12-2006

A Parametric Study of Water Vapor Condensation in Supersonic Nozzle Flow Fields

Todd Branson VanPelt
University of Tennessee - Knoxville

To the Graduate Council:

I am submitting herewith a thesis written by Todd Branson VanPelt entitled "A Parametric Study of Water Vapor Condensation in Supersonic Nozzle Flow Fields." I have examined the final electronic copy of this thesis for form and content and recommend that it be accepted in partial fulfillment of the requirements for the degree of Master of Science, with a major in Mechanical Engineering.

Roy J. Schulz, Major Professor

We have read this thesis and recommend its acceptance:

Basil N. Anatar, Frank G. Collins

Accepted for the Council:
Carolyn R. Hodges

Vice Provost and Dean of the Graduate School

(Original signatures are on file with official student records.)

To the Graduate Council:

I am submitting herewith a thesis written by Todd Branson VanPelt entitle “A Parametric Study of Water Vapor Condensation in Supersonic Nozzle Flow Fields.” I have examined the final electronic copy of this thesis for form and content and recommend that it be accepted in partial fulfillment of the requirements for the degree of Master of Science, with a major in Mechanical Engineering.

Roy J. Schulz
Major Professor

We have read this thesis and
recommend its acceptance:

Basil N. Antar

Frank G. Collins

Acceptance for the Council:

Anne Mayhew
Vice Chancellor and Dean of
Graduate Studies

(Original signatures are on file with official student records.)

A Parametric Study of Water Vapor Condensation in Supersonic Nozzle Flow Fields

A Thesis Presented for the
Master of Science Degree
The University of Tennessee

Todd Branson VanPelt
December 2006

Dedication

This thesis is dedicated to my heavenly father for providing me the knowledge, strength, perseverance, and determination to complete the work and to my savior, Jesus Christ, for his love, compassion, and forgiveness.

Acknowledgements

I would like to thank my advisor, Dr. Roy Schulz, for his guidance and support in my research and thesis preparation. To my thesis committee members, Drs. Basil Antar and Frank Collins, I am grateful for their effort in reviewing my thesis for the consideration of my final degree requirement of a Master of Science. In addition, I am in much appreciation to the faculty of the University of Tennessee Space Institute for furthering my education in engineering.

I am in forever in loving debt to my parents, Sterley and Bonnie VanPelt, and my two sisters, Sinda Buck and Cassie Rainwater, for whose encouragement and support helped me reach my goals. To my wife, Kerry VanPelt, I recognize her steadfast faith and love in me for which I am in very grateful.

Abstract

Combustion driven hypersonic and supersonic wind tunnels are impaired in their flight simulation abilities by the condensation of water vapor introduced into the test stream by the burning byproducts of air and hydrocarbon fuels. The purpose of this study is to evaluate the abilities of a condensation model to predict the beginning axial locations of vapor changing into liquid droplets and study the correlations with initial combustion chamber conditions. A test matrix with different fuels, chamber pressure, and equivalence ratio was applied to the FIRACON model written by Erickson, *et al.* [7] using the dimensions of the NASA Langley eight-foot-high heated wind tunnel nozzle.

The results indicate higher chamber pressure and fuel-air equivalence ratio cause water vapor molecules to nucleate and condense further upstream of the nozzle, where as higher temperature delayed the condensation event in the expanding nozzle flow. At this time, FIRACON's results can be considered qualitative in nature. General trends in the changes of the expanding flows due to varying initial chamber conditions can be seen, but the accuracy is unknown. A more thorough experimental and theoretical investigation of a condensing flow in a nozzle is needed to improve existing models before attaining results that could be considered relatively accurate or quantitative in nature.

Table of Contents

List of Tables

List of Figures

Nomenclature

A .....nozzle cross sectional area, m^2

$A_{n,k}$.....constant coefficients in *Equation* 2.43 for $C_{p,k}$

$a_{2,C}$.....initial approximation of mols of CO_2 per total mol equivalence of C in mixture

$B_{n,j}$ .....constant coefficient in *Equation* 2.38 for $K_{p,j}$

$C_{p,k}$.....molar heat capacity of species k, J/mol-K

$c_{p,c}$.....specific heat capacity of carrier gas, J/kg-K

$c_{p,k}$.....specific heat capacity of species k, J/kg-K

$D_{n,k}$ .....constant coefficients in *Equation* 2.73 for μ_k

$E_{n,k}$.....constant coefficients in *Equation* 2.76 for λ_k

F .....function defined by *Equation* 3.27

f .....factor to account for carrier gas defined by *Equation* 2.84

G.....function defined by *Equation* 2.53

h.....specific enthalpy of total mixture, J/kg

h_G.....specific enthalpy of gaseous mixture, J/kg

h_L .....specific enthalpy of liquid water, J/kg

h_0 .....stagnation specific enthalpy, J/kg

$\hat{h}_F, \hat{h}_{O_2}, \hat{h}_{N_2}$ .....specific enthalpy of fuel, O_2, and N_2 in feed, J/kg

$\hat{h}_0$ .....total specific enthalpy of feed to combustion chamber, J/kg

$\Delta h^0_{L,G,373.15}$ .....specific enthalpy of evaporation at 373.15 K, J/kg

J.....nucleation rate, droplet formed/m^3-s

$\overline{J}_j$ .....mean nucleation rate defined by *Equation* 3.24, droplets formed/m^3-s

$K_{p,j}$ .....equilibrium constant for reaction j

Kn.....Knudsen number defined in terms of r

Kn_* .....Knudsen number defined in terms of r_*

k.....Boltzmann constant, J/molecule-K

L .....latent heat of evaporation at $T_s(p_1)$, J/kg

$\tilde{\ell}$ .....mean free path, m

M .....mass of a water droplet, kg

m.....average molecular mass of gaseous mixture, kg/molecule

m_c .....average molecular mass of carrier gas, kg/molecule

m_1 .....molecular mass of water, kg/molecule

$\dot{m}$ .....mass flow rate, kg total mixture/s

n.....interation index and atoms of carbon per molecule of fuel

Δn^i .....number of droplets of kind i per mass of total mixture, droplet/kg

Pr.....Prandtl number defined in terms of $c_{p,1}$ in *Equation* 2.79

p.....pressure, N/m^2

p_1 .....partial pressure of water vapor, N/m^2

p_∞.....vapor pressure of water over a flat surface, N/m^2

p^0 .....standard state pressure, 0.101325 MN/m^2

Q.....Kantrowitz correction factor, *Equation* 2.72

q_c .....condensation coefficient

q_e .....evaporation coefficient

R .....universal gas constant 8.314J/mol-K

$\overline{R}$ .....specific gas constant for mixture, R/W, J/kg-K

R' .....universal gas constant, 1.987 cal/mol-K

$\overline{R}_c$ .....specific gas constant for carrier gas, R/W_c, J/kg-K

$\overline{R}_1$ .....specific gas constant for water, R/W_1, J/kg-K

r.....droplet radius, m

r_w .....nozzle radius, m

r_*.....critical droplet radius, m

s .....specific entropy of total mixture, J/kg-K

$s^0_{G,1}$.....specific entropy of water vapor at standard state pressure, J/kg-K

s_L .....specific entropy of liquid water, J/kg-K

$\Delta s^0_{L,G}$ .....specific entropy of evaporation at standard state pressure

T .....temperature, K

T_G .....temperature of gaseous mixture, K

T_L.....temperature of liquid water, K

T_R.....reduced temperature, T/T_c

T_c .....critical temperature of water, 647.3K

$T_s(p_1)$ .....saturation temperature based on partial pressure of water

t .....time, s

Δt.....time step, s

U.....velocity, m/s

W .....average molecular weight of gaseous mixture, kg/mol

W_c.....average molecular weight of carrier gas, kg/mol

W_k.....molecular weight of species k, kg/mol

w.....mass of liquid water per mass of total mixture

w_c.....mass of carrier gas per mass of total mixture

Δx .....computational step along nozzle, m

Y .....mol number of mixture, mols/kg

Y_C, Y_H, Y_O, Y_N .....equivalent total mols of elements C, H, O, and N per mass of total mixture, mols/kg

Y_k.....mol number of species k, mols/kg

Y_k^0 .....mol number of species k in gaseous mixture at point in nozzle where $J = J_{\min}$, mols/kg

$\hat{Y}_F, \hat{Y}_{O_2}, \hat{Y}_{N_2}$ .....mols of fuel, O_2, and N_2 per mass of total mixture in feed, mols/kg

y_k.....mol fraction of species k

Z_j.....parameter defined by *Equation* 3.28

z .....ratio of droplet radius to critcal radius, r/r_*

Greek:

α.....constant in *Equation* 2.88

α_c.....thermal accommodation coefficient for carrier gas interaction with water droplets

β.....constant in *Equation* 2.85; also Langmuir parameter

γ.....ratio of specific heats

δ.....parameter defined by *Equation* 2.92

δ^* .....nozzle boundary layer displacement thickness, m

ε.....allowable iteration error

$\eta_{H,C}$.....elemental ratio of hydrogen to carbon in mixture

$\eta_{N,O}$.....elemental ratio of nitrogen to oxygen in mixture

θ .....parameter defined by *Equation* 2.85

Λ.....parameter defined by *Equation* 2.86

λ .....thermal conductivity of gaseous mixture, J/s-m-K

μ .....viscosity of gaseous mixture, N-s/m^2

ν .....parameter defined be *Equation* 2.88

ξ.....parameter defined be *Equation* 2.87

ρ .....mass density, kg/m^3

σ.....surface tension, N/m

ϕ .....equivalence ratio

ψ.....parameter defined be *Equation* 2.90

Ω .....parameter defined be *Equation* 2.73

Subscripts:

c.....carrier gas

G.....gaseous mixture

i .....properties at interface between free molecular and continuum regimes

j .....location index along nozzle axis

k.....chemical species index (*k* = 1 denotes water vapor)

L .....liquid water

min .....minimum

n.....summation index

0.....stagnation conditions

s.....saturation condition, expect in *Equation* 2.13 where it is stoichiometric

condition

1.....water vapor

373.15.....evaluated at 373.15K

Superscripts:

i .....droplet type index

0.....conditions at point in nozzle where nucleation rate just begins, except p^0 denotes state pressure of 0.1401325 MN/m^2

′.....approximation

″.....alternate approximation

*.....sonic condition at nozzle throat

A caret over a symbol indicates the feed condition to combustor.

Chapter 1

Introduction

From the beginning of the Wright brother's first powered flight in 1903, to Charles Yeager's first manned airplane flight to exceed the speed of sound in level flight in 1947, and to the current development of NASA's X43 scramjet to achieve hypersonic flight, mankind is attempting to fly faster and faster. The design and development of aircrafts in the early twentieth century experienced many failures before successful operational aircrafts were attained. By the end of World War II, aircraft became increasingly expensive to develop and the costs of unsuccessful designs were growing. As a result, more emphasis was placed on the mathematical modeling and physical flight simulations before actual construction and manned flight-testing of an aircraft began.

To simulate aircraft flight, wind tunnels are used to study the effects of airflow over the surfaces. Supersonic wind tunnels are used to test aircraft flights beyond the speed of sound. Compression-driven supersonic wind tunnels operate by compressing air into large storage tanks and then releasing it through a supersonic nozzle into the wind tunnel test section. The airflow experiences a pressure and temperature drop as speeds approach Mach 1 in the throat of the converging-diverging nozzle section of the tunnel. After the flow reaches sonic velocity in the throat, the flow continues to expand isentropically to supersonic speeds through the diverging section of the tunnel's nozzle.

When the air expands past the throat, the temperature of the flow continues to decrease rapidly. In some cases, the temperature can become so low that air begins to liquefy. To combat this problem, the air stored in the tanks is heated so that when it is released into the tunnel and the temperature begins to decrease past the throat the temperature drop does not reach the point for air to liquefy. Moisture in the air can be another problem. The decreasing temperature in the diverging section of the nozzle in the wind tunnel will cause any water vapor contained in the air to condense into a liquid droplet state or crystallize into fine ice crystals. Water vapor condensation is prevented by drying the air to remove all the moisture before it is stored in the storage tanks of the compression-driven wind tunnel.

Wind tunnels driven by compressed air are typically limited to short burst of flows due to the volume in the supply tanks. For very high speed, or hypersonic flight simulations, where the Mach number exceeds about four, vitiated air at high pressure is used to drive wind tunnels. Vitiated “air” is air burned at a lean stoichiometry with a fuel, typically a hydrocarbon fuel. The expansion of the combustion products of the fuel and air form the test stream. Hydrocarbon fuels produce substantial amount of water vapor in the combustion products. Unlike the wind tunnels driven by compressed air in tanks, combustion driven wind tunnels are not able to remove the water vapor from the flow before expansion. The water vapor contained in the combustion products will condense in the expansion with a significant increase of the temperature in the expanding flow of the nozzle.

Background

Condensation is the phase change of water vapor into liquid or liquid into crystals or a solid phase. Around the beginning of the twentieth century, homogeneous nucleation theory was developed to predict condensations [1, 50]. The theory was applied to a variety of devices such as Wilson Cloud Chambers, steam turbine nozzles, and moisture-laden wind tunnel flows [1-24, 26-31, 34-38, 40-50]. In addition, the theory is used extensively to predict the condensation of alloy phases formed in sprays of fine liquid metal that cool and solidify.

The formation of water vapor alters the supersonic nozzle flow substantially. Heybey [20] in 1942 observed the following consequences of the airflow expanding and cooling in the nozzle to form liquid water droplets:

1.) heat is released into the gas flow by the phase change of water vapor into liquid drops,

2.) a loss of gas mass flow with increased specific volume,

3.) a change in specific heat, gas constant, and molecular weight of the gas flow, and

4.) the one phase flow becoming a two-phase flow, gas and liquid.

These changes also cause changes in Mach number, velocity, temperature, pressure, total temperature, and total pressure. With these changes, the supersonic wind tunnel will not operate at its designed test conditions. The flight simulation, therefore, will not experience the proper simulations.

In some test facilities, it has been observed that water vapor condensation did not occur until the flow reached a condition of saturation or slight supersaturation, and continued expanding through the nozzle at an equilibrium saturation condition. Past researchers like Gyarmathly [15], Wegener and Mack [44], and others claim the condensing water vapor happens suddenly at a “condensation shock”, some distance past the initial saturation point in the nozzle flow, far into the supersaturation regime. Where the metastable equilibrium state of the flow collapses, and experiences a condensation generated discontinuity in the flow, something like a shock wave occurs. Heybey [20] also described it as a “condensation shock”. To reconcile the two viewpoints of equilibrium saturated expansion versus supersaturated expansion followed by a condensation shock, is the recognition that the condensation process depends on the number and type of nucleation sites for minute water molecules to form.

For wind tunnels with airflow containing particulates of dust or rust, heterogeneous nucleation sites will trigger condensation to occur as soon as it can and continue in an apparent equilibrium process. For clean air with few or no particulates, homogenous nucleation happens where liquid water molecules form molecular aggregates of a few dozen to serve as the nucleation sites. It takes time and distance downstream of the saturation point in the nozzle for these homogeneous nucleation sites to form, thus, the “shock-like” appearance of the “sudden” condensation, in relatively clean tunnel and nozzle flow expansion.

FIRACON

Researchers at NASA Langely have encountered condensation problems with their eight-foot high heated wind tunnel (8ft HHT). This tunnel provides a simulation of hypersonic flow by the combustion of various fuels and air, enriched with oxygen if necessary, at high pressures followed by an expansion of the products of combustion

through the nozzle producing the hypersonic flow. Commonly used fuels are methane, propane, and iso-butane. The combustion products of these fuels contain a substantial amount of water vapor. Erickson, *et al.* [7] has observed that the condensation depends on the fuel type, equivalence ratio, and heat losses from the flowing gas neglecting any consideration of soot formation. These variables, and the pressure at which combustion occurs, determine the characteristics of homogenous nucleation driven condensation in wind tunnels.

Erickson, *et al*. [7], developed a code, FIRACON, to predict the homogenous nucleation of growth of water droplet in combustion driven hypersonic wind tunnel flows. The starting point of the work was based on Young's [48, 49] work of water droplet formation by condensation in the expansion of pure steam. Young's work was modified and expanded to include the rapid expansion of combustion products in wind tunnel nozzles.

Purpose of Present Study

The problem of water vapor condensation in wind tunnel test facilities has yet to be resolved. It has been observed that after the initial condensation point and some distance downstream, the flow can experience a re-vaporization or evaporation of the water droplets. In addition, re-vaporization is expected downstream of shock waves generated by the test article in the tunnel. In either case, the occurrence of condensation is detrimental to wind tunnel operations. The purpose of this study is to examine the current capability of predicting the axial locations in a Mach 8 blow-down wind tunnel where condensation begins, and to correlate these locations with the initial combustion chamber conditions. The program written by Erickson, *et al.* [7], FIRACON, was obtained and made operational for desktop computers. The present study used the existing dimensions of the NASA Langley eight-foot-high heated wind tunnel. A test matrix was developed to explore the possible effects of fuel type, equivalence ratio, and chamber pressure on the predicted initial beginning locations water vapor condensation by homogenous nucleation. The following chapters briefly outline the theory used in FIRACON, and the

steps or process by which FIRACON predicts water condensation in combustion-driven supersonic/hypersonic wind tunnels.

Chapter 2

Theory Used in FIRACON

This chapter summarizes the theoretical models and sub-models that Erickson, *et al.* [7] assembled in order to carry out a one-dimensional flow calculation of a hydrocarbon combustion gas, expanding supersonically in a nozzle, with a prediction of water vapor condensation into microscopic water droplets. Water droplet growth by continued condensation on each droplet group according to size is also predicted. In addition, the initiation of the liquid water content of the flow and its increase by continued droplet condensation is predicted.

Flow Equations

For quasi-one-dimensional flow the gas phase continuity equation is expressed as

$$\dot{m} = \frac{\rho_{\mathrm{G}} A U}{1-w} . \qquad (Eq.\ 2.1)$$

This equation applies through the nozzle expansion from no liquid water present ($w = 0$) to water being present. It is assumed the condensed liquid water and the gaseous mixture have the same velocity. The momentum equation is expressed as

$$\frac{(1-w)\,dp}{\rho_{\mathrm{G}}} = -UdU . \qquad (Eq.\ 2.2)$$

The energy equation is

$$h_0 = (1-w)\,h_{\mathrm{G}} + \sum_i w^i h_{\mathrm{L}}^i + \frac{U^2}{2} , \qquad (Eq.\ 2.3)$$

where the first term on the right side is expressed as

$$(1-w)\,h_{\mathrm{G}} = (1-w-w_{\mathrm{c}})\,h_{\mathrm{G},1} + w_c h_{\mathrm{G,c}} . \qquad (Eq.\ 2.4)$$

For the point where water condenses and chemical reactions cease, the energy equation becomes

$$h_0 = h_{G,1} dw - \sum_i w^i dh_L^i - \sum_i h_L^i dw^i . \qquad (Eq.\ 2.5)$$

Stoichiometric Relationships

The elemental chemical composition of the reacting flows is defined by Erickson, *et al.* [7] as being composed of carbon, C, hydrogen, H, oxygen, O, and nitrogen, N. The elemental constants are first determined from a specified equivalence ratio, ϕ, expressed as

$$\phi = \frac{Y_{\mathrm{H}}/2 + 2Y_{\mathrm{C}}}{Y_{\mathrm{O}}}. \qquad (Eq.\ 2.6)$$

A characteristic expression that expresses the conservation of elemental mass of the four elemental species is given as

$$12Y_C + Y_H + 16Y_O + 14Y_N = 1000. \qquad (Eq.\ 2.7)$$

The specified nitrogen-to-oxygen ratio, $\eta_{\mathrm{N,O}}$, and the hydrogen-to-carbon ration, $\eta_{\mathrm{H,C}}$, are inputed as constants based on the oxidizer and the fuel type specified for the combustion, respectively. The elemental constants are then expressed as

$$Y_{\mathrm{O}} = \frac{500}{8 + 7\eta_{\mathrm{N,O}} + \phi\left[\left(12 + \eta_{\mathrm{H,C}}\right)/\left(4 + \eta_{\mathrm{H,C}}\right)\right]}, \qquad (Eq.\ 2.8)$$

$$Y_{\mathrm{C}} = \frac{2\phi Y_{\mathrm{O}}}{4 + \eta_{\mathrm{H,C}}}, \qquad (Eq.\ 2.9)$$

$$Y_{\mathrm{N}} = \eta_{\mathrm{N,O}} Y_{\mathrm{O}}, \text{ and} \qquad (Eq.\ 2.10)$$

$$Y_{\mathrm{H}} = \eta_{\mathrm{H,C}} Y_{\mathrm{C}}. \qquad (Eq.\ 2.11)$$

The reaction in the combustor is assumed limited to hydrocarbons (C_nH_m) burning with an oxygen and nitrogen mixture. The stoichiometric reaction assumed is

$$\mathrm{C}_n\mathrm{H}_m + \left(n + \frac{m}{4}\right)\mathrm{O}_2 = n\mathrm{CO}_2 + \frac{m}{2}\mathrm{H}_2\mathrm{O}. \qquad (Eq.\ 2.12)$$

The stoichiometric ratio of fuel to oxygen is defined as

$$\left(\frac{\hat{Y}_F}{\hat{Y}_{O_2}}\right)_s = \frac{4}{n\left(4 + \eta_{H,C}\right)} \qquad (Eq.\ 2.13)$$

followed by the total mols of fuel per mass of total mixture in feed, $\hat{Y}_{\mathrm{F}}$, expressed as

$$\hat{Y}_{\mathrm{F}} = \frac{4}{n\left(4+\eta_{\mathrm{H,C}}\right)}\hat{Y}_{\mathrm{O}_2} \qquad (Eq.\ 2.14)$$

with the nitrogen as

$$\hat{Y}_{\mathrm{N}_2} = \eta_{\mathrm{N,O}}\hat{Y}_{\mathrm{O}_2}, \text{ and} \qquad (Eq.\ 2.15)$$

the oxygen defined as

$$\hat{Y}_{\mathrm{O}_2} = \frac{Y_{\mathrm{O}}}{2}. \qquad (Eq.\ 2.16)$$

Substituting the expression for $\hat{Y}_{\mathrm{O}_2}$, above the authors obtain

$$\hat{Y}_{O_2} = \frac{250}{8+7\eta_{\mathrm{N,O}}+\phi\left[\left(12+\eta_{\mathrm{H,C}}\right)/\left(4+\eta_{\mathrm{H,C}}\right)\right]}. \qquad (Eq.\ 2.17)$$

In the flow region where nucleation and droplet growth begins, it is assumed by Erickson, *et al*. [7] the decreased temperature has reached the point where the temperature dependent properties of the chemical composition has no significant effect (chemically frozen). Only changes due to the formation of water are considered, which decreases the amount of H_2O in the gas or vapor phase. The mols of water vapor, Y_1, in the flow is defined as

$$Y_1 = \frac{Y_1^0 - w/W}{1-w}. \qquad (Eq.\ 2.18)$$

The rest of the chemical species, Y_{k}, are then defined as

$$Y_k = \frac{Y_k^0}{1-w} \qquad (Eq.\ 2.19)$$

for $k > 1$, where k is an index related to the ten molecular compounds assumed to form the combustion gas. The average molecular weight of the gaseous mixture, W, is then determined by

$$W = \frac{1}{\sum_{k=1}^{10} Y_k} \qquad (Eq.\ 2.20)$$

and with water being present it becomes

$$W = \frac{1-w}{Y^0 - w/W_1} \qquad (Eq.\ 2.21)$$

where

$$Y^0 = \sum_{k=1}^{10} Y_k^0 \ . \qquad (Eq.\ 2.22)$$

In addition, the mol fraction of any species, y_k, in the gaseous mixture is

$$y_k = Y_k W \ . \qquad (Eq.\ 2.23)$$

The average molecular weight of the carrier gases, W_c, excluding water, is determined from

$$W_c = \sum_{k=2}^{10} \frac{Y_k W_k}{Y - Y_1} \qquad (Eq.\ 2.24)$$

or

$$W_c = \sum_{k=2}^{10} \frac{y_k^0 W_k}{1 - y_1^0} . \qquad (Eq.\ 2.25)$$

Equilibrium Chemical Composition

Only ten molecular species are considered for the combustion products, numbered 1 through 10 in the following order: H_2O, CO_2 CO, O_2, H_2, N_2, H, O, OH, and NO. Six equilibrium reactions are considered with six corresponding equilibrium relations. The reactions and equilibrium constants are as follows.

For $CO_2 + H_2 \rightarrow CO + H_2O$ $\qquad (Eq.\ 2.26)$

$$K_{p,1} = \frac{Y_1 Y_3}{Y_2 Y_5} . \qquad (Eq.\ 2.27)$$

For $2CO_2 \rightarrow 2CO + O_2$, $\qquad (Eq.\ 2.28)$

$$K_{p,2} = \frac{Y_3^2 Y_4}{Y_2^2 Y} \frac{p}{p^0} . \qquad (Eq.\ 2.29)$$

For $H_2 + O_2 \rightarrow 2OH$, $\qquad (Eq.\ 2.30)$

$$K_{p,3} = \frac{Y_9^2}{Y_4 Y_5} . \qquad (Eq.\ 2.31)$$

For $H_2 \rightarrow 2H$, $\qquad (Eq.\ 2.32)$

$$K_{p,4} = \frac{Y_8^2}{Y_4 Y} \frac{p}{p^0}. \quad (Eq.\ 2.33)$$

For $O_2 \rightarrow 2O$, (*Eq.* 2.34)

$$K_{p,5} = \frac{Y_8^2}{Y_4 Y} \frac{p}{p^0}. \quad (Eq.\ 2.35)$$

For $O_2 + N_2 \rightarrow 2NO$, (*Eq.* 2.36)

$$K_{p,6} = \frac{Y_{10}^2}{Y_4 Y_6}. \quad (Eq.\ 2.37)$$

The variation of the equilibrium constants with temperature are obtained with curve fits of the form

$$K_{p,j} = \exp\left(\sum_{n=1}^{6} B_{n,j} T_G^{n-2} \right). \quad (Eq.\ 2.38)$$

Four elemental atom balance equations are needed to close the system of equations and solve for the equilibrium molecular composition. They are given as follows:

$$Y_H = 2Y_1 + 2Y_5 + Y_7 + Y_9, \quad (Eq.\ 2.39)$$

$$Y_O = Y_1 + 2Y_2 + Y_3 + 2Y_4 + Y_8 + Y_9 + Y_{10}, \quad (Eq.\ 2.40)$$

$$Y_N = 2Y_6 + Y_{10}, \text{ and} \quad (Eq.\ 2.41)$$

$$Y_C = Y_2 + Y_3. \quad (Eq.\ 2.42)$$

Thermodynamic Relations and Properties

Many thermodynamic relations and properties are needed to determine the characteristics of the expanding flow with condensation. To begin, the molar heat capacity at a constant pressure for each chemical species, $C_{p,k}$, is obtained as curve fits of the form

$$C_{p,k} = \sum_{n=1}^{6} A_{n,k} T_G^{n-2}. \quad (Eq.\ 2.43)$$

The specific heat capacity at a constant pressure, $c_{p,k}$, is then expressed as

$$c_{p,k} = \frac{C_{p,k}}{W_k}. \quad (Eq.\ 2.44)$$

In addition, the specific heat for water vapor, $c_{\mathrm{p},1}$, is also defined by a curve fit as

$$c_{\mathrm{p},1} = \frac{\sum_{n=1}^{6} A_{n,1} T_{\mathrm{G}}^{n-2}}{W_1}. \qquad (Eq.\ 2.45)$$

The ratio of specific heats for water vapor, γ_1, is given as

$$\gamma_1 = \frac{c_{\mathrm{p},1}}{c_{\mathrm{p},1} - \bar{R}_1}. \qquad (Eq.\ 2.46)$$

The specific heat capacity at constant pressure for carrier a gas, $c_{\mathrm{p,c}}$, is

$$c_{\mathrm{p,c}} = \frac{\sum_{k=2}^{10} y_k^0 C_{\mathrm{p},k}}{\left(1 - y_1^0\right) W_1} \qquad (Eq.\ 2.47)$$

and the ratio of the specific heats for the carrier gas, γ_{c}, is

$$\gamma_{\mathrm{c}} = \frac{c_{\mathrm{p,c}}}{c_{\mathrm{p,c}} - \bar{R}_{\mathrm{c}}}. \qquad (Eq.\ 2.48)$$

The specific enthalpy of the gaseous mixture, h_{G}, is expressed as

$$h_{\mathrm{G}} = \sum_{k=1}^{10} Y_k \left[A_{1,k} \ln T_{\mathrm{G}} + \sum_{n=2}^{6} \frac{A_{n,k} T_{\mathrm{G}}^{n-1}}{n-1} + A_{7,k} \right] \qquad (Eq.\ 2.49)$$

and the specific enthalpy of water vapor in the mixture, $h_{\mathrm{G},1}$, is

$$h_{\mathrm{G},1} = \frac{\left[A_{1,1} \ln T_{\mathrm{G}} + \sum_{n=2}^{6} \frac{A_{n,1} T_{\mathrm{G}}^{n-1}}{n_1} + A_{7,1} \right]}{W_1} \qquad (Eq.\ 2.50)$$

The specific entropy of the gaseous mixture, s_{G}, is given by

$$\begin{aligned} s_G = & \sum_{k=1}^{10} Y_k \left[\frac{-A_{1,k}}{T_G} + \left(A_{2,k} - R'\right) \ln T_G + \sum_{n=3}^{6} \frac{A_{n,k} T_G^{n-2}}{} + A_{8,k} \right] \\ & - \bar{R} \ln \rho_G - \bar{R} \ln\left(\frac{R}{p^0}\right) - R \sum_{k=1}^{10} Y_k \ln Y_k. \end{aligned} \qquad (Eq.\ 2.51)$$

The gas density, ρ_{G}, is also related to the gas entropy, s_{G}, state pressure, p^0, and gas temperature, T_{G}, by

$$\rho_{\mathrm{G}} = \exp\left[\frac{G - s_{\mathrm{G}} - \bar{R}\ln\left(R/p^{0}\right) - R\sum_{k=1}^{10} Y_k \ln Y_k}{\bar{R}}\right] \qquad (Eq.\ 2.52)$$

where

$$G = \sum_{k=1}^{10} Y_k \left[\frac{-A_{1,k}}{T_{\mathrm{G}}} + \left(A_{2,k} - R'\right)\ln T_{\mathrm{G}} + \sum_{n=3}^{6} \frac{A_{n,k} T_{\mathrm{G}}^{n-2}}{n-2} + A_{8,k}\right]. \qquad (Eq.\ 2.53)$$

The ideal gas equation of state for the gaseous mixture equation is assumed as

$$p = \rho_{\mathrm{G}} \bar{R} T_{\mathrm{G}} \qquad (Eq.\ 2.54)$$

where

$$\bar{R} = \frac{R}{W} \quad \text{and} \quad W = \left(\sum_{k=1}^{10} Y_k\right)^{-1}. \qquad (Eq.\ 2.55)$$

For the flow region where nucleation and droplet growth occur, additional terms are needed for the specific enthalpy and entropy of liquid water. The enthalpy is defined from

$$h_{\mathrm{L}} - h_{\mathrm{L},373.15} = \left(4.2\times10^{3}\right)\left(T - 373.15\right) \text{ and} \qquad (Eq.\ 2.56)$$

$$\Delta h^{0}_{\mathrm{L,G},373.15} = h_{\mathrm{G},1,373.15} - h_{\mathrm{L},373.15}, \qquad (Eq.\ 2.57)$$

so that the specific enthalpy of liquid water is specified as

$$h_{L} = \left(4.2\times10^{3}\right)T - \left(17.1174\times10^{6}\right). \qquad (Eq.\ 2.58)$$

The specific entropy of liquid is acquired in a similar fashion. Beginning with the specific entropy of evaporation of water at 1atm and 373.15K

$$\Delta s^{0}_{L,G,373.15} = \frac{\Delta h^{0}_{L,G,373.15}}{373.15} = 6.0485\times10^{3}\ \mathrm{J/kg-K}, \qquad (Eq.\ 2.59)$$

the entropy of water at 1atm and 373.15K, $s^{0}_{G,1}$, is defined using

$$s^{0}_{G,1} = \frac{\left[-A_{1,1}/T_{G} + A_{2,1}\ln T_{G} + \sum_{n=3}^{6} \frac{A_{n,1} T_{G}^{n-2}}{n-2} + A_{8,1}\right]}{W_{1}}. \qquad (Eq.\ 2.60)$$

Given

$$s_{\mathrm{L}} - s_{\mathrm{L},373.15} = \left(4.2\times10^{3}\right)\ln\frac{T}{373.15}, \qquad (Eq.\ 2.61)$$

and

$$\Delta s^{0}_{\mathrm{L},373.15} = s^{0}_{\mathrm{G},373.15} - s_{\mathrm{L},373.15}, \qquad (Eq.\ 2.62)$$

the specific entropy of liquid water, s_{L}, is obtained as

$$s_{\mathrm{L}} = 4.2\times10^{3}\ln T - 20.0149\times10^{3}. \qquad (Eq.\ 2.63)$$

In addition, the specific latent heat of evaporation of water, L, is also needed and expressed as

$$L = h_{\mathrm{G},1} - h_{\mathrm{L}}. \qquad (Eq.\ 2.64)$$

By substitution of these parameters, then

$$L = h_{\mathrm{G},1} - 4.2\times10^{3}T + 17.1175\times10^{6}. \qquad (Eq.\ 2.65)$$

The vapor pressure of water, p_{∞}, is obtain from the equation

$$p_{\infty} = \exp\left(55.897 - \frac{6641.7}{T} - 4.4864\ln T\right). \qquad (Eq.\ 2.66)$$

Young [47, 48] expressed the surface tension of water as

$$\sigma = \left(82.27 + 75.612T_{\mathrm{R}} - 256.889T_{\mathrm{R}}^{2} + 95.928T_{\mathrm{R}}^{3}\right)\times10^{-3} \qquad (Eq.\ 2.67)$$

where

$$T_{\mathrm{R}} = \frac{T}{T_{\mathrm{c}}}. \qquad (Eq.\ 2.68)$$

Erickson, *et. al*. [7] use the same equation. The critical droplet radius at nucleation is obtained from classical theory as

$$r_{*} = \frac{2\sigma}{\rho_{\mathrm{L}}\bar{R}_{1}T_{\mathrm{G}}\ln\left(p_{1}/p_{\infty}\right)} \qquad (Eq.\ 2.69)$$

where $p_{1} = y_{1}p$.

Nucleation Rate

Erickson, *et al*., [7] modify Young's expression [47, 48] for the nucleation rate of a pure steam flow to include the effects of a carrier gas. Erickson, *et al*. [7] defends this by the argument that "nucleation depends on collision between water molecules in the

gaseous phase and clusters of water molecules, both of which are proportional to the density of water vapor." Therefore, the density of water vapor in a gaseous mixture is expressed as

$$\rho_{G,1} = \frac{y_1 m_1}{m}\rho_G \,. \qquad (Eq.\ 2.70)$$

Then, Young's [47, 48] modified nucleation rate that includes a carrier gas is derived as

$$J = \frac{q_c}{1+Q}\left(\frac{y_1 m_1}{m}\right)^2\left(\frac{2\sigma}{\pi m_1^3}\right)^{1/2}\frac{\rho_G^2}{\rho_L}\times\exp\left(\frac{-4\pi r_*^2\sigma}{3kT_G}\right). \qquad (Eq.\ 2.71)$$

q_c is the condensation coefficient, argued to by Young [47, 48] to be unity and the non-isothermal correction, Q, factor given by Kantrowitz [22] expressed as

$$Q = \frac{2(\gamma_1 - 1)}{\gamma_1 + 1}\frac{L}{\bar{R}_1 T_G}\left(\frac{L}{\bar{R}_1 T_G} - \frac{1}{2}\right) \qquad (Eq.\ 2.72)$$

Transport Properties

Various transport properties are needed for the flow region where droplet growth is considered. The temperature in this region is consequently low due to the flow expansion in the nozzle. Only a narrow range of a data is needed for viscosity and thermal conductivity for temperatures in the range of 200 to 500K. As an additional result, only seven chemical species (H_2O, CO_2, CO, O_2, H_2, N_2, and NO) are present in significant quantities at low temperatures.

The viscosity of the gaseous mixture is obtain first from the individual viscosity, μ_k, of each species

$$\mu_k = \sum_{n=1}^{4} D_{n,k} T_G^{n-1}\,, \qquad (Eq.\ 2.73)$$

then the viscosity of the gaseous mixture using Touloukian, *et al.* [39] expression is obtained from

$$\mu = \sum_{k=1}^{10}\frac{\mu_k}{1+\frac{1}{Y_k}\sum\limits_{\substack{\ell=1\\ \ell\neq k}}^{10} Y_\ell \phi_{k,\ell}} \qquad (Eq.\ 2.74)$$

where

$$\phi_{k,1} = \frac{\left[1+\left(\mu_k/\mu_1\right)^{1/2}\left(W_1/W_k\right)^{1/4}\right]^2}{\left\{8\left[1+\left(W_k/W_1\right)\right]\right\}^{1/2}}. \qquad (Eq.\ 2.75)$$

Thermal conductivity of the gaseous mixture is solved for in the same matter. First, the thermal conductivity of each species, λ_k, is obtain from

$$\lambda_k = \sum_{n=1}^{4} E_{n,k} T_G^{n-1}, \qquad (Eq.\ 2.76)$$

and then used to find the thermal conductivity for gaseous mixture

$$\lambda = \frac{1}{2}\left[W \sum_{k=1}^{10} Y_k \lambda_k + \frac{1}{W \sum_{k=1}^{10} Y_k/\lambda_k} \right]. \qquad (Eq.\ 2.77)$$

The mean free path, $\tilde{\ell}$, is obtained from

$$\tilde{\ell} = 1.5\mu \frac{\sqrt{\bar{R}T_G}}{p}, \qquad (Eq.\ 2.78)$$

The Prandtl number, Pr, is given as

$$\mathrm{Pr} = \frac{c_{p,1}\mu}{\lambda}, \qquad (Eq.\ 2.79)$$

where the specific heat at constant pressure for water vapor, $c_{p,1}$, is used. The Knudsen number, Kn, of the water droplets is obtained from

$$\mathrm{Kn} = \frac{\tilde{\ell}}{2r}, \qquad (Eq.\ 2.80)$$

and a second Knudsen, Kn^*, number in terms of the critical droplet radius, r^*, as

$$\mathrm{Kn}^* = \frac{\tilde{\ell}}{2r^*}. \qquad (Eq.\ 2.81)$$

Droplet Growth

Erickson, *et al.* [7] rewrite the integrated droplet growth equation given by Young [47, 48] for droplets with the $z = \frac{r}{r^*} \geq 1.1$ as

$$\frac{\theta^3}{\theta+1}\ln\frac{z_{j+1}+\theta}{z_j+\theta}+\left(\frac{1}{\theta+1}+\Omega\right)\ln\frac{z_{j+1}-1}{z_j-1}+$$
$$(\Omega+1-\theta)\left(z_{j+1}-z_j\right)+\tfrac{1}{2}\left(z_{j+1}^2-z_j^2\right)=\Lambda\Delta T. \qquad (Eq.\ 2.82)$$

In addition, this equation applies when a carrier gas is present with Ω defined as

$$\Omega=\frac{\xi(1-\nu)\mathrm{Kn}^*}{\mathrm{Pr}\,f} \qquad (Eq.\ 2.83)$$

where f is defined as

$$f=y_1\left(\frac{m_1}{m}\right)^{1/2}+(1-y_1)\left(\frac{m_c}{m}\right)^{1/2}\left[\frac{(\gamma_c+1)\gamma_1 c_{p,c}}{(\gamma_1+1)\gamma_c c_{p,1}}\right]. \qquad (Eq.\ 2.84)$$

The other parameters used in *Equations* 2.82 and 2.83 is defined as

$$\theta=2\beta\mathrm{Kn}^*, \qquad (Eq.\ 2.85)$$

$$\Lambda=\lambda\frac{\left[T_s(p_1)-T_G\right]}{L\rho_L r^{*2}}, \qquad (Eq.\ 2.86)$$

$$\xi=\frac{\sqrt{8\pi}}{1.5}\frac{2\gamma_1}{(\gamma_1+1)}, \text{ and} \qquad (Eq.\ 2.87)$$

$$\nu=\frac{\bar{R}_1 T_s(p_1)}{L}\left[\alpha+\frac{1}{2}-\frac{2-q_c}{2q_c}\frac{\gamma_1+1}{2\gamma_1}\frac{c_{p,1}T_s(p_1)}{L}\frac{f}{y_1}\left(\frac{m}{m_1}\right)^{1/2}\right]. \qquad (Eq.\ 2.88)$$

The ratio of specific heat and heat capacity, γ_1, and $c_{p,1}$, for water vapor at the saturation temperature, $T_s(p_1)$, are based on partial pressure of water in the mixture.

For droplet growth where $z=\frac{r}{r^*}<1.1$, the integrated droplet growth equation is given as

$$z_{j+1}=1+\frac{r_{*,j}}{r_{*,j+1}}(z_j-1)\exp(\psi\Delta t)-\frac{1}{\psi r_{*,j+1}}\frac{dr_*}{dt}\exp(\psi\Delta t-1) \qquad (Eq.\ 2.89)$$

where the parameter, ψ, is defined as

$$\psi=\frac{fp}{r_j\sqrt{2\pi\bar{R}T_G}}\frac{\gamma_1+1}{2\gamma_1}\frac{c_{p,1}}{L_{\rho L}}\frac{1}{1-\nu}\left[T_s(p_1)-T_G\right] \qquad (Eq.\ 2.90)$$

The other parameters f and v are defined previously. The temperature of the liquid droplets are obtained from Young's [47, 48] theory as

$$T_L = T_G + \frac{\left(1 - r_*/r\right)\left[T_s\left(p_1\right) - T_G\right]}{1 - \nu\delta} \qquad (Eq.\ 2.91)$$

where the parameter δ is given by Erickson, *et al.*[7] by

$$\delta = \frac{\xi\,\mathrm{Kn}/\mathrm{Pr}}{\dfrac{f}{1+2\beta\mathrm{Kn}} + \dfrac{\xi\mathrm{Kn}}{\mathrm{Pr}}}, \text{ and} \qquad (Eq.\ 2.92)$$

the parameter ξ is defined previously.

Entropy Production Equation

Young [47, 48] developed a method of solving for expanding stream flow that replaced the differential form of the momentum equation with an equation for the increase in entropy due to water condensation. Erickson, *et al.* [7] applied Young's theory [47, 48] to the case where a carrier gas is present and obtained the expression for entropy change as

$$ds = \left\{L - c_{\mathrm{p},1}\left[T_{\mathrm{s}}\left(p_1\right) - T_{\mathrm{G}}\right]\right\}\left\{\frac{1}{T_{\mathrm{G}}} - \frac{1}{T_{\mathrm{s}}\left(p_1\right)}\right\} dw. \qquad (Eq.\ 2.93)$$

Chapter 3

FIRACON's Procedures

This chapter gives a brief outline of the numerical process by which the FIRACON code predicts the one-dimensional, chemical equilibrium supersonic expansion of combustion gases with a condensing species, water vapor. FIRACON carries out this process in three distinct and separate sequential steps called PART 1, PART 2, and PART 3 presented respectively in this thesis. These "parts" correspond, approximately to the sequence of calculation steps in FIRACON. The main part of the Fortran source code for FIRACON is given in the report by Erickson, *et al*. [7].

Input for FIRACON

The first task of FIRACON is to obtain the data input via the subroutine DATAII. Erickson *et al.*, [7] originally inputed the data by data statements. In the present study, this is changed to a predefined input files read by FIRACON. The file CASEDATA.INPUT is called from DATAII and read into the program. The initial conditions in the combustor are set by the inputed initial temperature, (K); initial Pressure, (N/m^2); and the temperature of the fuel feed, (K). The fuel is defined by setting the enthalpy of the fuel at the feed temperature, (CAL/MOL), the elemental ratio of hydrogen to carbon in the mixture, and the number of atoms of carbon in a molecule of fuel. The oxidant is defined by the equivalence ratio and elemental ratio of nitrogen to oxygen in the mixture. The expansion nozzle is defined by the diameter of nozzle throat, (m), the corresponding X and Y wall coordinates for the tunnel geometry, a predetermined boundary layer displacement thickness, and the final X, (m) used to terminate calculations. In addition, a minimum value for the nucleation rate, J, (Droplets Formed/m^3-S), is inputted to define the start or initiation of the nucleation and condensation processes in the expansion. The step width, X (m), for PART 3 Calculations is also inputted.

Two more additional files, PLOT.INPUT and CONST.INPUT, are read into the program. PLOT.INPUT is not used in the present study because it is used by FIRACON to plot the results onto specific equipment at the NASA Langley facility. The file

CONST.INPUT is an additional file to specify constants used in FIRACON's calculation.

The input parameters for CASEDATA.INPUT are defined as:

T0 .....initial temperature, (K)

P0 .....initial pressure, (N/M^2)

DSTAR .....diameter of nozzle throat, (M^3)

HFUEL .....enthalpy of the fuel at the feed temperature, (CAL/MOL)

TFEED .....temperature of the feed, (K)

PHI1 .....equivalence ratio

RHC .....elemental ratio of hydrogen to carbon in mixture

RNO .....elemental ratio of nitrogen to oxygen in mixture

JMIN .....beginning nucleation rate for PART 3, (Droplets Formed/M^3-S)

NATOM.....number of carbon atoms in a molecule of fuel

IOUT .....output level prescribed as:

0 - standard summary output,

1 - extended output, or

2 - debug output

SWPO .....printed output switch prescribe as:

0 - do not print output, or

1 - print output

SWGO.....graphic output switch prescribe as:

0 - do not plot output, or

1 - plot output

SWEND .....end of data switch prescribe as:

0 - if data encountered, process it, or

1 - if end of data encountered, stop

NA.....number of axial positions, *X*, defining nozzle geometry

DELX.....axial step width for PART 3 calculations (m)

XLAST.....final *X*,(m) (used to terminate calculations)

XA.....nozzle *X* coordinates

RWA .....wall coordinates for defining tunnel geometry

DELSTR .....boundary layer displacement thickness for tunnel geometry.

The order and placement of the preceding parameters are illustrated in *Table* 3.1 as the structure for CASEDATA.INPUT file.

The input parameters for CONST.INPUT are defined as:

IPLTRD.....integer flag to indicate if auto-scaling is to be used on the plots

0 - use auto-scaling, or

1 - do not use auto-scaling

JSTOP .....maximum number of bands in PART 3 dimension statements

JDB .....debug print control for PART 3

DBLIT.....routine for all band numbers greater than or equal to JBD

QC.....condensation coefficient

ALPHA .....constant in *Equation* 2.88

ALPHAC.....thermal accommodation coefficient for carries gas interaction with water droplets

BETA .....Langmuir parameter

RHOL.....density of water, (kg/m^3)

CVRAT.....convergence ratio for DEL/CV

ARAT.....convergence ratio for *A'/A*

DT1 .....temperature step for PART 1, (K)

DT2 .....temperature step for PART 2, (K)

EPS.....convergence array:

1 - Newton Iteration to solve equation (57)

2 - newton iteration to solve equation (111)

***Table* 3.1: File Structure of CASEDATA.INPUT.**

T0	P0	DSTAR	HFUEL	TFEED
PHI1	RHC	RNO	JMIN	
NATOM	IOUT	SWPO	SWGO	SWEND
NA	DELX	XLAST		
XA(I)	RWA(I)	DELSTR(I)		

3 - pressure convergence in PART 1

4 - mass flux convergence in PART 1

5 - pressure convergence in PART 2

6 - newton iteration for T(J-1) in PART 3

7 - temperature convergence

8 - newton iteration for *X* as a function of A),

TC .....critical temperature of water, (K)

K.....Boltzmann constant, (J/molecule-K)

CAPR.....universal gas constant, (J/mol-K)

M1.....molecular mass of water, (kg/molecule)

W.....molecular weight table, (kg/mol)

DY.....estimates of standard deviation used for curve fitting the nozzle wall coordinates

The order and placement of these parameters are illustrated in *Table* 3.2 as the structure for CONST.INPUT file.

***Table* 3.2: File Structure of CONST.INPUT.**

IPLTRD	JSTOP	JDB	RHOL	
QC	ALPHA	ALPHAC	BETA	RHOL
CVRAT	ARAT	DT1	DT2	
(EPS(I), I=1,8)				
TC	K	CAPR	M1	
(W(I),I=1,10)				
(DY(I), I=1,10)				

PART 1 Procedures

PART 1 of FIRACON deals with setting the feed condition to the combustor, solving for the adiabatic flame temperature, determining the chemical composition of the combustion products at a stagnation temperature that allows for heat loss, and specific mass flow rate. The stagnation conditions in the combustor are defined by the hydrogen to carbon ratio, $\eta_{H,C}$; number of carbon atoms in a molecule of fuel, η; fuel equivalence ratio ϕ; feed temperatures of fuel, air, and oxygen: $\hat{T}_F$, $\hat{T}_{air}$, and $\hat{T}_{O_2}$; and pressure in combustion chamber, p_0. The specific enthalpies of fuel, oxygen, and nitrogen, $\hat{h}_F$, $\hat{h}_{O_2}$, and $\hat{h}_{N_2}$, are determined from the fuel and feed temperature. The mols of fuel, oxygen, and nitrogen per mass of the total mixture ($\hat{Y}_F$, $\hat{Y}_{O_2}$, and $\hat{Y}_{N_2}$), are determined by first solving for oxygen from *Equation* 2.17 and then solving for fuel and nitrogen from *Equations* 2.14 and 2.15. The total specific enthalpy is then determined from

$$\hat{h}_0 = Y_F h_F + Y_{O_2} h_{O_2} + Y_{N_2} h_{N_2} . \qquad (Eq.\ 3.1)$$

The next major task of PART 1 is solving for the chemical equilibrium composition and the corresponding flame temperature. The combustion products included ten species numbered from 1 to 10 in the following order: H_2O, CO_2 CO, O_2, H_2, N_2, H, O, OH, and NO. As listed in chapter 2, six reactions are considered with six corresponding equilibrium relations. The reactions and equilibrium relations are defined earlier by *Equations* 2.26 - 2.37 and recall that the temperature dependency of the equilibrium constants is given by the curve fits in the *Equation* 2.38.

Four elemental balance equations are needed to solve the equilibrium relations. They are given in *Equation* 2.39 to 2.42. The constants, Y_H, Y_O, Y_N, and Y_C are determined from the specification of elemental hydrogen-to-carbon ration, $\eta_{H,C}$, elemental nitrogen-to-oxygen ration, $\eta_{N,O}$, and the equivalence ratio, ϕ, from the expressions in *Equation* 2.8 to 2.11. The composition is initially solved for H_2O, CO_2, CO, O_2, and N_2 with $Y_5 = Y_7 = Y_8 = Y_9 = Y_{10} = 0$ by successive approximation of *Equations* 2.39 - 2.42 based on an assumed initial temperature as a first guess. Then, the species mol numbers and the mol number of the mixture are obtained from:

$$Y_1 = \frac{Y_{\mathrm{H}}}{2}. \qquad (Eq.\ 3.2)$$

$$Y_2 = a_{2,\mathrm{C}} Y_{\mathrm{C}}, \qquad (Eq.\ 3.3)$$

$$Y_3 = Y_C - Y_2, \qquad (Eq.\ 3.4)$$

$$Y_4 = \frac{Y_{\mathrm{O}} - Y_{\mathrm{C}} - Y_1 - Y_2}{2} \qquad (Eq.\ 3.5)$$

$$Y_6 = \frac{Y_{\mathrm{N}}}{2}, \text{ and} \qquad (Eq.\ 3.6)$$

$$Y = \frac{Y_{\mathrm{H}} + Y_{\mathrm{O}} + Y_{\mathrm{N}} + Y_{\mathrm{C}} - Y_1 - Y_2}{2}. \qquad (Eq.\ 3.7)$$

With the initial approximation for the five major species, the mole numbers are then recalculated by successive approximation method, with the mol number based on the equations that follow:

$$Y_3 = Y_2 \left(\frac{K_{p,2} Y}{Y4} \frac{p^0}{p} \right)^{1/2}, \qquad (Eq.\ 3.8)$$

$$Y_5 = \frac{Y_1 Y_3}{K_{p,1} Y_2}, \qquad (Eq.\ 3.9)$$

$$Y_{10} = \left(K_{p,6} Y_4 Y_6 \right)^{1/2}, \qquad (Eq.\ 3.10)$$

$$Y_6 = \frac{Y_N - Y_{10}}{2}, \qquad (Eq.\ 3.11)$$

$$Y_9 = \left(K_{p,3} Y_4 Y_5 \right)^{1/2}, \qquad (Eq.\ 3.12)$$

$$Y_7 = \left(K_{p,4} Y_5 \frac{p^0}{p} \right)^{1/2}, \qquad (Eq.\ 3.13)$$

$$Y_8 = \left(K_{p,5} Y_4 \frac{p^0}{p} \right)^{1/2}, \qquad (Eq.\ 3.14)$$

$$Y_1 = \frac{Y_{\mathrm{H}} - 2Y_5 - Y_7 - Y_9}{2}, \qquad (Eq.\ 3.15)$$

$$Y_2 = Y_C - Y_3, \qquad (Eq.\ 3.16)$$

and an equation for Y_4 of the form

$$Y_4 = \frac{\left[Y_4 + \frac{Y_O - Y_C - Y_1 - Y_2 - Y_8 - Y_9 - Y_{10}}{2} \right]}{2} \qquad (Eq.\ 3.17)$$

Used to damp numerical oscillations in the successive approximation technique at high temperatures. The total mixture mol number is given by

$$Y = \sum_{k=1}^{10} Y^k \,. \qquad (Eq.\ 3.18)$$

Once all ten species are solved for at a given temperature, then the specific enthalpy of the mixture is determined by *Equation* 2.49. The specific enthalpy of the mixture, h_G, is compared to the total feed enthalpy, $\hat{h}_0$. If the specific enthalpy of the mixture is greater than the total feed enthalpy, temperature is decreased. Correspondingly, temperature is increased when h_G is less than $\hat{h}_0$. The adiabatic flame temperature is obtained when $h_G = \hat{h}_0$.

The stagnation conditions in the combustor do not account for heat loss, but a user specified heat loss can be included in the flame temperature calculations if a stagnation temperature, T_0, that is less than the adiabatic flame temperature is inputted. With, T_0, the chemical composition is determined by the preceding scheme just described. The stagnation enthalpy, h_0, is determined by *Equation* 2.49 and the stagnation entropy, s_0, is determined from *Equation* 2.51.

The mass flow rate leaving the combustor chamber is determined first by assuming an equilibrium isentropic expansion to a choked throat condition. An approximate pressure, *p*', is determined from a select temperature difference, ΔT, that defines a new gas temperature, *T*. With a newly selected temperature, the chemical equilibrium composition is determined. The density of the flow is thus determined from the function *G*, defined as *Equation* 2.53 and used in *Equation* 2.52. Now with gas density, ρ_G, and the composition determined, pressure is computed from *Equation* 2.54. An iteration process of comparing *p* and *p'* continues till *p* is sufficiently close to *p'*, thus, the pressure is determined followed by the velocity from

$$U = \left[2\left(h_0 - h_G \right) \right]^{1/2} . \qquad (Eq.\ 3.19)$$

The mass flux, $\rho_G U$, is calculated at selected temperatures corresponding to successive locations along the nozzle. The maximum mass flux , $\rho_G^* U^*$, occurs at the nozzle throat where the nozzle's cross sectional area, A^*, is known. The mass flow rate is given as

$$\dot{m} = \rho_G^* U^* A^* . \qquad (Eq.\ 3.20)$$

The result is the calculated mass flow rate of total mixture at the throat of the nozzle.

PART 2 Procedures

PART 2 is an equilibrium calculation of the flow expanding in the nozzle from the throat to the maximum specified length input. The flow's expansion is assumed to be isentropic while remaining in chemical equilibrium with no liquid water formation. The nucleation rate is computed for each expansion step to determine when to begin PART 3.

With isentropic expansion, the entropy and enthalpy at each step is assume to be $s = s_0$ and $h_0 =$ constant along the nozzle. Given the throat temperature and pressure, T^* and p^*, a temperature T less than T^* is selected then pressure, p, is determine by iteration and the corresponding ρ_G, h_G, and U are computed using the same scheme as PART 1. The area of the nozzle corresponding to the new position at T less than T^* is computed from

$$A = \frac{\dot{m}}{\rho_G U} . \qquad (Eq.\ 3.21)$$

The location in the nozzle, x, is then determined from a scheme that relates the cross sectional area as a function of nozzle position, x.

The nucleation rate, J, is determined at each computation step in the nozzle from *Equation* 2.71 with the following *Equations* 2.46, 2.50, 2.65, 2.66, 2.67, and 2.68. J_{min} is designated in CASEDATA.INPUT as the minimal significant value of J, were droplet nucleation is assumed a priori to begin. The nucleation rate, J, is compared to J_{min} to determine the point in the nozzle expansion where the flow field data is stored to be used by the calculation procedures in PART 3 that predicts nucleation and droplet growths. For this study, the value of J_{min} is set at 10^{15}, suggested by Erickson, et al. [7].

PART 3 Procedures

PART 3 of FIRACON is responsible for calculating the flow field in the nozzle at, and downstream of, the initial station where significant nucleation is defined (by specifying J_{min}) to begin. The nucleation of groups of micro-droplets, the growth of these groups of micro-droplets by condensation, and the changes to the state of the gas flow are computed in PART 3. Note, except for the water vapor content of the flow, all other species are assumed to be fixed or frozen in composition from this station onward.

PART 3 begins with the flow field data stored by PART 2 of the program that corresponds to the nozzle station where J was first calculated to be equal to, or greater than, J_{min}. The numerical model or process by which PART 3 calculates the water vapor condensation, droplet nucleation and changes in the gas flow properties in the expansion are described briefly below.

The computation begins at the step $j = 1$ where the nucleation rate exceeded the minimal value, J_{min}. The computation proceeds by finding the flow properties at the following steps. First, the axial distance is represented as

$$x_{j+1} = x_j + \Delta x \qquad (Eq.\ 3.22)$$

and the corresponding nozzle area is obtain from the curve fit of the input nozzle contour,

$$A_{j+1} = f\left(x_{j+1}\right). \qquad (Eq.\ 3.23)$$

Solutions for all the properties at the $j + 1^{th}$ position are based on an iteration scheme by adjusting T_{j+1} as the primary variable with a secondary loop within. Temperature, pressure, and velocity at the $j + 1^{th}$ position are first set to be equal to the value at position j. As the iterations scheme proceeds, T_{j+1} is adjusted with $T'_{j+1} = T_{j+1}$ defined to test for convergence.

The calculation of the mean nucleation rate of new droplets is continued by Young's [48, 49] suggestion to vary J as $\exp(kx)$ in the form

$$\overline{J}_i = \frac{J_{j+1/2} - J_{j-1/2}}{\ln \dfrac{J_{j+1/2}}{J_{j-1/2}}} \qquad (Eq.\ 3.24)$$

where $J_{j+1/2}$ and $J_{j-1/2}$ are computed from *Equation* 2.71. The number of new droplets formed at the j^{th} position is solved for by

$$\Delta n^{i=j} = \frac{\overline{J}_j A_j \Delta x}{\dot{m}} \qquad (Eq.\ 3.25)$$

where the droplets size of this condensation group will change as the group moves downstream, but the number of drops in the group remain constant.

The condensing group of droplets diameter growth in size at each $j + 1^{th}$ positions is determined from *Equation* 2.82 if $z_j^i = \frac{r_j^i}{r_{*,j}} \geq 1.1$ for the group, or using *Equation* 2.89 if $z_j^i = r_j^i / r_{*,j} < 1.1$. The time interval in these two equations corresponds to the step size x defined as

$$\Delta t = \frac{2\Delta x}{U_j + U_{j+1}} \qquad (Eq.\ 3.26)$$

For a condensed group's droplet radius of $z_j^i = r_j^i / r_{*,j} \geq 1.1$, *Equation* 2.82 is rewritten as

$$F = Z_{j+1} - Z_j - \Lambda \Delta t \qquad (Eq.\ 3.27)$$

where

$$z_j = \frac{\theta^3}{\theta+1}\ln\left(z_j^i + \theta\right) + \left(\frac{1}{\theta+1} + \Omega\right)\ln\left(z_j^i - 1\right) \qquad (Eq.\ 3.28)$$
$$\left(\Omega + 1 - \theta\right) z_j^i + \tfrac{1}{2} z_j^{i^2}$$

The solution of the droplet radius is solved using a Newton iteration scheme in the form

$$\frac{dF}{dz_{j+1}^i} = \frac{\theta^3}{\left(\theta+1\right)\left(z_{j+1}^i + \theta\right)} + \frac{1 + \Omega\left(\theta+1\right)}{\left(\theta+1\right)\left(z_{j+1}^i - 1\right)} + z_{j+1}^i\left(\Omega + 1 - \theta\right) \qquad (Eq.\ 3.29)$$

so that the n^{th} iteration is

$$z_{j+1}^i\left(n+1\right) = z_{j+1}^i\left(n\right) - \frac{F\left(n\right)}{dF\left(n\right)/dz_{j+1}^i}. \qquad (Eq.\ 3.30)$$

Then, the droplet radius is solved for by

$$r_{j+1}^i = z_{j+1}^i r_{*,j}. \qquad (Eq.\ 3.31)$$

Young [47, 48] argued that the gaseous mixtures' properties between j^{th} and $j+1^{\text{th}}$ positions do not significantly change, so that r_{j+1}^{i} is computed with only knowledge of the properties at the j^{th} position.

For a droplet radius of $z_j^i = \frac{r_j^i}{r_{*,j}} < 1.1$, *Equation* 2.89 requires knowledge of $r_{*,j+1}$ and all properties of the j^{th} position with the following expression

$$\frac{dr_*}{dt} = \frac{r_{*,j+1} - r_{*,j}}{\Delta t}. \qquad (Eq.\ 3.32)$$

Young [48, 49] assumed the parameter ψ to be as given by *Equation* 2.90, and to be constant between the j^{th} and the $j+1^{\text{th}}$ position, but the solution of z_{j+1}^{i} from *Equation* 2.89 requires a knowledge of $r_{*,j+1}$, which is successively revised from $r_{*,j+1}$ using the revised values of T_{j+1}.

The mass of liquid water in each condensation group, per total mass of mixture, is expressed as

$$w_{j+1}^{i} = \tfrac{4}{3}\pi\rho_L \left(r_{j+1}^{i}\right)^3 \Delta n^i \qquad (Eq.\ 3.33)$$

for droplets of type i at the $j+1^{\text{th}}$ position, where the total mass of liquid water per total mass of mixture at the $j+1^{\text{th}}$ position is

$$w_{j+1} = \sum_{i=1}^{j+1} w_{j+1}^{i}. \qquad (Eq.\ 3.34)$$

Before enthalpy and entropy of the liquid water in the mixture is calculated, the temperature of the liquid water droplets of the i^{th} type, $T_{L,j+1}^{i}$, is determined from *Equation* 2.91. $T_{L,j+1}^{i}$ is then used in *Equation* 2.58 to obtain $h_{L,j+1}^{i}$ for the final calculation of the enthalpy of liquid water,

$$h_{L,j+1} = \sum_i w_{j+1}^{i} h_{L,j+1}^{i}. \qquad (Eq.\ 3.35)$$

Entropy of the liquid water is determined by first using *Equation* 2.63 to obtain $s_{L,j+1}^{i}$ and the determining the total entropy from

$$s_{L,j+1} = \sum_i w_{j+1}^{i} s_{L,j+1}^{i}. \qquad (Eq.\ 3.36)$$

The next step of PART 3 is to compute the entropy increase from the formation of liquid by replacing *ds* by Δs_j and *dw* by Δw_j where

$$\Delta w_j = w_{j+1} - w_j \qquad (Eq.\ 3.37)$$

in *Equation* 2.93. Temperature and pressure used in *Equation* 2.93 are defined as

$$T_G = \frac{T_{G,j+1} + T_{G,j}}{2}, \text{ and} \qquad (Eq.3.38)$$

$$p = \frac{p_{j+1} + p_j}{2}. \qquad (Eq.\ 3.39)$$

L is evaluated at $T_s(p_1)$ and $c_{p,1}$ is evaluated at T_G. Therefore, the entropy production was expressed as

$$s_{j+1} = s_j + \Delta s_j. \qquad (Eq.\ 3.40)$$

The temperature of the gas, T_G, is solved by an iteration scheme attempting to find a value of $T_{G,j+1}$ satisfying the independent computation of $s_{G,j+1}$. In addition, $\rho_{G,j+1}$ is determined from another iteration scheme using the known flow area at $j + 1^{th}$ position. For further details, refer to the Erickson, *et. al.*, [7] report.

Chapter 4

Development of Test Matrix

In order to carry out the study of the effects of fuel type, equivalence ratio, and chamber pressure on the beginning of nucleation and condensation in combustion driven, supersonic nozzle flow, some representative cases had to be defined in order to make the necessary comparisons. These cases were defined to include representative, nominal, or typical types of fuel used in vitiated-heated wind tunnels and other representative blow-down facilities. In addition, equivalence ratios and chamber pressures were selected that would give reasonably high stagnation temperatures and pressure, also representative of real test facility operations. *Tables* 4.1 lists the chamber pressure and equivalence ratios selected for the Methane fuel cases to be discussed. The chamber pressures and equivalence ratios in this table are representative for the Propane, Butane, and Iso-Butane cases studied in addition. The Methane is abbreviated as METH followed by a sequence of numbers with the second number representing the set of five initial pressures, and the third for the four sets of equivalence ratios chosen.

Reasons for Case Selections

Four equivalence ratios ϕ of 0.6, 0.7, 0.8, and 0.9 were chosen for two reasons. One, the different equivalence ratio resulted in different chamber temperatures in the combustor, so that the results can be compared to different initial temperatures. Second, the different equivalence ratio also resulted in different concentrations of combustion product species to be compared to the nucleation and condensation in the expanding flow, especially the water vapor species. Five sets of chamber pressures were selected to represent the various operation conditions, so that the results could be correlated to the chamber pressure.

Calculated Results Presentations

The results of the study can be found in the appendixes of this paper. Ten different plots are presented for the different characteristics of the flow where ‘distance’ refers to

***Table 4.1*: Cases Selected for Discussion**

Case Designation	T_0 (K)	P_0 (N/m^2)	ϕ
METH 1.1.1	1560	6.8948E+05	0.6
METH 1.1.2	1740	6.8948E+05	0.7
METH 1.1.3	1900	6.8948E+05	0.8
METH 1.1.4	2050	6.8948E+05	0.9
METH 1.2.1	1560	1.3790E+06	0.6
METH 1.2.2	1740	1.3790E+06	0.7
METH 1.2.3	1900	1.3790E+06	0.8
METH 1.2.4	2050	1.3790E+06	0.9
METH 1.3.1	1560	2.0684E+06	0.6
METH 1.3.2	1740	2.0684E+06	0.7
METH 1.3.3	1900	2.0684E+06	0.8
METH 1.3.4	2050	2.0684E+06	0.9
METH 1.4.1	1560	2.7579E+06	0.6
METH 1.4.2	1740	2.7579E+06	0.7
METH 1.4.3	1900	2.7579E+06	0.8
METH 1.4.4	2050	2.7579E+06	0.9
METH 1.5.1	1560	3.4474E+06	0.6
METH 1.5.2	1740	3.4474E+06	0.7
METH 1.5.3	1900	3.4474E+06	0.8
METH 1.5.4	2050	3.4474E+06	0.9

Note: Methane (CH_4) is represented as METH.

axial distance downstream of the nozzle throat plane. All of these eleven plot sets are listed below with the preceding letter indicating in which appendix they appear:

A.) the nucleation rate vs. distance,

B.) critical droplet radius vs. distance,

C.) the mass fraction of water to the total flow mixture vs. distance,

D.) mixture velocity vs. distance,

E.) Mach number vs. distance,

F.) mixture static temperature vs. distance,

G.) mixture stagnation temperature vs. distance,

H.) mixture static pressure vs. distance,

I.) mixture stagnation pressure vs. distance, and

J.) water vapor saturation pressure vs. distance.

Although the droplet temperatures are calculated by FIRACON, they are not presented in this thesis. The data just described are plotted along the axial location in the nozzle, starting from the throat to the end of the nozzle. The plots, excluding pressure and stagnation pressure, are grouped together for each initial chamber pressures. The two pressures sets are grouped with the same equivalence ratios. This is for aesthetic reasons, so the comparisons of different chamber pressure are not overlapping each other. The results of PART 2 of FIRACON are plotted showing the corresponding expansions without condensation. The nucleation rates plotted in *Figures* A-1 through A-5 corresponds to values for supersaturated flow all the way to the nozzle exit without liquid water condensations. PART 3 is plotted with a heavier weighted line over the results of PART 2, representing flow calculations with water vapor droplet nucleation and liquid water condensation induced changes to the expanding flow.

All the test cases were applied to the dimensions of NASA Langley 8-Foot, High Temperature Tunnel (8-Ft HTT). According to NASA Langley web page (http://wte.larc.nasa.gov), the tunnel is a combustion-heated hypersonic blow down-to-atmosphere wind tunnel. Flight simulations are possible for ranges of Mach numbers from four through seven, with altitude ranges of 50,000 to 120,000ft. The test section is 8ft in diameter and 12ft long. The Langley 8-Ft HTT is used to test large models

including air-breathing hypersonic propulsion systems, and structural and thermal systems. As of now, stable wind tunnel test conditions are limited to 60 seconds. The typical flow medium is pressurized combustion products of methane and air. The flow is enriched with additional oxygen for air-breathing propulsion tests.

Difficulties with Some Calculated Cases

Not all the cases from the test matrix listed in *Table* 4.1 are represented in the *Figures* A though J (appendixes A through J). The cases METH 1.1.4, and METH 1.3.4 are not because FIRACON failed in PART 1 to complete the calculations for the combustion chamber conditions. On the other hand, the METH 1.2.4, METH 1.4.4, and METH 1.5.4 cases did not result in significant nucleation or condensation, so they are not plotted in *Figures* C (Appendix C) and *Figures* D, (Appendix D), but their calculated results from PART 2 are shown in the rest of the figures.

The illustrated results of PART 2 show very smooth lines, which is to be expected for an isentropic, one-dimension expansion of the flow, but some of the computed cases in PART 3 illustrate numerical instability in the calculations. In addition, PART 3 failed to complete calculations in all cases because of the lack of convergence in the calculation of the entropy change in the flow caused by the formation of the liquid water drops. This can be seen by the prematurely terminated lines of the results for PART 3 in all the figures. The instability of PART 3 of FIRACON may be due to the degree of numerical precision inherent in 32 bit desktop computers. FIRACON is written by Erickson, *et al*. [7] to run on a NASA Langley mainframe computer with much greater numerical precision. In the present study, the code was converted and recompiled to run on a desktop computer. Some of the equations had to be broken down into pieces in order for the FORTRAN compiler to work. Compiling in double precision was also attempted. Never the less, as described above some numerical instability were observed in the output of several of the cases run, and all cases failed to complete.

In the present study, the most important parameter or results are the axial locations where the computed nucleation rate exceeded the minimal rate defined as the value where condensation begins. The locations in the nozzle where condensation begins were

calculated in the completely functioning PART 2 of FIRACON. The premature terminated lines from the results of PART 3 begin to illustrate the changes in the flow properties, compared to single-phase isentropic isentropic expansion, due to water vapor condensation in the nozzle.

Chapter 5

Results and Discussions

The approach taken to review, analyze, and discuss the results of the study is to consider the plotted results shown in *Figures* A-1 through J-5, presented in the appendixes A through J. Not all of the figures and tables contained in the appendixes will be discussed, since many of these figures show results very similar to previous figures to be analyzed and discussed in this chapter.

Fuel

Results for vitiated combustion of three other fuels, Propane, Butane, and Iso-Butane, were attained in addition by FIRACON. The input conditions, chamber pressure and equivalence ratio listed in *Table* 4.1 for Methane, were the same applied to these three fuels. The only difference in the initial conditions was the total temperatures in the chamber. FIRACON determines the chambers total temperature by calculating the adiabatic flame temperature then deducts an assumed fixed heat loss. A second comparison was done between Methane and Propane with the same initial total pressure, equivalence ratio, and total temperature. The relative differences among the calculated flow properties results along the nozzle between Methane and Propane calculated flow properties only ranged between 0.0 and 0.3%. This insignificant difference suggest the water vapor nucleation rate, condensation, and sub sequential changes in the isentropic flow expansion are not considerably change by the resulting combustion by products composition for a given fuel, but by the resulting chamber temperature. Therefore, only the results for the Methane cases are presented for discussion.

Nucleation Rate at the Initiation of Nucleation and Droplet Growth

Figures A-1 through A-5, Appendix A, display the nucleation rates as a function of axial distance, for methane driven combustion products in the supersonic expansions. The effects of equivalence ratio on nucleation rate are seen for each of the five chamber stagnation pressures chosen. Generally for a given chamber stagnation pressure, nucleation begins earlier, or further upstream, with the lowest equivalence ratio. This is

because the lowest combustion driven chamber temperature occurs at the lowest equivalence ratio, with succeeding higher chamber temperatures at higher equivalence ratios.

The effect of each stagnation pressure is just the opposite. The higher the stagnation chamber pressure, the further upstream (toward the nozzle throat) the initiation of the nucleation and condensation process begins.

In order to more clearly show the characteristics of the supersonic expansions with condensation, a series of tables is presented containing data extracted from the calculations. The first table is *Table* 5.1 where values for the droplet nucleation rate, *J*, are listed for two axial positions in the nozzle. The first listed value of *J* is labeled at axial position 2. This is the point where the results of the FIRACON program indicate the beginning of significant water droplet formation. Position 3 is downstream of position 2; position 2 is the axial position where the nucleation rate reaches the value equal to the input, arbitrary J_{min} value, which triggers the initiation of the nucleation calculation process in FIRACON. The next value of *J* tabulated for each case in *Table* 5.1 is position 3; where the nucleation and condensation process begins to significantly change the flow field parameters such as Mach number, velocity, static pressure and temperature, and so forth. The nucleation rates indicated in the table thus represent critical values illustrative of the process of a water vapor condensation and droplet nucleation in a combustion-driven or vitiated air, supersonic and hypersonic wind tunnels, over a wide range of combustion stoichiometries and chamber pressures.

Critical Droplet Radius at the Initiation of Nucleation and Droplet Growth

Figures B-1 through B-5, Appendix B, show the predicted values of the critical droplet radius given by *Equation* 2.69 as a function of axial distance for the selected equivalence ratios and chamber pressure for Methane. The critical droplet radius has no meaning until saturation is reached; hence the distributions plotted show the critical droplet radius as zero up to the point of saturation in the nozzle. Interestingly, the largest critical radius is predicted at the respective saturation points for each equivalence ratio and for each chamber pressures. Note, also that once nucleation is initiated, the radius of

***Table* 5.1: Nucleation Rate at Two Significant Events.**

	Position 2		Position 3	
Case Designation	***x* (m)**	***J***	***x* (m)**	***J***
METH 1.1.1	5.69	3.76E+15	6.84	7.29E+19
METH 1.1.2	8.06	3.30E+15	10.41	2.69E+19
METH 1.1.3	12.59	1.46E+15	N/C	N/C
METH 1.1.4	N/D	N/D	N/D	N/D
METH 1.2.1	5.34	1.74E+16	5.99	5.21E+19
METH 1.2.2	7.35	3.61E+15	8.80	2.30E+19
METH 1.2.3	10.74	2.06E+15	13.99	3.65E+18
METH 1.2.4	N/SN	N/SN	N/SN	N/SN
METH 1.3.1	5.08	7.57E+15	5.63	5.21E+19
METH 1.3.2	6.97	3.52E+15	8.12	1.21E+19
METH 1.3.3	9.92	2.01E+15	12.02	5.29E+18
METH 1.3.4	N/D	N/D	N/D	N/D
METH 1.4.1	4.91	6.43E+15	5.41	6.58E+18
METH 1.4.2	6.76	7.51E+15	7.61	9.26E+18
METH 1.4.3	9.47	2.84E+15	11.12	6.49E+18
METH 1.4.4	N/SN	N/SN	N/SN	N/SN
METH 1.5.1	4.83	2.35E+16	5.18	3.37E+18
METH 1.5.2	6.57	6.93E+15	7.27	4.37E+18
METH 1.5.3	9.09	2.20E+15	10.59	7.39E+18
METH 1.5.4	N/SN	N/SN	N/SN	N/SN

Note: Position 2 represents the point where nucleation and condensation effects are beginning to be considered in the flow, and position 3 represent the point where the effects of the formation of water droplets begin to significantly change the flow properties. Nucleation Rate is represented as J, and the position in the nozzle as x. N/D indicates FIRACON's failure to complete calculations, N/SN indicates no significant nucleation, and N/C indicates no changes to the flow properties

the droplets begin to grow rapidly from their value at the initiation of nucleation (which equals the critical radius at that point). Also of interest are the sizes of the critical radii. At the initiation of nucleation the critical radii are of the order 3 to 5×10^{-10}m, or about, roughly, ½ nanometer. These are very small particles of liquid water. *Figures* B-6 through B-10 show the same results for the Propane cases.

Another key piece of information about the water vapor condensation process in computed cases are the values of the droplet critical radii at position 2 and 3 contained in *Table* 5.2. The droplet critical radii represent the probable radii of the initial stable droplet nuclei produced in the condensation process, as required by the quasi-equilibrium theory of nucleation. The magnitudes of these radii are of the order, as previously discussed, of about ½ nanometer. These radii can be compared to the radii of rust and dust or mote particles in wind tunnel flow when such data becomes available. Such a comparison will improve understanding of which mode of nucleation prevails in a given wind tunnel, homogenous nucleation or heterogeneous nucleation.

Mass Fraction of Condensed Liquid Water in the Mixture Expansion

Figure C-1 through C-5, Appendix C, show the mass fraction of condensed liquid water in the supersonically expanding mixture of combustion products as it flows through the nozzle, for Methane driven combustion. The liquid mixture fraction rises from zero at the point of nucleation and the initiation of condensation, to roughly 0.1 to 1.0 percent of the total mixture, at the termination of the calculations, depending, of course, on the particular equivalence ratio and chamber pressure of each case. The rapid rise of the formation of liquid water species indicates how rapidly condensation can deplete the mixture of the combustion product's water vapor to produce a condensed phase in the flow. Since gas or mixture velocities are of the order of 1800 – 2000m/s in the nozzle flow where condensation is occurring (see Appendix E), and condensation distances are of the order of a few meters, say 2m, the times for the condensation of the liquid water in the nozzle in expansions are of the order of

$$\tau_{condensation} \approx \frac{2\text{m}}{2000\,\text{m/s}} = 1\times10^{-3}\,\text{seconds}. \qquad (Eq\ 5.1)$$

***Table* 5.2: Critical Droplet Radius at Two Significant Events**.

	Position 2		Position 3	
Case Designation	***x* (m)**	***r** (m)**	***x* (m)**	***r** (m)**
METH 1.1.1	5.69	4.16E-10	6.84	2.79E-10
METH 1.1.2	8.06	4.00E-10	10.41	2.74E-10
METH 1.1.3	12.59	3.94E-10	N/C	N/C
METH 1.1.4	N/D	N/D	N/D	N/D
METH 1.2.1	5.34	4.28E-10	5.99	3.21E-10
METH 1.2.2	7.35	4.28E-10	8.80	3.11E-10
METH 1.2.3	10.74	4.18E-10	13.99	3.23E-10
METH 1.2.4	N/SN	N/SN	N/SN	N/SN
METH 1.3.1	5.08	4.56E-10	5.63	3.42E-10
METH 1.3.2	6.97	4.45E-10	8.12	3.40E-10
METH 1.3.3	9.92	4.36E-10	12.02	3.37E-10
METH 1.3.4	N/D	N/D	N/D	N/D
METH 1.4.1	4.91	4.71E-10	5.41	3.84E-10
METH 1.4.2	6.76	4.50E-10	7.61	3.59E-10
METH 1.4.3	9.47	4.44E-10	11.12	3.48E-10
METH 1.4.4	N/SN	N/SN	N/SN	N/SN
METH 1.5.1	4.83	4.67E-10	5.18	4.04E-10
METH 1.5.2	6.57	4.61E-10	7.27	3.80E-10
METH 1.5.3	9.09	4.57E-10	10.59	3.56E-10
METH 1.5.4	N/SN	N/SN	N/SN	N/SN

Note: Position 2 represents the point where nucleation and condensation effects are beginning to be considered in the flow, and position 3 represent the point where the effects of the formation of water droplets begin to significantly change the flow properties. Critical Droplet Radius is represented as r^*, and the position in the nozzle as x. N/D indicates FIRACON's failure to complete calculations, N/SN indicates no significant nucleation, and N/C indicates no changes to the flow properties

Thus, condensation starts and is significantly accomplished in only a few milliseconds.

Mixture Velocity and Mach Number Distributions in the Calculated Nozzle Flows

Figure D-1 through D-5, Appendix D, and *Figure* E-1 through E-5, Appendix E, show the velocities and Mach numbers, respectively, of the expanding flow of vitiated air from the combustion of methane and air along the nozzle from the throat to the exit. As stated in chapter two, the velocities of the water droplets formed are considered to be the same velocity as the expanding mixture. So, the plotted results represent the mixture of the water droplets and the combustion products forming a carrier gas.

As to be expected for a normal operation of a converging-diverging nozzle, the velocity and Mach number increase from the throat to the end of nozzle. The velocity increases rapidly just downstream of the throat and then reaches a point about midway through the nozzle where velocity and Mach number increase gradually. For the cases where nucleation and condensation occurs in the nozzle, the gas velocity increases and the Mach number decreases, due to the heat released by the condensation process. The decreases shown in Mach number are much greater than the slight increases in velocity.

The effects of the initial chamber pressure, equivalence ratio, and subsequent chamber temperatures are the same as stated earlier for each test case. In order to provide precise data on when the nucleation and condensation process begins, and when it begins to change the flow properties from their isentropic expansion values, *Table* 5.3 provides tabulated values of velocity at three axial positions, positions 1, 2, and 3. These are the same axial position explained previously with the addition of position 1 indicating the point where the flow becomes saturated. Again, the purpose of providing this data is to clarify the condition in the vitiated Mach 8 wind tunnel nozzle flows where the process of nucleation and condensation of water vapor begin to have important effect on the quality and quantities of the flow variables.

Table 5.4 provides the tabulated values of Mach number, corresponding to the velocity values at position 1, 2, and 3. As the data indicates, in a Mach 8 nozzle expansion for typical vitiated chamber condition and pressures the water vapor

***Table* 5.3: Velocity at Three Significant Events.**

	Position 1		Position 2		Position 3	
Case Designation	***x* (m)**	***U* (m/s^2)**	***x* (m)**	***U* (m/s^2)**	***x* (m)**	***U* (m/s^2)**
METH 1.1.1	4.29	1794.0	5.69	1818.3	6.84	1833.2
METH 1.1.2	5.68	1943.0	8.06	1967.0	10.41	1978.7
METH 1.1.3	7.53	2074.0	12.59	2096.5	N/C	
METH 1.1.4	N/D	N/D	N/D	N/D	N/D	N/D
METH 1.2.1	4.05	1788.0	5.34	1813.1	5.99	1824.3
METH 1.2.2	5.33	1937.3	7.35	1961.4	8.80	1974.5
METH 1.2.3	7.03	2068.8	10.74	2091.3	13.99	2098.8
METH 1.2.4	9.66	2190.8	N/SN	N/SN	N/SN	N/SN
METH 1.3.1	3.93	1785.0	5.08	1808.7	5.63	1817.4
METH 1.3.2	5.17	1934.4	6.97	1957.9	8.12	1976.8
METH 1.3.3	6.79	2066.1	9.92	2087.9	12.02	2094.9
METH 1.3.4	N/D	N/D	N/D	N/D	N/D	N/D
METH 1.4.1	3.82	1782.0	4.91	1805.8	5.41	1834.3
METH 1.4.2	5.10	1933.0	6.76	1955.8	7.61	1973.0
METH 1.4.3	6.60	2063.9	9.47	2085.7	11.12	2092.3
METH 1.4.4	8.85	2185.2	N/SN	N/SN	N/SN	N/SN
METH 1.5.1	3.72	1779.0	4.83	1804.3	5.18	1830.9
METH 1.5.2	4.95	1930.1	6.57	1953.7	7.27	1972.0
METH 1.5.3	6.44	2061.8	9.09	2083.7	10.59	2092.8
METH 1.5.4	8.71	2190.2	N/SN	N/SN	N/SN	N/SN

Note: Position 1 represents the point where the flow becomes saturated, position 2 represents the point where nucleation and condensation effects are beginning to be considered in the flow, and position 3 represent the point where the effects of the formation of water droplets begin to significantly change the flow properties. Velocity is represented as *U*, and the position in the nozzle as *x*. N/D indicates FIRACON's failure to complete calculations, N/SN indicates no significant nucleation, and N/C indicates no changes to the flow properties

***Table* 5.4: Mach number at Three Significant Events**.

	Position 1		Position 2		Position 3	
Case Designation	**x (m)**	**M**	**x (m)**	**M**	**x (m)**	**M**
METH 1.1.1	4.29	5.81	5.69	6.48	6.84	6.92
METH 1.1.2	5.68	6.33	8.06	7.10	10.41	7.55
METH 1.1.3	7.53	6.81	12.59	7.64	N/C	N/C
METH 1.1.4	N/D	N/D	N/D	N/D	N/D	N/D
METH 1.2.1	4.05	5.67	5.34	6.33	5.99	6.61
METH 1.2.2	5.33	6.18	7.35	6.91	8.80	7.25
METH 1.2.3	7.03	6.67	10.74	7.44	13.99	7.72
METH 1.2.4	9.66	7.12	N/SN	N/SN	N/SN	N/SN
METH 1.3.1	3.93	5.61	5.08	6.20	5.63	6.45
METH 1.3.2	5.17	6.11	6.97	6.79	8.12	7.10
METH 1.3.3	6.79	6.59	9.92	7.32	12.02	7.58
METH 1.3.4	N/D	N/D	N/D	N/D	N/D	N/D
METH 1.4.1	3.82	5.55	4.91	6.12	5.41	6.37
METH 1.4.2	5.10	6.08	6.76	6.73	7.61	6.98
METH 1.4.3	6.60	6.53	9.47	7.24	11.12	7.48
METH 1.4.4	8.85	6.97	N/SN	N/SN	N/SN	N/SN
METH 1.5.1	3.72	5.48	4.83	6.08	5.18	6.28
METH 1.5.2	4.95	6.01	6.57	6.66	7.27	6.88
METH 1.5.3	6.44	6.48	9.09	7.17	10.59	7.41
METH 1.5.4	8.71	6.94	N/SN	N/SN	N/SN	N/SN

Note: Position 1 represents the point where the flow becomes saturated, position 2 represents the point where nucleation and condensation effects are beginning to be considered in the flow, and position 3 represent the point where the effects of the formation of water droplets begin to significantly change the flow properties. Mach number is represented as *M*, and the position in the nozzle as *x*. N/D indicates FIRACON's failure to complete calculations, N/SN indicates no significant nucleation, and N/C indicates no changes to the flow properties.

condensation process beings to affect flow variables in the Mach number ranges from 5 to 7. Refer to *Table* 5.4 for details.

Mixture Static Temperature and Pressure Distributions Along the Nozzle

Figures F-1 through F-5, Appendix F, plot the static temperature for the overall flow of the expanding gas in the nozzle for the methane cases. The static pressure distribution along the nozzle is illustrated in *Figures* H-1 and H-5, Appendix H, for the methane driven combustion cases. Both static temperature and pressure decrease for the isentropic expansion of the mixture, but at the point where the formation of water droplets by nucleation and condensation, the static temperature and pressure both increase. The relative change in magnitude of temperature is much greater than the relative change in pressure. Also, the change in temperature in the nozzle happens at a faster rate than the increase in static pressure.

To clarify the nature of the conditions where condensation effects on flow quality become important, *Tables* 5.5 and 5.6 have been prepared and are shown. *Table* 5.5 provides the tabulated values of mixture static temperature at positions 1, 2, and 3. As indicated, condensation begins to be important at relatively low static temperatures. Table 5.6 shows the corresponding data for static pressures.

Mixture Stagnation Temperature Distribution Along the Nozzle

As shown in *Figures* G-5 through G-5, Appendix G, for the expanding products of the combustion of methane and vitiated air, the stagnation temperature along the nozzle experiences a brief drop just past the throat and then rises quickly in a short distance. This effect is due to the equilibrium chemistry of the exhaust products wherein the heat of dissociation of some of the chemical species is recovered as these species recombine. After the increase, the stagnation temperature remains constant or slightly decreasing along the nozzle for the rest of the expanding isentropic flow. For cases with calculated condensation of the water vapor, the stagnation temperature abruptly increases where condensation becomes significant. As observed earlier, the higher the chamber pressure, the sooner, or closer to the throat, the effects of nucleation and condensation of water

***Table* 5.5: Static Temperature at Three Significant Events**.

	Position 1		Position 2		Position 3	
Case Designation	***x* (m)**	***T* (K)**	***x* (m)**	***T* (K)**	***x* (m)**	***T* (K)**
METH 1.1.1	4.29	242.0	5.69	199.6	6.84	178.2
METH 1.1.2	5.68	238.0	8.06	193.6	10.41	173.4
METH 1.1.3	7.53	233.3	12.59	189.6	N/C	N/C
METH 1.1.4	N/D	N/D	N/D	N/D	N/D	N/D
METH 1.2.1	4.05	252.0	5.34	208.2	5.99	193.3
METH 1.2.2	5.33	248.0	7.35	203.5	8.80	187.1
METH 1.2.3	7.03	242.3	10.74	198.8	13.99	185.9
METH 1.2.4	9.66	237.4	N/SN	N/SN	N/SN	N/SN
METH 1.3.1	3.93	257.0	5.08	215.6	5.63	201.3
METH 1.3.2	5.17	253.0	6.97	209.6	8.12	196.0
METH 1.3.3	6.79	247.0	9.92	204.7	12.02	192.1
METH 1.3.4	N/D	N/D	N/D	N/D	N/D	N/D
METH 1.4.1	3.82	262.0	4.91	220.5	5.41	210.1
METH 1.4.2	5.10	255.5	6.76	213.3	7.61	202.0
METH 1.4.3	6.60	251.0	9.47	208.7	11.12	196.7
METH 1.4.4	8.85	246.3	N/SN	N/SN	N/SN	N/SN
METH 1.5.1	3.72	267.0	4.83	223.0	5.18	215.6
METH 1.5.2	4.95	260.5	6.57	217.0	7.27	207.4
METH 1.5.3	6.44	254.8	9.09	212.4	10.59	200.4
METH 1.5.4	8.71	249.8	N/SN	N/SN	N/SN	N/SN

Note: Position 1 represents the point where the flow becomes saturated, position 2 represents the point where nucleation and condensation effects are beginning to be considered in the flow, and position 3 represent the point where the effects of the formation of water droplets begin to significantly change the flow properties. Static Temperature is represented as *T*, and the position in the nozzle as *x*. N/D indicates FIRACON's failure to complete calculations, N/SN indicates no significant nucleation, and N/C indicates no changes to the flow properties

***Table* 5.6: Static Pressure at Three Significant Events**.

	Position 1		Position 2		Position 3	
Case Designation	***x* (m)**	***P* (N/m^2)**	***x* (m)**	**P (N/m^2)**	***x* (m)**	***P* (N/m^2)**
METH 1.1.1	4.29	430.4	5.69	215.5	6.84	142.7
METH 1.1.2	5.68	228.6	8.06	108.7	10.41	72.5
METH 1.1.3	7.53	130.1	12.59	61.5	N/C	N/C
METH 1.1.4	N/D	N/D	N/D	N/D	N/D	N/D
METH 1.2.1	4.05	996.4	5.34	501.4	5.99	382.5
METH 1.2.2	5.33	530.9	7.35	260.0	8.80	187.8
METH 1.2.3	7.03	299.0	10.74	146.2	13.99	113.6
METH 1.2.4	9.66	177.7	N/SN	N/SN	N/SN	N/SN
METH 1.3.1	3.93	1604.4	5.08	852.2	5.63	665.5
METH 1.3.2	5.17	856.3	6.97	434.2	8.12	325.4
METH 1.3.3	6.79	481.8	9.92	243.9	12.02	193.1
METH 1.3.4	N/D	N/D	N/D	N/D	N/D	N/D
METH 1.4.1	3.82	2293.5	4.91	1232.1	5.41	979.5
METH 1.4.2	5.10	1183.5	6.76	616.6	7.61	488.1
METH 1.4.3	6.60	681.4	9.47	348.7	11.12	280.6
METH 1.4.4	8.85	408.1	N/SN	N/SN	N/SN	N/SN
METH 1.5.1	3.72	3069.6	4.83	1602.8	5.18	1354.5
METH 1.5.2	4.95	1587.3	6.57	820.0	7.27	668.4
METH 1.5.3	6.44	899.3	9.09	464.7	10.59	372.8
METH 1.5.4	8.71	524.4	N/SN	N/SN	N/SN	N/SN

Note: Position 1 represents the point where the flow becomes saturated, position 2 represents the point where nucleation and condensation effects are beginning to be considered in the flow, and position 3 represent the point where the effects of the formation of water droplets begin to significantly change the flow properties. Saturation Pressure Ratio is represented as P_{bar}, and the position in the nozzle as x. N/D indicates FIRACON's failure to complete calculations, N/SN indicates no significant nucleation, and N/C indicates no changes to the flow properties.

vapor begin to increase the stagnation temperature. With higher chamber temperatures, corresponding to larger equivalence ratios, the effects of the formation of the liquid water droplets causes changes later in the flow, or further past the throat.

Stagnation Pressure Distribution Along the Nozzle

The stagnation pressure distribution along the nozzle for the Methane cases are shown in Appendix I in *Figures* I-1 through I-4 grouped together by equivalence ratios. The stagnation pressure continues to increase from nozzle's throat to the nozzle's exit plane for the equilibrium isentropic expansions, but for cases with condensation, at the point when nucleation and condensation begin to affect the flow properties, the stagnation pressure abruptly drops off. Comparing *Figures* I-1 through I-4 for each equivalence ratio, it can be seen that the higher the chamber pressure the sooner stagnation pressure will experience a dramatic drop from the presence of condensed water vapor in the flow. Comparing the equivalence ratios shows that for a higher equivalence ratio, the later or further from the nozzle the stagnation pressure drop off occurs.

Saturation Pressure Ratio Distributions Along the Nozzle

Figure J-1 through J-5 in Appendix J plot the saturation pressure ratio of the expanding flow. The flow becomes supersaturated sooner or closer to the throat for lower equivalence ratios and, the flow becomes supersaturated faster for higher chamber pressures. The saturation pressure ratio is defined as the ratio of partial pressure of the water vapor in the gas mixture to the saturation pressure of water at the gas temperature. Mathematically,

$$\overline{P} = \frac{x_{\mathrm{wv}} P_{\mathrm{gas}}}{P_{\mathrm{sat}}(T_{gas})} \qquad (Eq.\ 5.2)$$

where x_{wv} is the mole fraction of the water vapor, P_{gas} is the mixture static pressure, and P_{sat} is the water saturation pressure at the gas mixture temperature, T_{gas}. From *Figures* J-1 to J-5 , values of $\overline{\mathrm{P}}$ have been extracted at three axial positions: the axial position where the flow first saturates; the position where condensation first begins to be observed at some significant degree; and the position where the condensation begins to have a

significant affect on the flow properties. The values of $\overline{P}$ at these locations are tabulated in *Table* 5.7.

***Table* 5.7: Saturation Pressure Ratio at Three Significant Events**.

	Position 1		Position 2		Position 3	
Case Designation	***x* (m)**	**P_{bar}**	***x* (m)**	**P_{bar}**	***x* (m)**	**P_{bar}**
METH 1.1.1	4.29	1.00	5.69	79.73	6.84	1716.9
METH 1.1.2	5.68	1.00	8.06	112.90	10.41	2529.7
METH 1.1.3	7.53	1.00	12.59	136.33	N/C	N/C
METH 1.1.4	N/D	N/D	N/D	N/D	N/D	N/D
METH 1.2.1	4.05	1.00	5.34	56.75	5.99	360.59
METH 1.2.2	5.33	1.00	7.35	64.18	8.80	552.80
METH 1.2.3	7.03	1.00	10.74	79.43	13.99	466.49
METH 1.2.4	9.66	1.00	N/SN	N/SN	N/SN	N/SN
		1.00				
METH 1.3.1	3.93	1.00	5.08	37.80	5.63	193.99
METH 1.3.2	5.17	1.00	6.97	47.07	8.12	238.24
METH 1.3.3	6.79	1.00	9.92	57.64	12.02	287.85
METH 1.3.4	N/D	N/D	N/D	N/D	N/D	N/D
METH 1.4.1	3.82	1.00	4.91	30.48	5.41	86.32
METH 1.4.2	5.10	1.00	6.76	41.78	7.61	149.24
METH 1.4.3	6.60	1.00	9.47	48.57	11.12	206.96
METH 1.4.4	8.85	1.00	N/SN	N/SN	N/SN	N/SN
METH 1.5.1	3.72	1.00	4.83	29.88	5.18	60.19
METH 1.5.2	4.95	1.00	6.57	35.34	7.27	97.18
METH 1.5.3	6.44	1.00	9.09	40.23	10.59	162.10
METH 1.5.4	8.71	1.00	N/SN	N/SN	N/SN	N/SN

Note: Position 1 represents the point where the flow becomes saturated, position 2 represents the point where nucleation and condensation effects are beginning to be considered in the flow, and position 3 represent the point where the effects of the formation of water droplets begin to significantly change the flow properties. Saturation Pressure Ratio is represented as P_{bar}, and the position in the nozzle as x. N/D indicates FIRACON's failure to complete calculations, N/SN indicates no significant nucleation, and N/C indicates no changes to the flow properties.

Chapter 6

Conclusions

Many theories describing water vapor nucleation with resulting condensation exist, although none has yet to be conclusively studied and applied successfully to supersonic or hypersonic wind tunnels to investigate methods of alleviating flow degradation. The engineers at NASA Langley attempted by developing the FIRACON code to model water vapor condensation and its effect on their hypersonic test facility. FIRACON is a scale dependent model using homogenous nucleation theory representing a finite nucleation rate of water vapor condensing in an expanding flow of vitiated combustion products supplemented by the addition of oxygen to simulate true atmospheric conditions.

The purpose of this study was to use FIRACON to examine the possible effects of fuel type, equivalence ratio, and chamber pressure on the predicted initial beginning locations of water vapor condensation in a hypersonic wind tunnel like the Langely's eight-foot high heated wind tunnel. It was observed fuel type did not have a direct effect, but the resulting chamber temperature from the fuel and air combustion, and also chamber pressures, influenced where condensation effects started in the nozzle. Higher chamber temperatures caused changes further downstream of the nozzle's throat. Increases in chamber pressure and fuel-air equivalence ratio resulted in a quicker condensation event changing the isentropic expansion in the nozzle. To reduce the degradation of the flow field effects caused by condensation, any possible changes to increase chamber temperatures and reducing the pressure and equivalence ratio would improve the expanding flow's ideal conditions.

Limits of Homogenous Nucleation Theory

Applying the FIRACON code to combustion driven supersonic and hypersonic test facilities is limited by it use of homogenous nucleation theory. Most test facilities are unable to provide a completely clean flow without rust or some other particles entrained in the flow. Homogenous nucleation theory applies to the rate of water vapor molecules combining with each other and growing size to condense into liquid water droplets. This theory does not account for dust or other type of particles serving as nucleation site for

water molecules to collect and grow in size. This commonly occurring microscope particle laden flow increases the condensation rate due to the additional nucleation sites for water vapor molecules to collect. A more appropriate theory to apply would be a heterogeneous nucleation theory. This theory would account for particles entrained in the flow serving as a trigger point for water vapor nucleation. Although more appropriate, the difficulty in applying the heterogeneous nucleation theory is the requirement of knowing exactly the dust and other particle composition in the flow field with their representative group size for this application to be effective.

Recommendations

Vitiated combustion driven supersonic and hypersonic wind tunnel test facilities need an improved condensation model before operating conditions or facility upgrades are made. The model would have to based on an heterogeneous nucleation theory to account for microscopic dust or other particles entrained in the flow. Any attempts to completely remove the particles for a clean flow would be difficult to accomplish and maintain.

Before attempts are made to write a condensation model solving for a heterogeneous nucleation, more research needs to be performed to better understand the physical phenomena. A complete analysis of the heat and mass transfer of the sub-microscopic, nano-sized condensate particles among the non-equilibrium gas phase is required to improve the modeling equations for an expanding two phase flow in a nozzle. A more accurate model would also include the effect of the expanding flows crossing shockwaves in a wind tunnel.

Condensation data in an expanding flow that is required for any conclusive analysis purpose is very limited. A systematic experimental study is needed to investigate moist air expanding through a small, well instrumented nozzle. This flow should also be seeded to various degrees for analytical comparison to better understand heterogeneous nucleation processes. Until a thorough experimental and theoretical investigation of the dynamics of a condensing flow in a nozzle is completed, modeling programs cannot be applied successfully to combustion driven wind tunnels for making operation and design improvements.

References

1.) Abraham, F. F., *Homogeneous Nucleation Theory*, Academic Press, New York and London, 1974, (Library of Congress Catalog Card Number 73-7439).

2.) Becker, J. V., "Results of Recent Hypersonic and Unsteady Flow Research at the Langley Aeronautical Laboratory," *Journal of Applied Physics*, Vol. 21, No. 7, pp. 619-628, July 1950.

3.) Binnie, A. M. and Green, B. E., "An Electrical Detector of Condensation in High-Velocity Streams," *Proc. Royal Society of London*, Series A, Vol. 181, pp. 134-154, 1943.

4.) Binnie, A. M. and Woods, M. W., "The Pressure Distribution in a Convergent-Divergent Steam Nozzle," Institute of Mechanical Engineers, Proceedings, Vol. 138, pp. 229-266, London, 1938.

5.) Chen, M-S., "The Condensation by Heterogeneous Droplet Nucleation in Boundary Layers," Ph.D. Dissertation, Department of Mechanical Engineering, College of Engineering Kansas State University, Manhattan, Kansas, 1984.

6.) Dunning, W. J., "Nucleation: Homogeneous and Heterogeneous," Discussions, No. 30, *The Physical Chemistry of Aerosols*, Faraday Division of the Chemical Society (Great Britain), pp. 9-19, 1961.

7.) Erickson, W. D., Mall, G. H. and Prabhu, Ramadas K., "Finite Rate Water Condensation in Combustion-Heated Wind Tunnels," NASA Technical Paper No. TP-2833, National Aeronautics and Space Administration, September 1988.

8.) Farley, F. J. M., "The Theory of the Condensation of Supersaturated Ion-free Vapor," *Proc. Of Royal Society of London*, Volume A212, pp. 530-542, 1952.

9.) Feder, J., Russell, K. C., Lothe, J. and Pound, G. M., "Homogeneous Nucleation and Growth of Droplets in Vapors," *Advances in Physics*, Vol. 15, pp. 111-178, 1966.

10.) Fletcher, N. H. "Size Effects in Heterogeneous Nucleation," *Journal of Chemical Physics*, Vol. 29, No. 2, pp. 572-576, September 1958.

11.) Fletcher, N. H., "Ice Crystal Nucleation by Aerosol Particles," Discussions, No. 30, *The Physical Chemistry of Aerosols*, Faraday Division of the Chemical Society (Great Britain), pp. 39-45, 1961.

12.) Frank, W., "Condensation Phenomena in Supersonic Nozzles," *Acta Mechanica*, Vol. 54, pp. 135-156, 1985.

13.) Gouse, Jr., S. W. and Brown, G. A., "A Survey of the Velocity of Sound in Two-

Phase Mixtures," ASME Publication 64-WA/FE35, presented at the Winter Annual Meeting, Nov. 29-Dec. 4, New York, NY, 1964.

14.) Griffin, J. L., "Digital Computer Analysis of Condensation in Highly Expanded Flows," Aerospace Research Laboratories Report (ARL 63-206), Office of Aerospace Research, United States Air Force, November 1963.

15.) Gyarmathy, G., "Basic Notions," Chapter 1 in *Two-Phase Steam Flow in Turbines and Separators*, M. J. Moore and C. H. Sieverding, Editors, Hemisphere Publishing Corporation, Washington and London, 1976 (ISBN 0-07-042992-8).

16.) Gyarmathy, G., "Condensation in Flowing Steam," Chapter 3 in *Two-Phase Steam Flow in Turbines and Separators*, M. J. Moore and C. H. Sieverding, Editors, Hemisphere Publishing Corporation, Washington and New York, 1976 (ISBN 0-07-042992-8).

17.) Harding, L. J., "A Digital Computer Program for Condensation in Expanding One Component Flows," Aerospace Research Laboratories Report (ARL 65-58), Office of Aerospace Research, United States Air Force, March 1965.

18.) Hansen, C. F. and Nothwang, G. J., "Condensation of Air in Supersonic Wind Tunnels and It's Effects on Flow About Models," NACA Technical Note 2690, Washington, April 1952.

19.) Hazen, W. E., "Some Operating Characteristics of the Wilson Cloud Chamber," Review of Scientific Instruments, Vol. 13, pp. 247-257, June 1942.

20.) Heybey, W., "Analytical Treatment of Normal Condensation Shock," NACA Technical Memorandum 1174, July 1947, a translation of "Analytische Behandlung des geraden Kondensationsstosses," Heeres-Versuchsstells, Peenemunde, Archiv Nr. 66/72, Marz 30, 1942.

21.) Hill, P. G., "Condensation of Water Vapor During Supersonic Expansion in Nozzles," *Journal of Fluid Mechanics*, Vol. 25, Part 3, pp. 593-620, July 1966.

22.) Kantrowitz, A., "Nucleation in Very Rapid Vapor Expansions," *Journal of Chemical Physics*, Vol. 19, No. 9, pp. 1097-1100, September 1951.

23.) Kang, S-W., "Analysis of Condensation Droplet Growth in Rarified and Continuum Environments," *AIAA Journal*, Vol. 5, No. 7, pp. 1288-1295, July 1967.

24.) Mason, B. J., "Nucleation of Water Aerosols," Discussions, No. 30, *The Physical Chemistry of Aerosols*, Faraday Division of the Chemical Society (Great Britain), pp. 21-38, 1961.

25.) McBride, B. J., and Gordon, S., "Computer Program for Calculation of Complex Chemical Equilibrium Compositions and Applications: Part I Analysis, Part II Users Manual and Program Description," NASA Reference Publication 1311 (1994, 1996).

26.) Miller, R. C., Anderson, R. J. and Kassner, J. L., Jr., "Evaluation of the Classical Theory of Nucleation Using Expansion Chamber Measurements of the Homogeneous Nucleation Rate of Water from the Vapor," *Proceedings of International Conference on Colloids and Surfaces*, 50th Colloid and Surface Science Symposium, San Juan, Puerto Rico, Vol. 2, pp. 1-21, 1976.

27.) Moore, M. J., Walters, P. T., Crane, R. I. And Davidson, B. J., "Predicting the Fog-Drop Size in Wet-Steam Turbines," Conference on Heat and Fluid Flow in Steam and Gas Turbine Plants, Conference Publication 3, Institute of Mechanical Engineers, (C37/73), pp. 101-109, 1973.

28.) Nagamatsu, H. T., "Summary of Recent GALCIT Hypersonic Experimental Investigations," *Journal of the Aeronautical Sciences*, pp. 165-172, March 1955.

29.) Nguyen, D. L., Winter, E. R. F. and Greiner, M., "Sonic Velocity in Two-Phase Systems," International J. of Multiphase Flow, Vol. 7, pp 311-320, 1981.

30.) Oswatitsch, K. "Kondensation ser Scheinungen in Uberschalldusen," Z. Angew, Math. Mech., Vol. 22, No. 1, pp. 1-14, 1942.

31.) Perrell, E. R., Erickson, W. D. and Candler, G. V., "Numerical Simulation of Nonequilibrium Condensation in a Hypersonic Wind Tunnel," *AIAA Journal of Thermophysics and Heat Transfer*, Vol. 10, No.2, pp. 277-283, April-June 1996.

32.) Powell, E. S., "An Improved Procedure for Calculating the Aerothermodynamic Properties of a Vitiated Air Test Medium," AIAA Paper No. AIAA-85-0913, presented at the AIAA 20th Thermophysics Conference, Williamsburg, Virginia, June 19-21, 1985.

33.) Powell, E., "A Simplified Engineering Model for Preliminary Facility Design," AIAA Paper No. AIAA-92-5044, presented at the AIAA Fourth International Aerospace Planes Conference, Orlando, Florida, December 1-4, 1992.

34.) Probstein, R. F., "Time Lag in the Self-Nucleation of a Supersaturated Vapor," *Journal of Chemical Physics*, Vol. 19, No. 5, pp. 619-626, May 1951.

35.) Pouring, A. A., "Thermal Choking and Condensation in Nozzles," *Physics of Fluids*, Vol. 8, No. 10, pp. 1802-1810, October 1965.

36.) Sivier, K. R., "Digital Computer Studies of Condensation in Expanding One-

Component Flows," Aerospace Research Laboratories Report (ARL 65-234), Office of Aerospace Research, United States Air Force, November 1965.

37.) Stever, H. G. and Rathbun, K. C., "Theoretical and Experimental Investigation of Condensation of Air in Hypersonic Wind Tunnels," NACA Technical Note 2559, Washington, November 1951.

38.) Tempelmeyer, K. E., Nesbitt, M. H., and Carpenter, L. R., "Theoretical Predictions of Inviscid Pressure Distribution and Heat Transfer Rates Over Simple Bodies in Air and Combustion Gas Test Media at Hypersonic Speeds," Arnold Engineering Development Center Technical Note (AEDC TN-60-207), Air Research and Development Command, AEDC, TN, 37389, March 1961.

39.) Touloukain, Y. S.; Saxien, S. C.; and Hestermans, P.: *Viscousity. Thermophysical Properties of Matter, Volume II*, IFI/Plenum, c. 1975

40.) Turnbull, D., "Transient Nucleation," Metals Technology (Previous title: Journal of the Institute of Metals), American Institute of Mining and Metallurgical Engineers, Technical Publication No. 2365, pp. 1-10, June 1948.

41.) Wallace, G. B., One-Dimensional Two-Phase, McGraw-Hill Book Company, New York, NY, 1969.

42.) Walters, P. T., "Optical Measurements of Water Droplets in West Steam Flows," Conference on Heat and Fluid Flow in Steam and Gas Turbine Plants, Conference Publication 3, Institute of Mechanical Engineers, (C32/73), pp. 66-74, 1973.

43.) Wegener, P. P. and Caligostro, D. J., "Periodic Nozzle Flow with Heat Addition," *Combustion Science and Technology*, Vol. 6, pp. 269-277, 1973.

44.) Wegener, P. P. and Mack, L. M., "Condensation in Supersonic and Hypersonic Tunnels," Advances in Applied Mechanics, Vol. 5, pp. 307-442, 1958.

45.) Wegener, P. P. and Pouring, A. A., "Experiments on Condensation of Water Vapor by Homogeneous Nucleation in Nozzles," *Physics of Fluids*, Vol. 7, No. 3, pp. 352-361, March 1964.

46.) Wegener, P. P., "Condensation Phenomena in Nozzles," *Heterogeneous Combustion*, pp. 701-724, AIAA Progress in Astronautics and Aeronautics, Vol. 15, H. G. Wolfhard, I. Glassman, and L. Green, Jr., Editors, Academic Press, 1964.

47.) Yang, W-T., "A Study of Homogeneous Nucleation from Vapor to Droplets," Ph.D. Dissertation presented to the Faculty of Yale University in candidacy for the Degree of Doctor of Philosophy, Yale University of Engineering, 1963.

48.) Young, J. B., “The Spontaneous Condensation of Steam in Supersonic Nozzles,” *Physico-Chemical Hydrodynamics*, Vol. 1, No. 3, pp. 57-82, 1982.

49.) Young, J. B., “Spontaneous Condensation of Steam in Supersonic Nozzles, Part I: Nucleation and Droplet Growth, Part II: Numerical Methods and Comparison to Experimental Results,” Report CUED/A·Turbo/TR-97, Department of Engineering, University of Cambridge, England, 1980.

50.) *Nucleation*, A. C. Zettlemoyer, Editor, Marcel Dekker, Inc., New York, 1969, (Library of Congress Catalog Card Number 70-77144).

Appendixes

Appendix A
Illustrations of the Nucleation Rate of Liquid Water Droplets Along the Nozzle

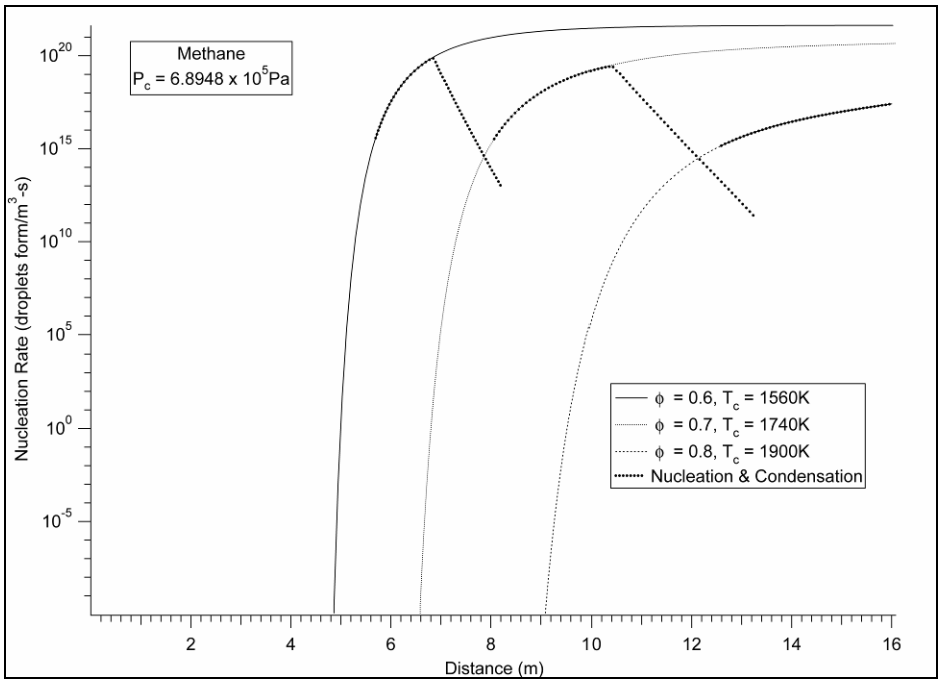

***Figure* A-1: Nucleation Rate of Liquid Water Droplets Along the Nozzle for Cases METH 1.1.1, 1.1.2, and 1.1.3.**

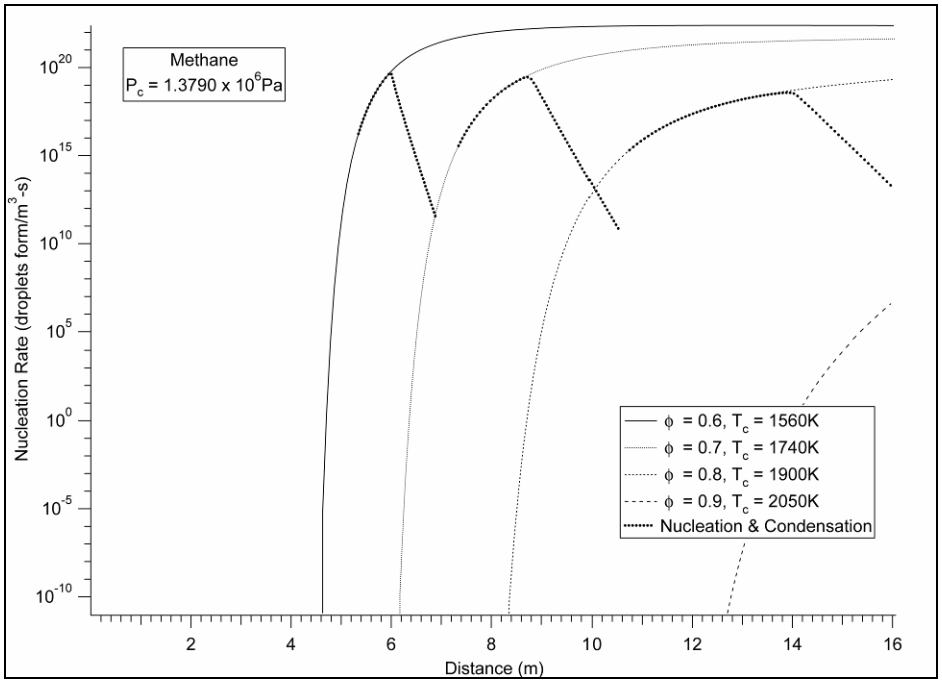

***Figure* A-2: Nucleation Rate of Liquid Water Droplets Along the Nozzle for Cases METH 1.2.1, 1.2.2, 1.2.3 and 1.2.4.**

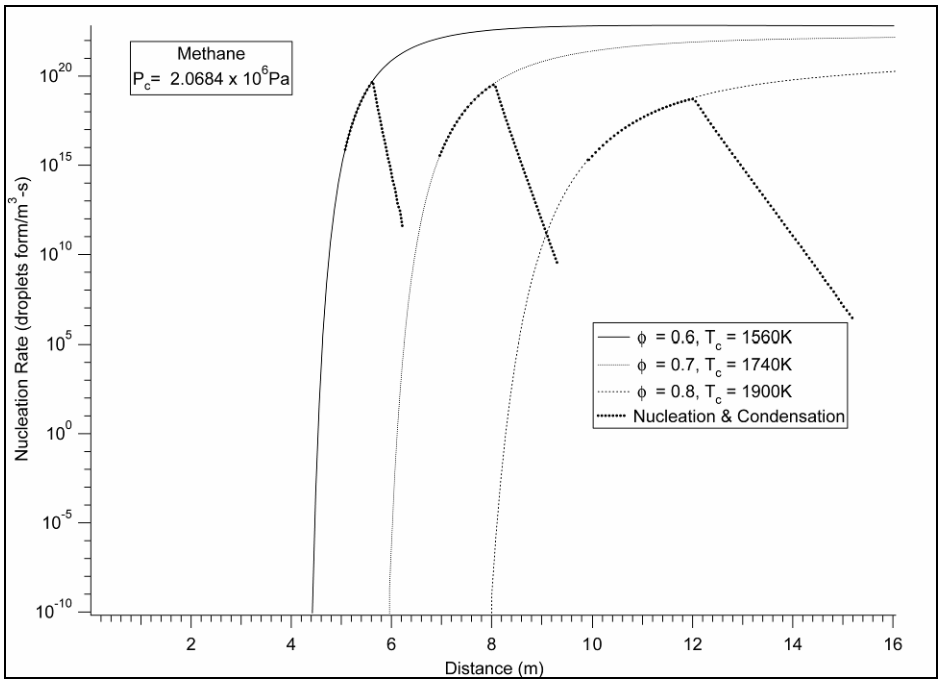

***Figure* A-3: Nucleation Rate of Liquid Water Droplets Along the Nozzle for Cases METH 1.3.1, 1.3.2, and 1.3.3.**

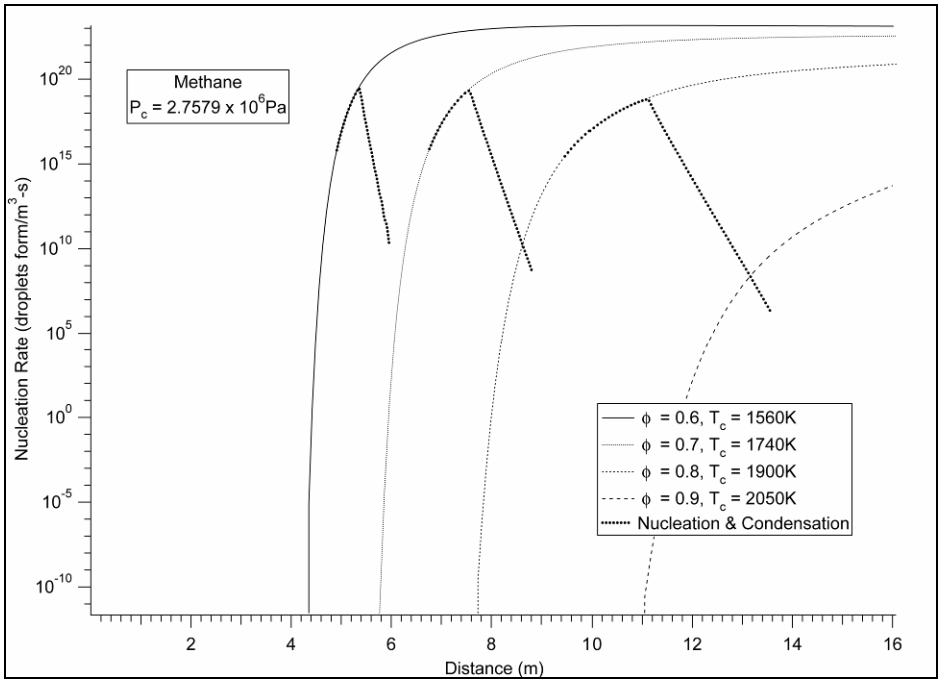

***Figure* A-4: Nucleation Rate of Liquid Water Droplets Along the Nozzle for Cases METH 1.4.1, 1.4.2, 1.4.3, and 1.4.4**

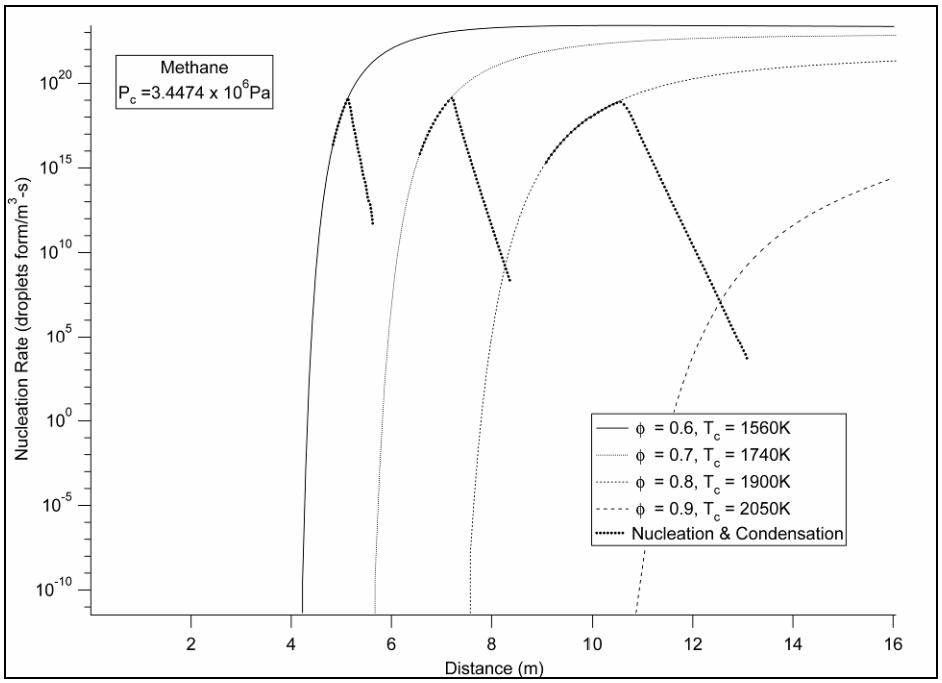

***Figure* A-5: Nucleation Rate of Liquid Water Droplets Along the Nozzle for Cases METH 1.5.1, 1.5.2, 1.5.3, and 1.5.4.**

Appendix B
Illustrations of the Critical Droplet Radius of Liquid Water Along the Nozzle

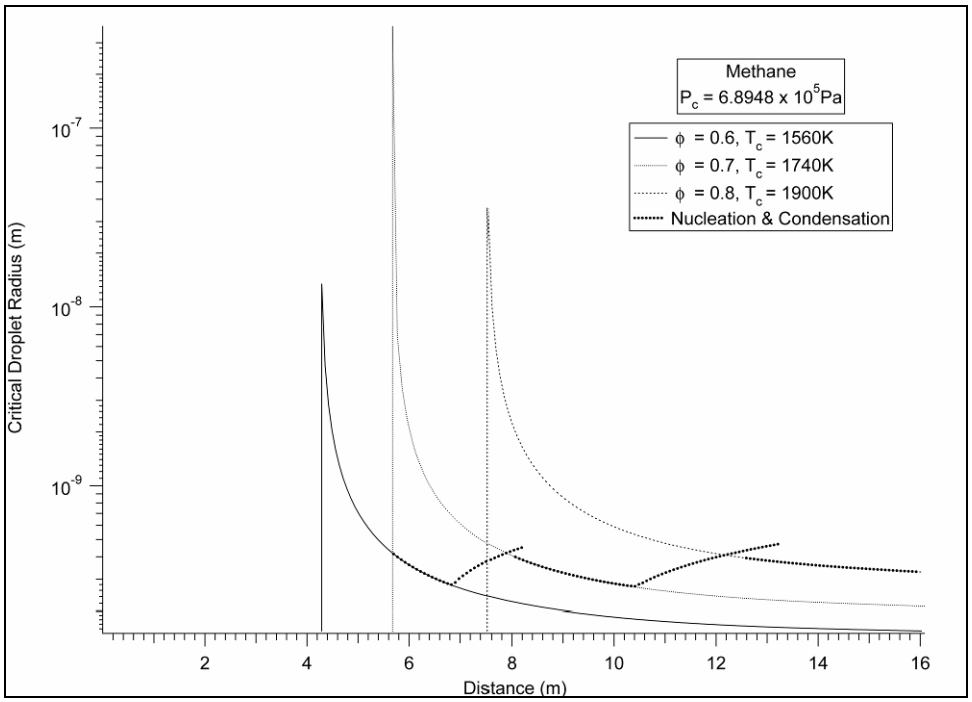

***Figure* B-1: Critical Droplet Radius of Liquid Water Along the Nozzle for Cases METH 1.1.1, 1.1.2, and 1.1.3.**

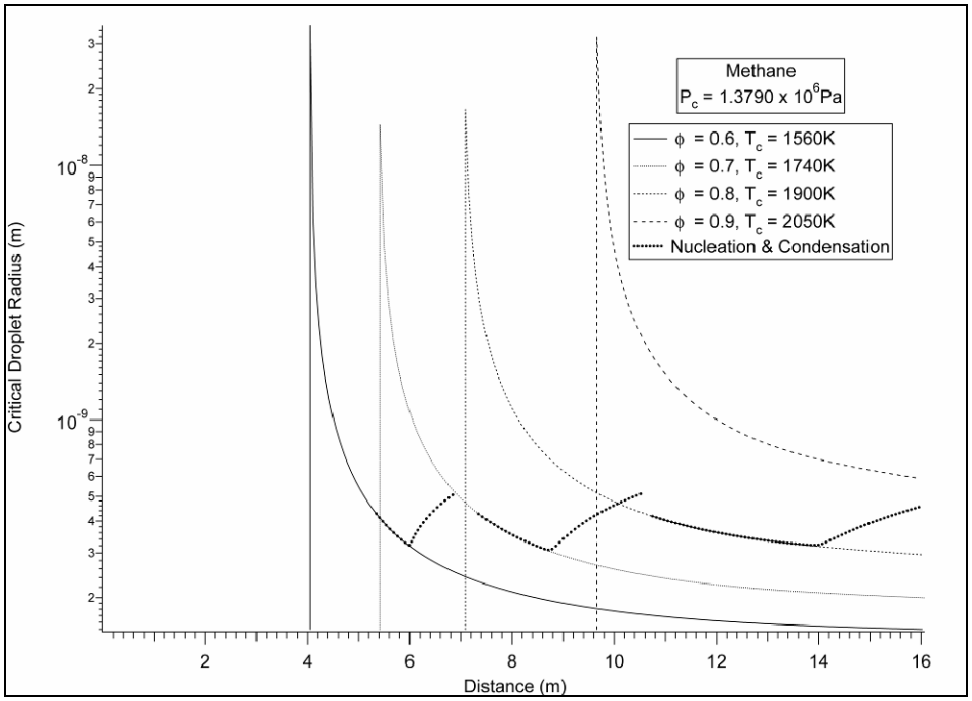

***Figure* B-2: Critical Droplet Radius of Liquid Water Along the Nozzle for Cases METH 1.2.1, 1.2.2, 1.2.3, and 1.2.4.**

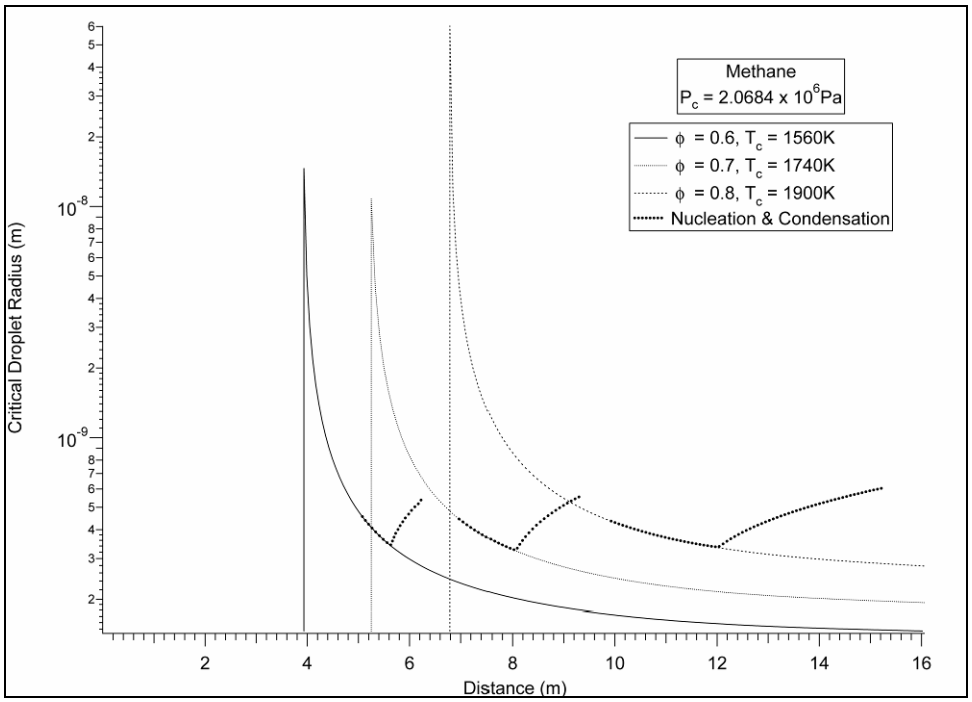

***Figure* B-3: Critical Droplet Radius of Liquid Water Along the Nozzle for METH 1.3.1, 1.3.2, and 1.3.3.**

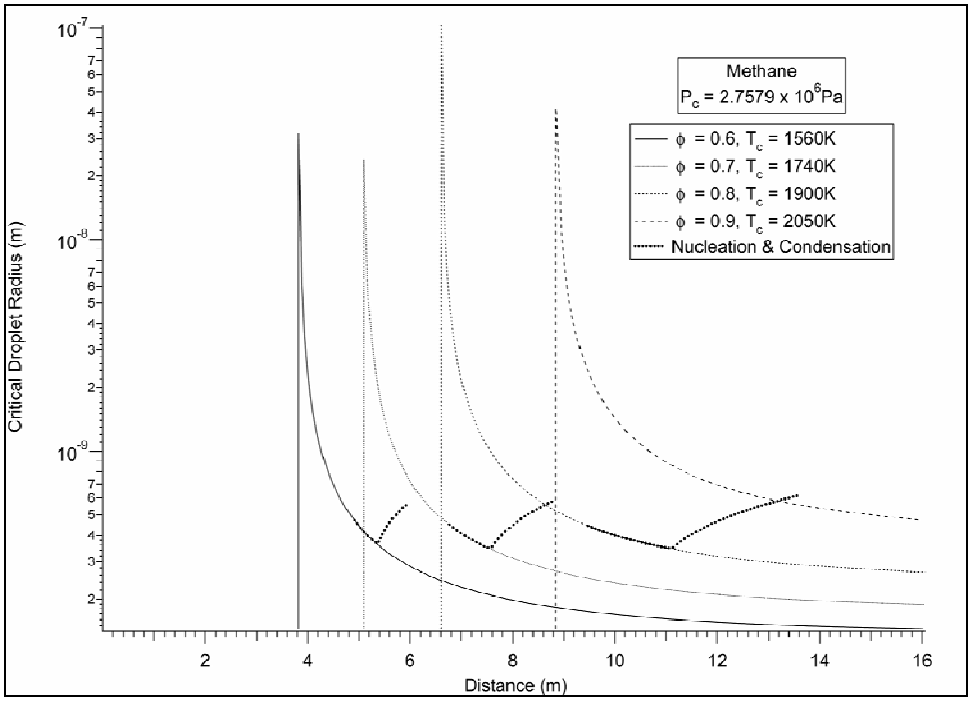

***Figure* B-4: Critical Droplet Radius of Liquid Water Along the Nozzle for Cases METH 1.4.1, 1.4.2, 1.4.3, and 1.4.4.**

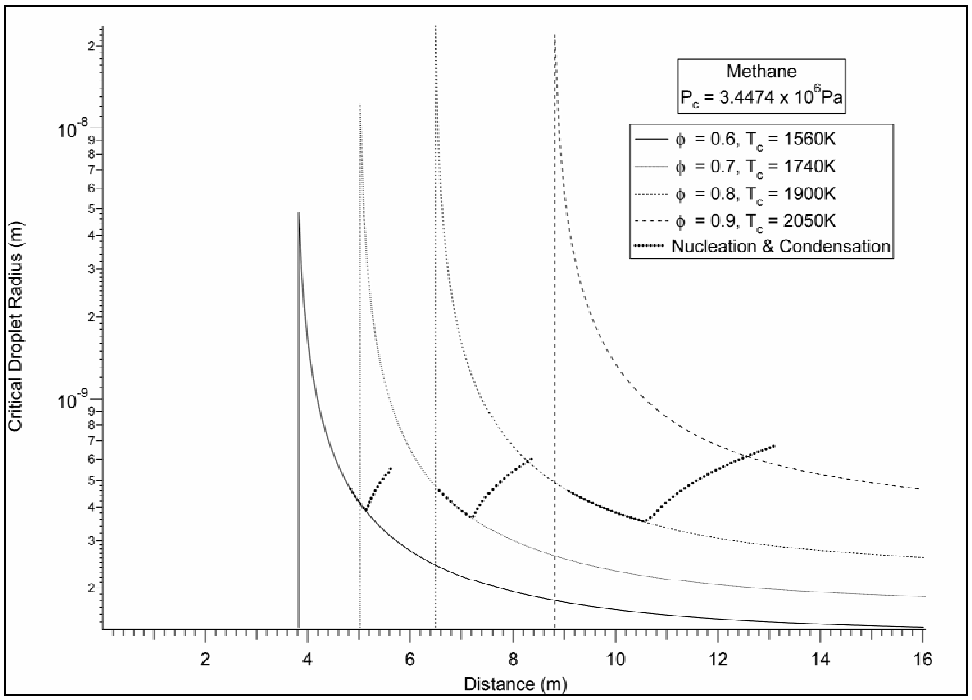

***Figure* B-5: Critical Droplet Radius of Liquid Water Along the Nozzle for Cases METH 1.5.1, 1.5.2, 1.5.3, and 1.5.4.**

Appendix C
Illustrations of the Mass Fraction of Liquid Water Along the Nozzle

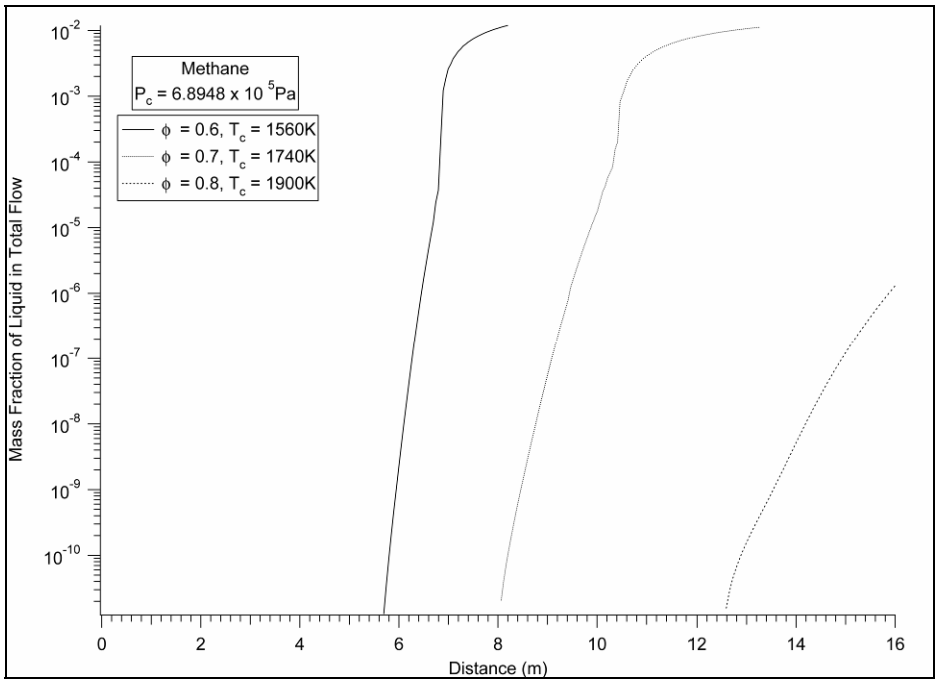

***Figure* C-1: Mass Fraction of Liquid Water Along the Nozzle for Cases METH 1.1.1, 1.1.2, and 1.1.3.**

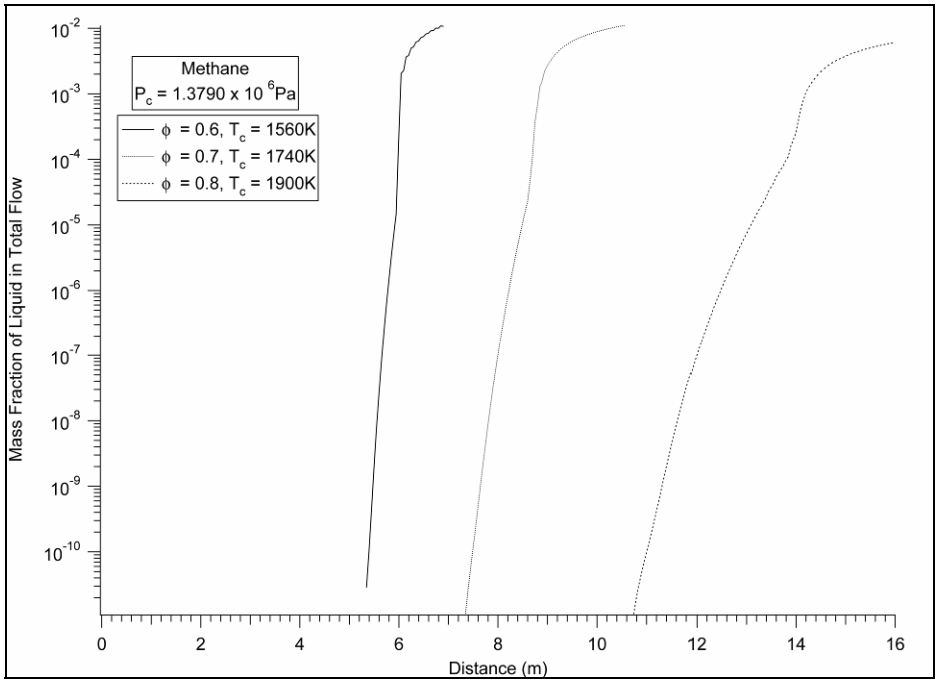

***Figure* C-2: Mass Fraction of Liquid Water Along the Nozzle for Cases METH 1.2.1, 1.1.2, and 1.2.3.**

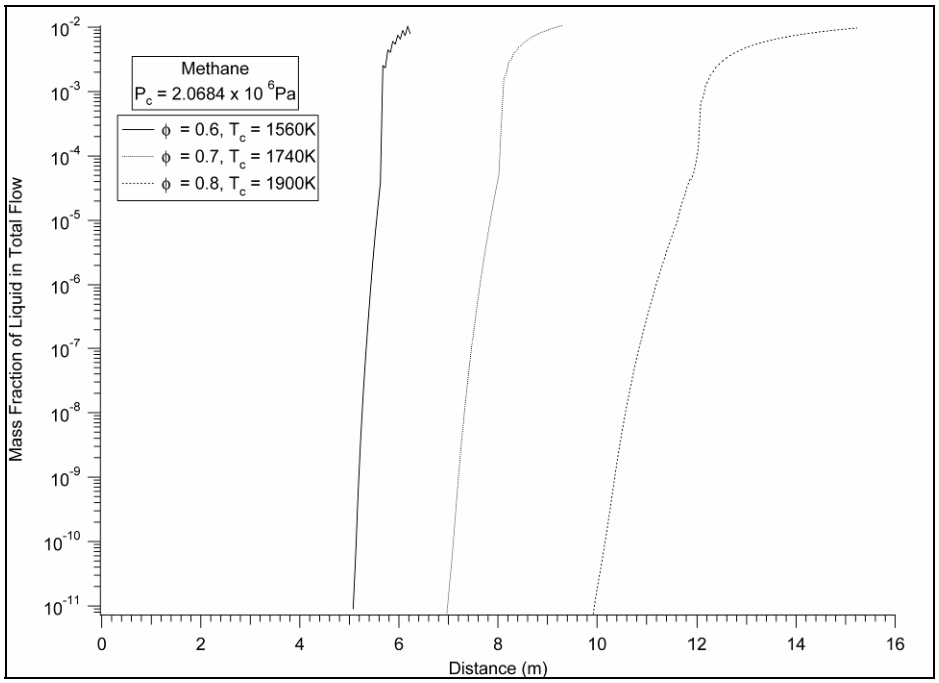

***Figure* C-3: Mass Fraction of Liquid Water Along the Nozzle for Cases METH 1.3.1, 1.3.2, and 1.3.3.**

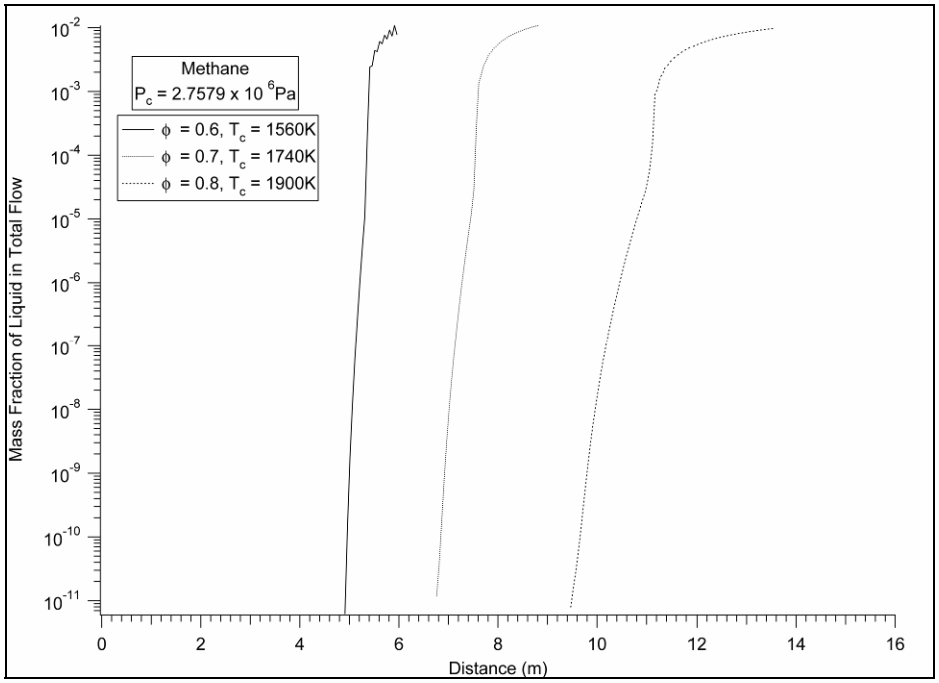

***Figure* C-4: Mass Fraction of Liquid Water Along the Nozzle for Cases METH 1.4.1, 1.4.2, and 1.4.3.**

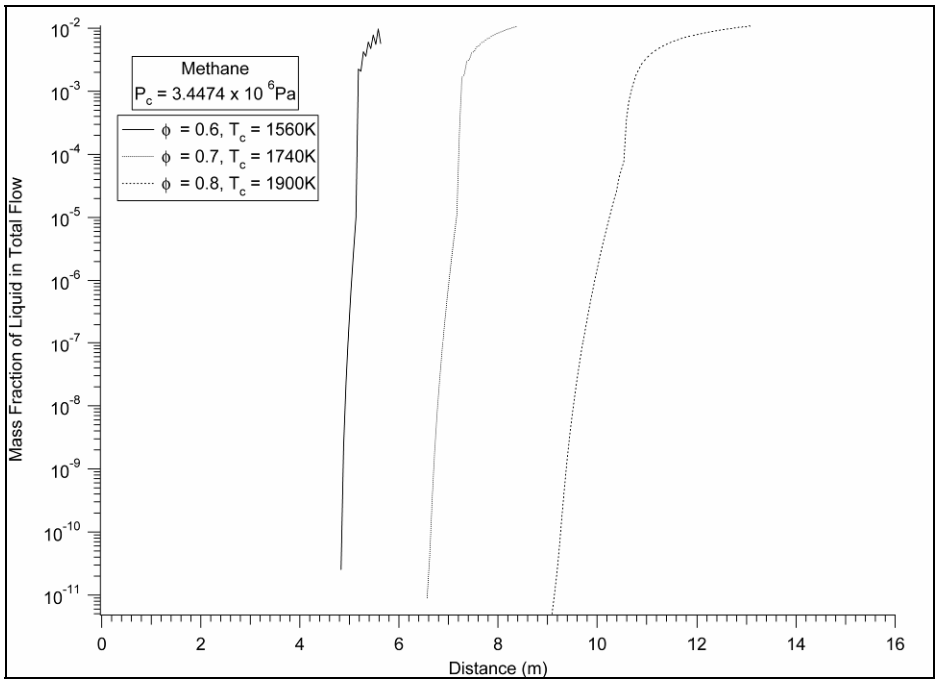

***Figure* C-5: Mass Fraction of Liquid Water Along the Nozzle for Cases METH 1.5.1, 1.5.2, and 1.5.3.**

Appendix D
Illustrations of the Mixture Velocity Distribution Along the Nozzle

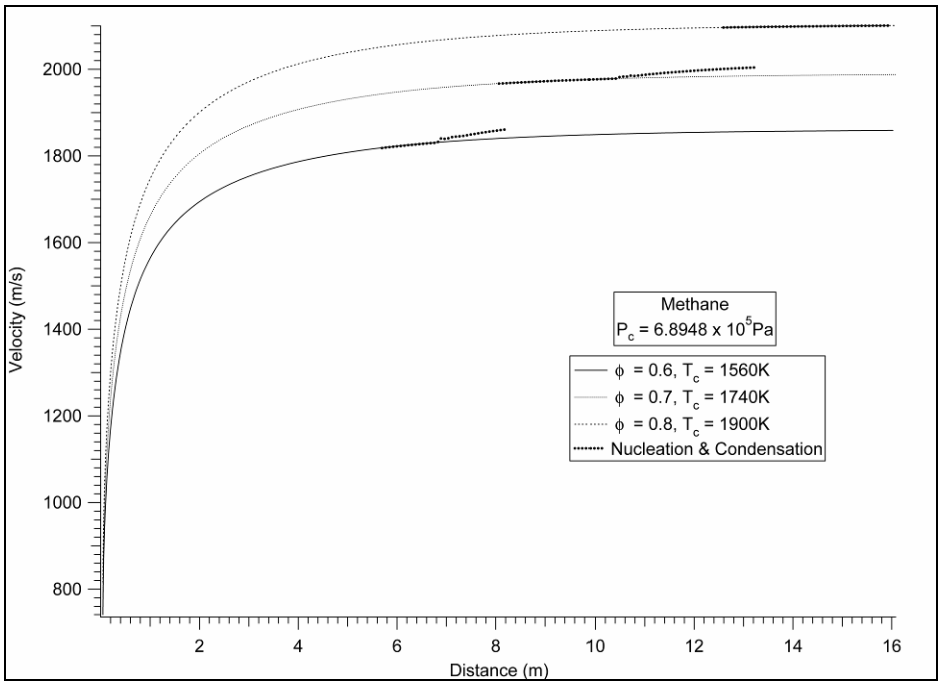

***Figure* D-1: Mixture Velocity Distribution Along the Nozzle for Cases METH 1.1.1, 1.1.2, and 1.1.3.**

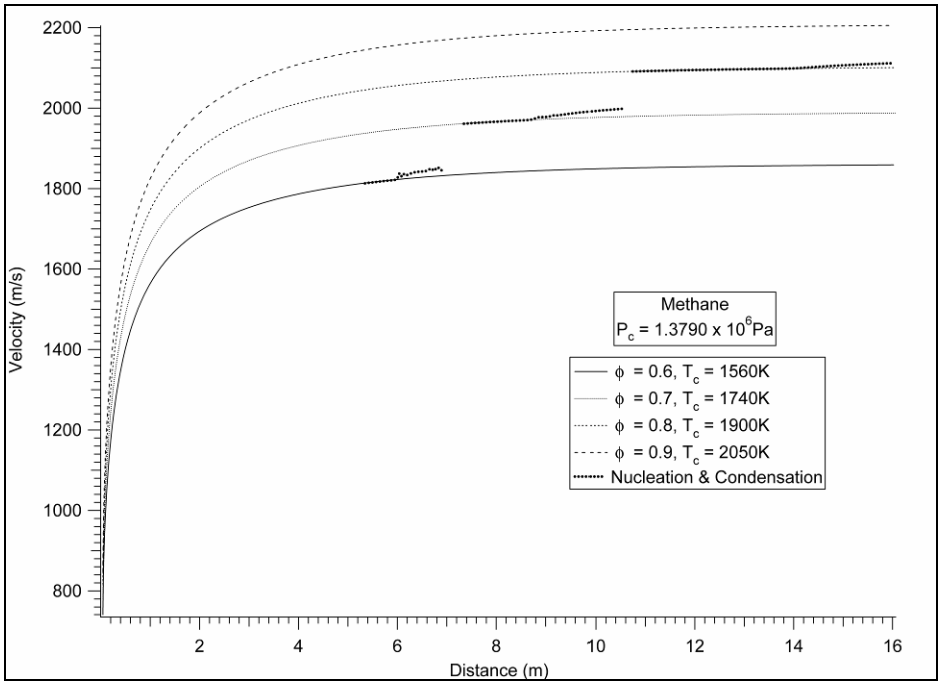

***Figure* D-2: Mixture Velocity Distribution Along the Nozzle for Cases METH 1.2.1, 1.2.2, 1.2.3, and 1.2.4.**

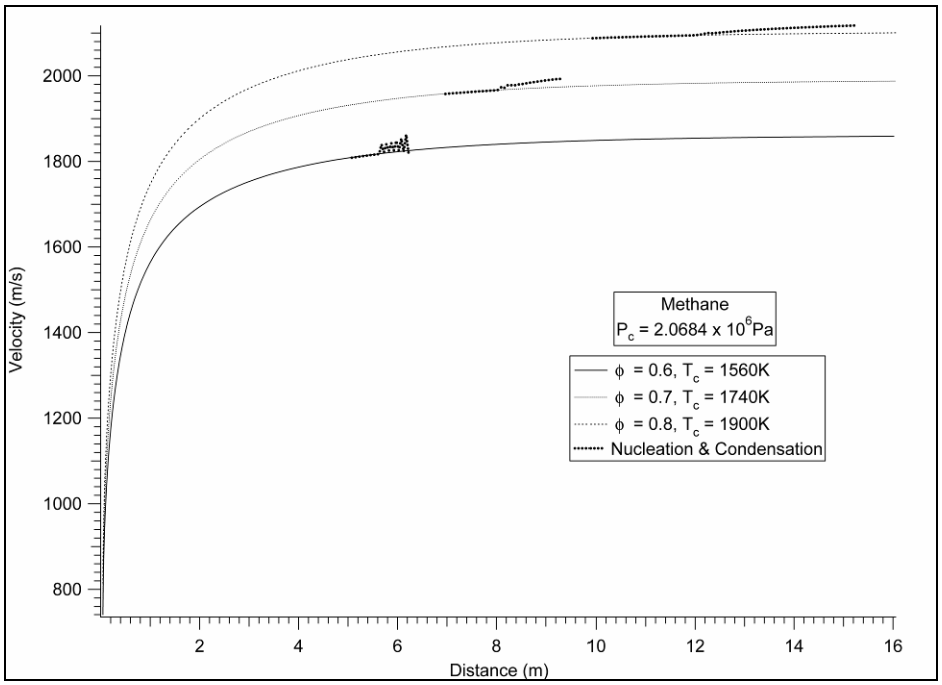

***Figure* D-3: Mixture Velocity Distribution Along the Nozzle for Cases METH 1.3.1, 1.3.2,and 1.3.3.**

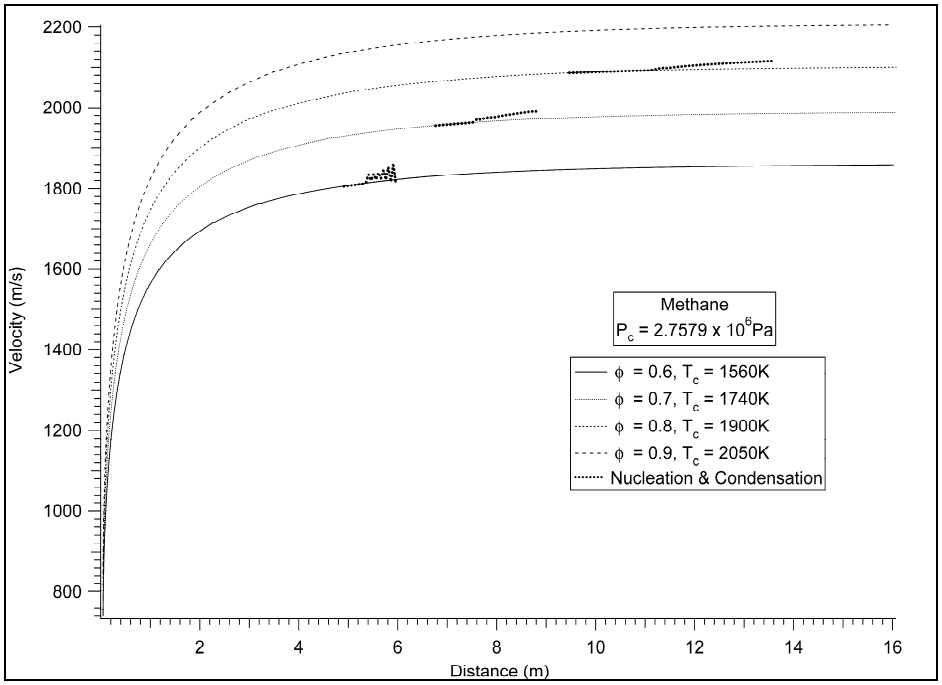

***Figure* D-4: Mixture Velocity Distribution Along the Nozzle for Cases METH 1.4.1, 1.4.2, 1.4.3, and 1.4.4.**

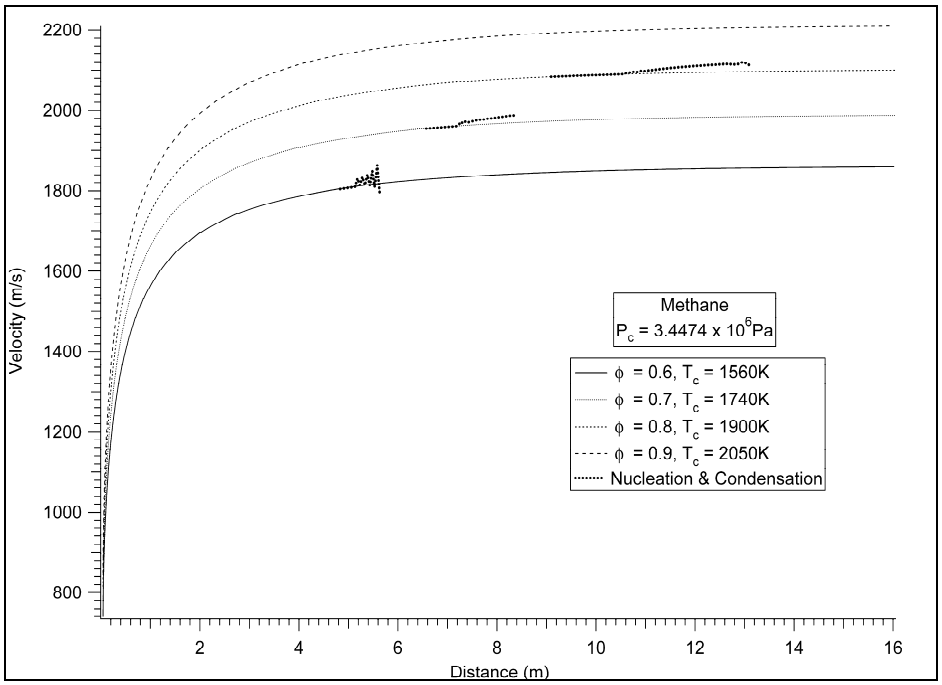

***Figure* D-5: Mixture Velocity Distribution Along the Nozzle for Cases METH 1.5.1, 1.5.2, 1.5.3, and 1.5.4.**

Appendix E
Illustrations of the Mixture Mach Number Distribution Along the Nozzle

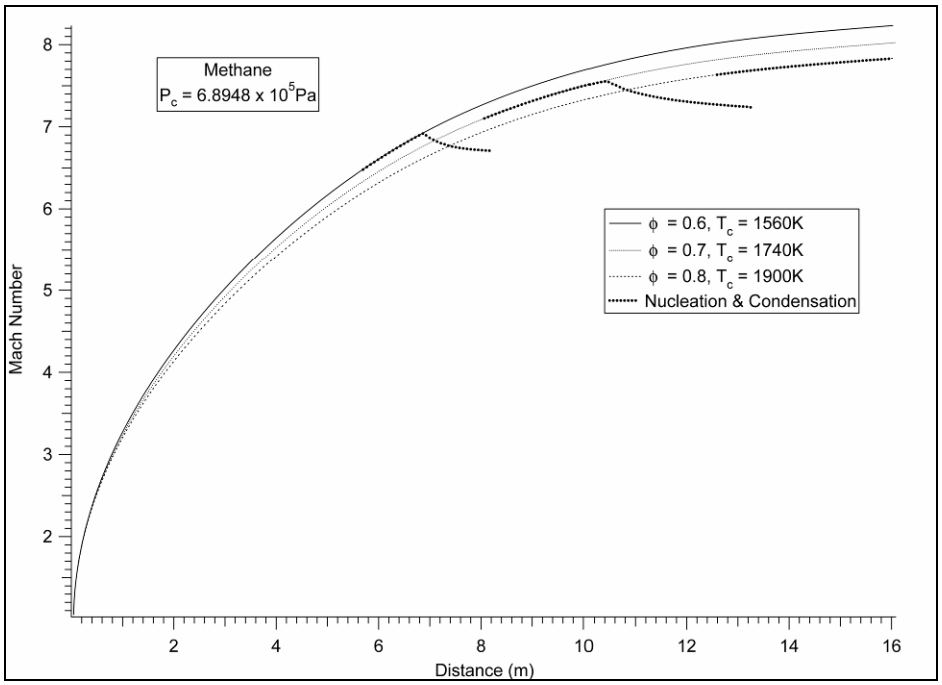

***Figure* E-1: Mixture Mach Number Distribution Along the Nozzle for Cases METH 1.1.1, 1.1.2, and 1.1.3.**

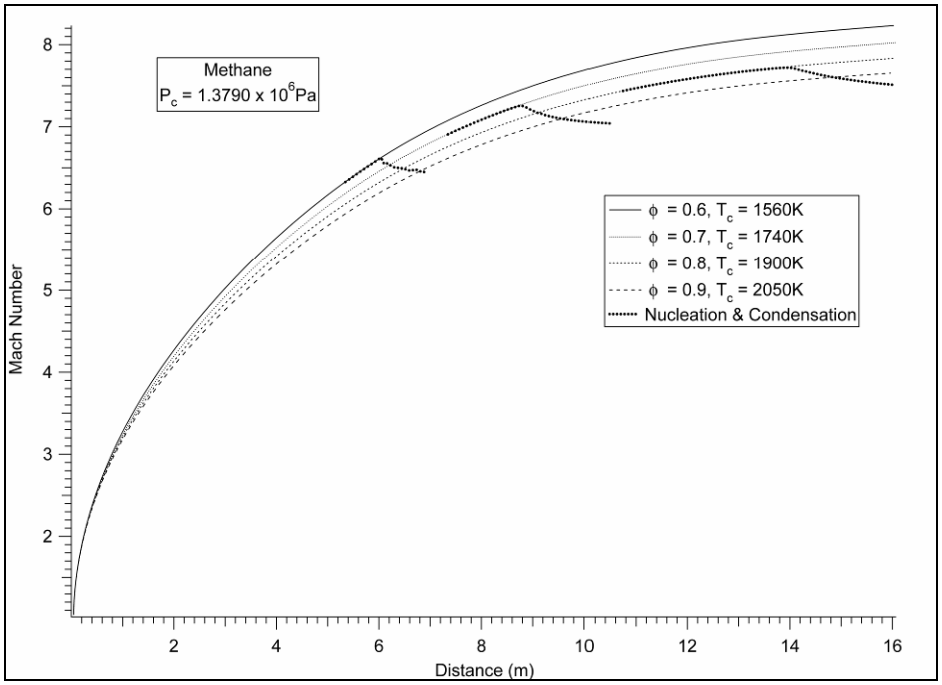

***Figure* E-2: Mixture Mach Number Distribution Along the Nozzle for Cases METH 1.2.1, 1.2.2, 1.2.3, and 1.2.4.**

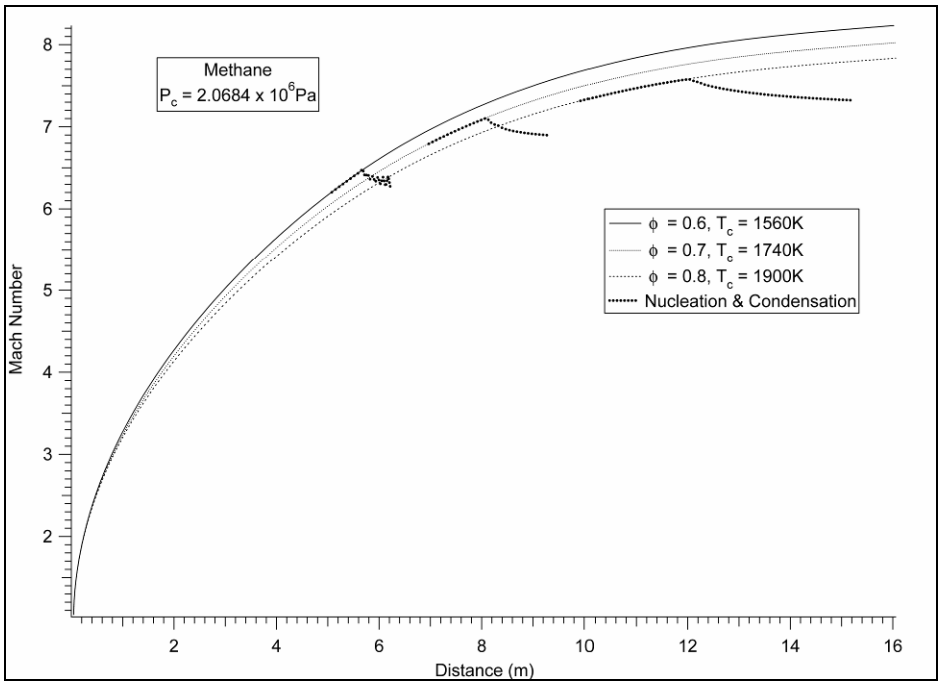

***Figure* E-3: Mixture Mach Number Distribution Along the Nozzle for Cases METH 1.3.1, 1.3.2, and 1.3.3.**

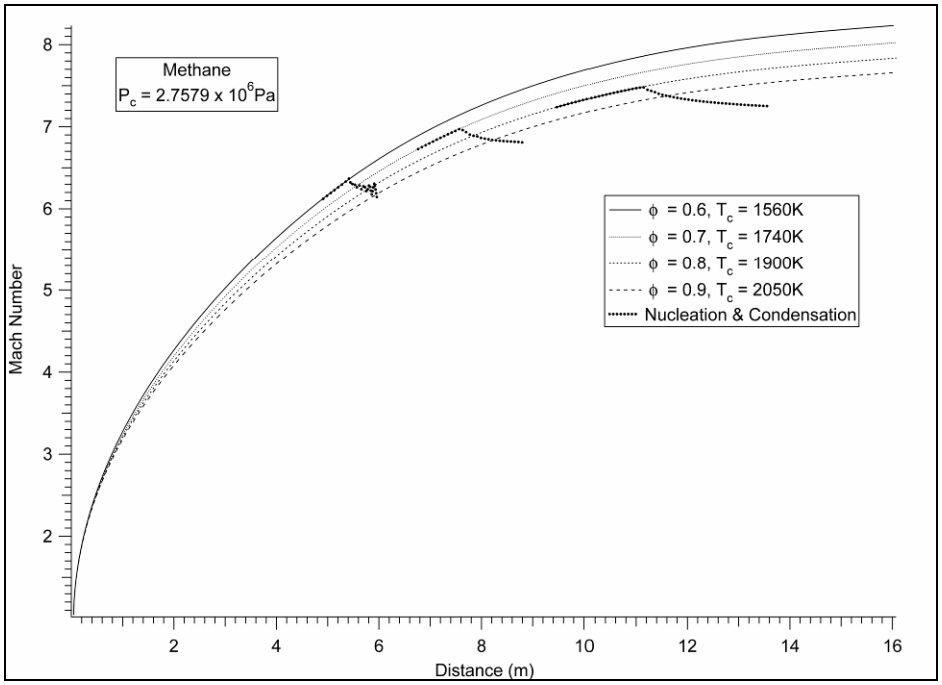

***Figure* E-4: Mixture Mach Number Distribution Along the Nozzle for Cases METH 1.4.1, 1.4.2, 1.4.3, and 1.4.4.**

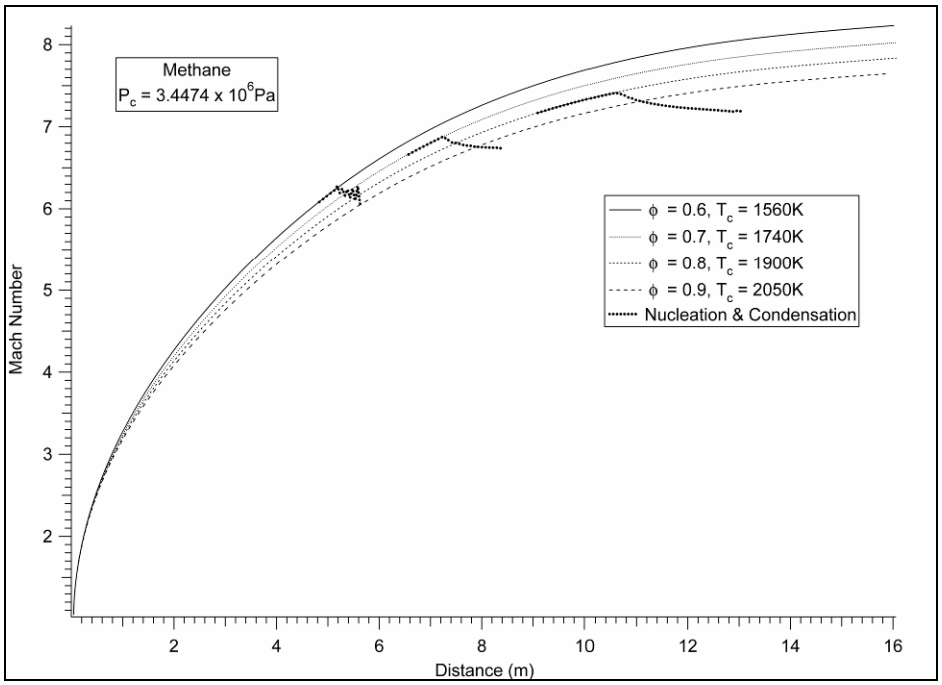

***Figure* E-5: Mixture Mach Number Distribution Along the Nozzle for Cases METH 1.5.1, 1.5.2, 1.5.3, and 1.5.4.**

Appendix F
Illustrations of the Mixture Static Temperature Distribution Along the Nozzle

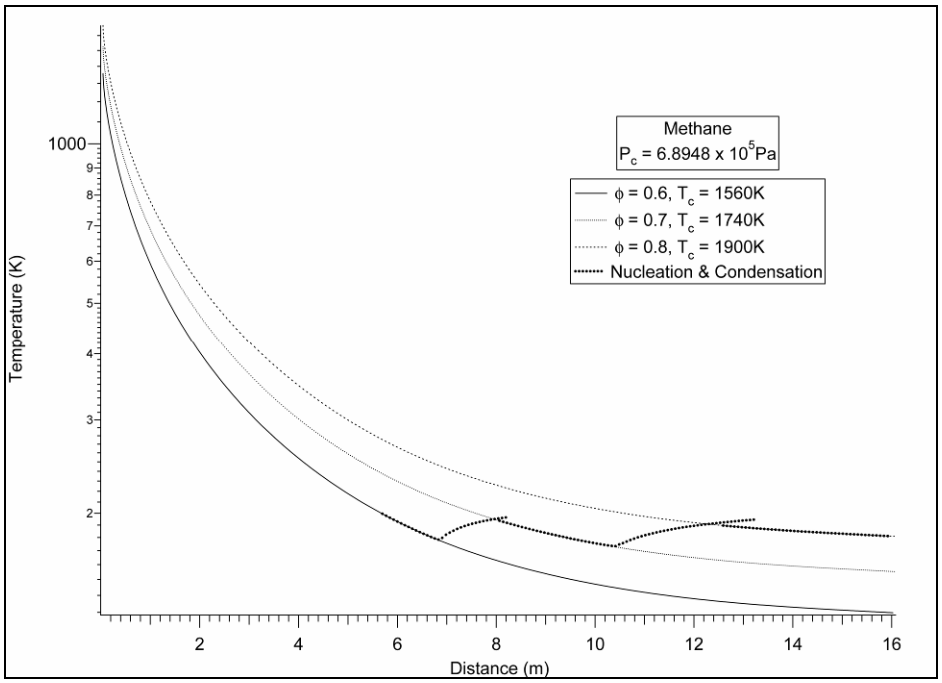

***Figure* F-1: Mixture Static Temperature Distribution Along the Nozzle for Cases METH 1.1.1, 1.1.2, and 1.1.3.**

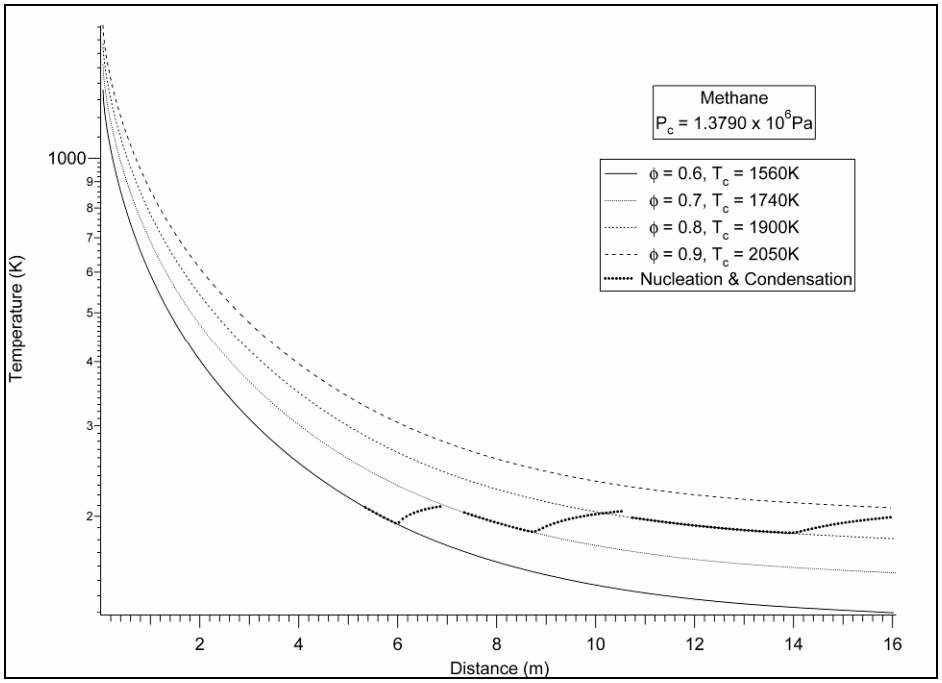

***Figure* F-2: Mixture Static Temperature Distribution Along the Nozzle for Cases METH 1.2.1, 1.2.2, 1.2.3, and 1.2.4.**

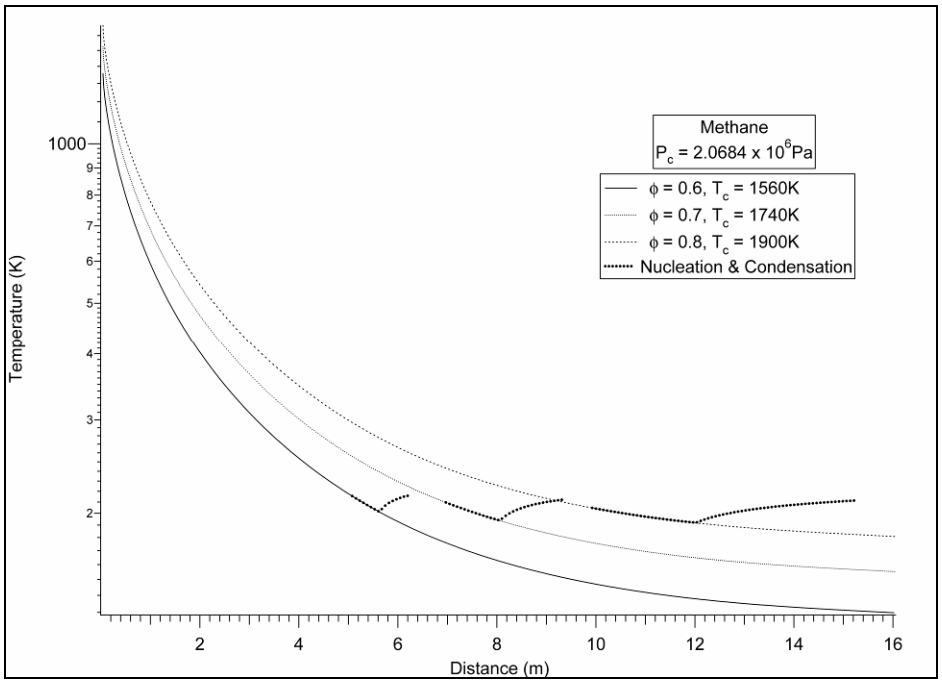

***Figure* F-3: Mixture Static Temperature Distribution Along the Nozzle for Cases METH 1.3.1, 1.3.2, and 1.3.3.**

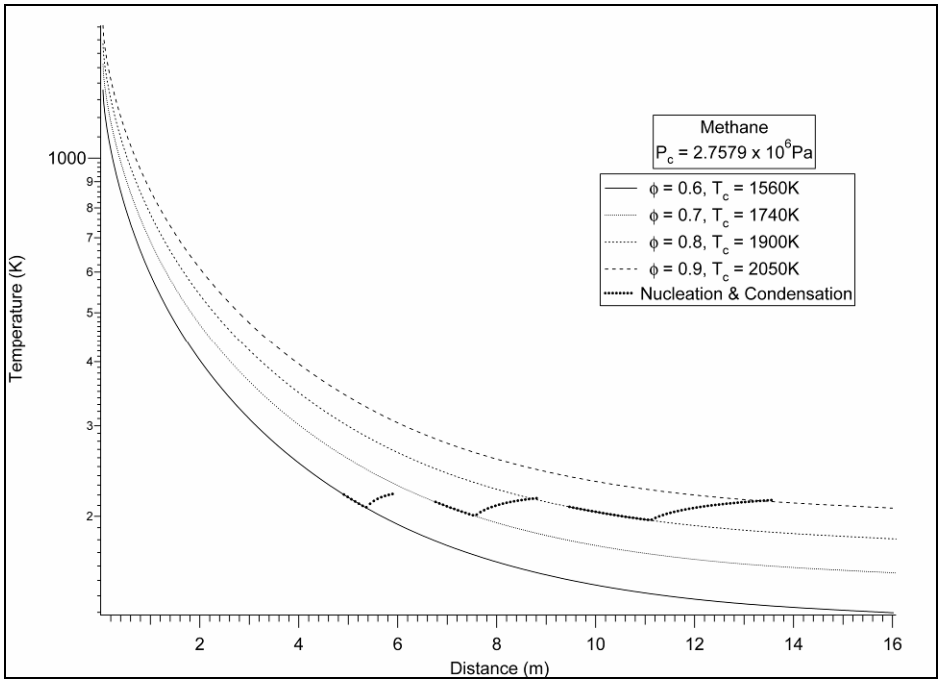

***Figure* F-4: Mixture Static Temperature Distribution Along the Nozzle for Cases METH 1.4.1, 1.4.2, 1.4.3, and 1.4.4.**

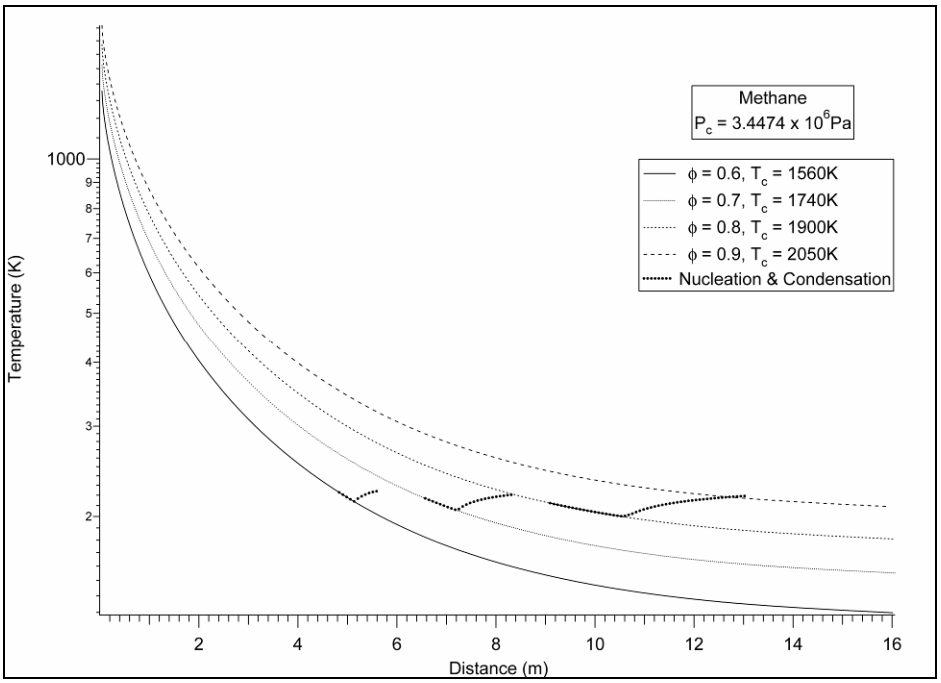

***Figure* F-5: Mixture Static Temperature Distribution Along the Nozzle for Cases METH 1.5.1, 1.5.2, 1.5.3, and 1.5.4.**

Appendix G
Illustrations of the Mixture Stagnation Temperature Distribution Along the Nozzle

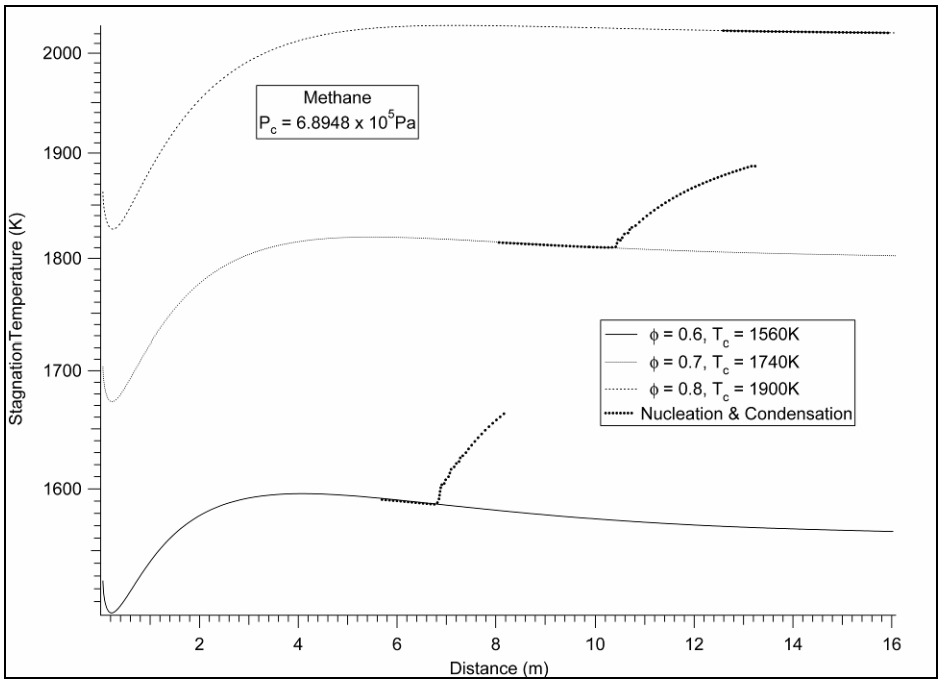

***Figure* G-1: Mixture Stagnation Temperature Distribution Along the Nozzle for Cases METH 1.1.1, 1.1.2, and 1.1.3.**

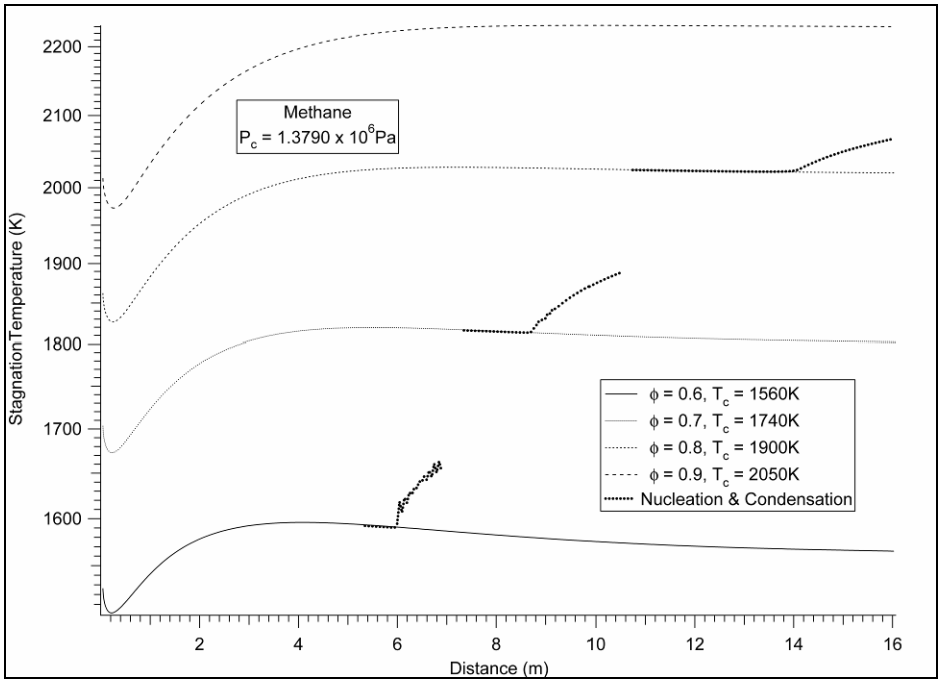

***Figure* G-2: Mixture Stagnation Temperature Distribution Along the Nozzle for Cases METH 1.2.1, 1.2.2, 1.2.3, and 1.2.4.**

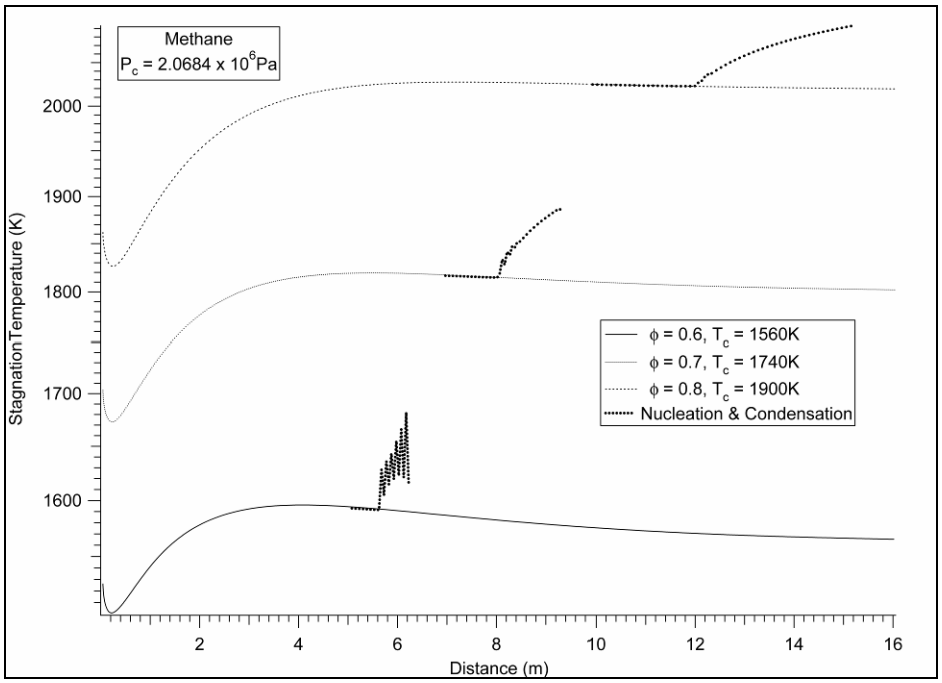

***Figure* G-3: Mixture Stagnation Temperature Distribution Along the Nozzle for Cases METH 1.3.1, 1.3.2, and 1.3.3.**

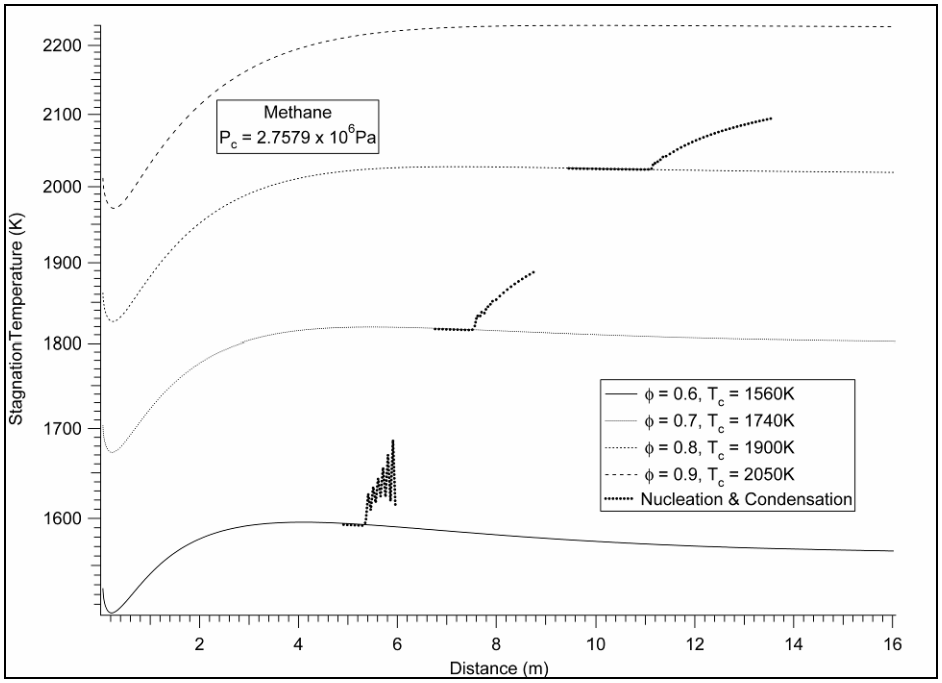

***Figure* G-4: Mixture Stagnation Temperature Distribution Along the Nozzle for Cases METH 1.4.1, 1.4.2, 1.4.3, and 1.4.4.**

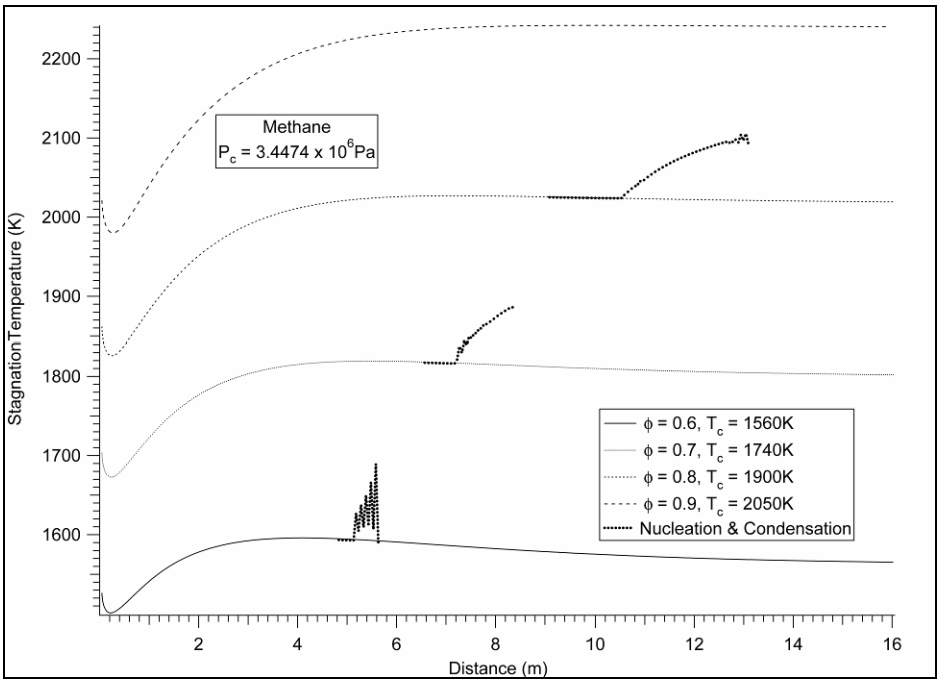

***Figure* G-5: Mixture Stagnation Temperature Distribution Along the Nozzle for Cases METH 1.5.1, 1.5.2, 1.5.3, and 1.5.4.**

Appendix H
Illustrations of the Mixture Static Pressure Distribution Along the Nozzle

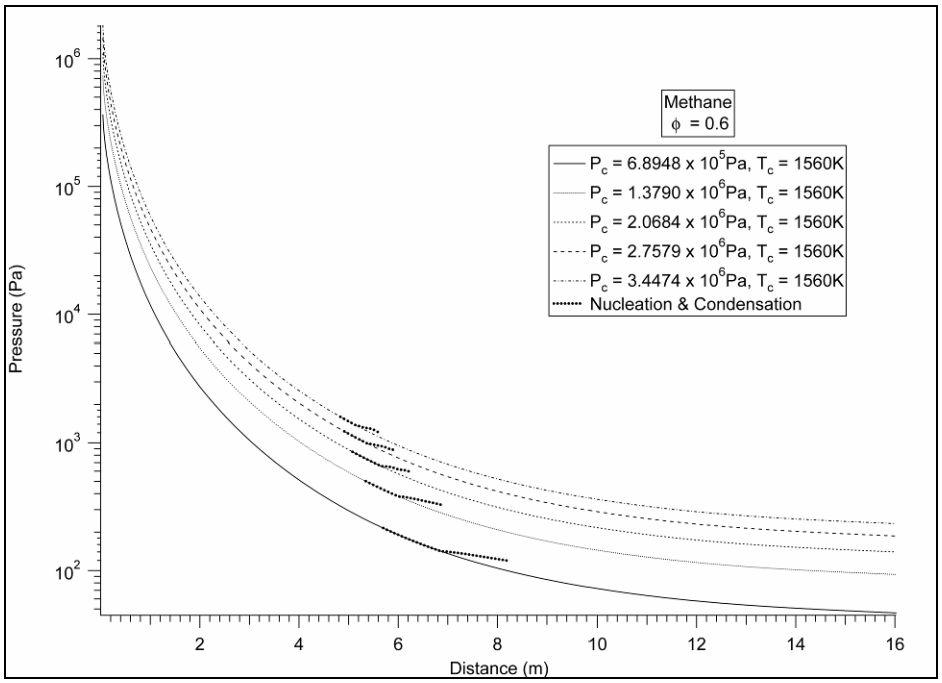

***Figure* H-1: Mixture Static Pressure Distribution Along the Nozzle for Cases METH 1.1.1, 1.2.1, 1.3.1, 1.4.1, and 1.5.1.**

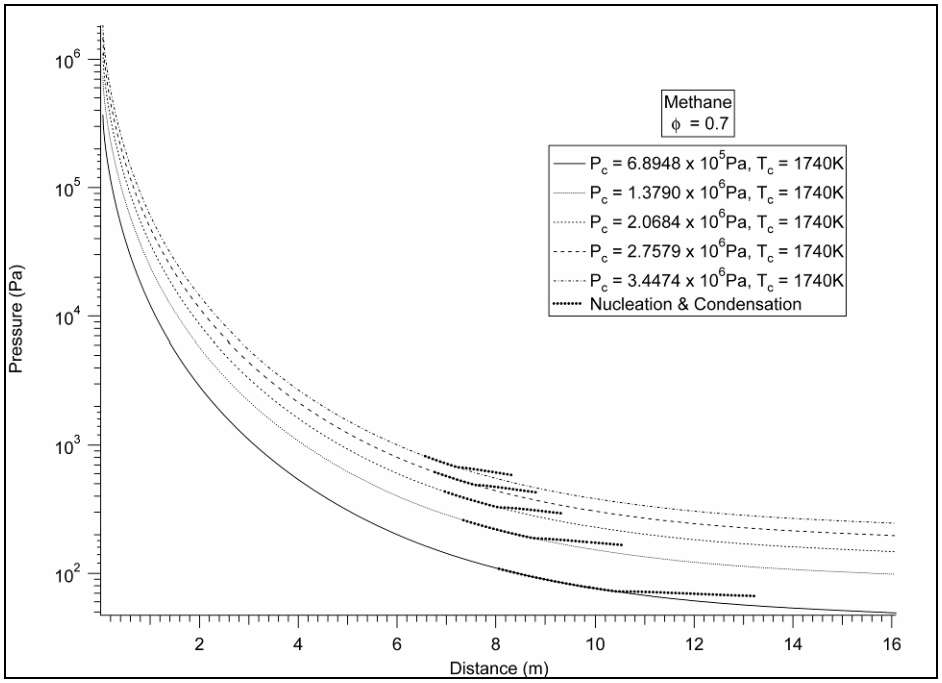

***Figure* H-2: Mixture Static Pressure Distribution Along the Nozzle for Cases METH 1.1.2, 1.2.2, 1.3.2, 1.4.2, and 1.5.2.**

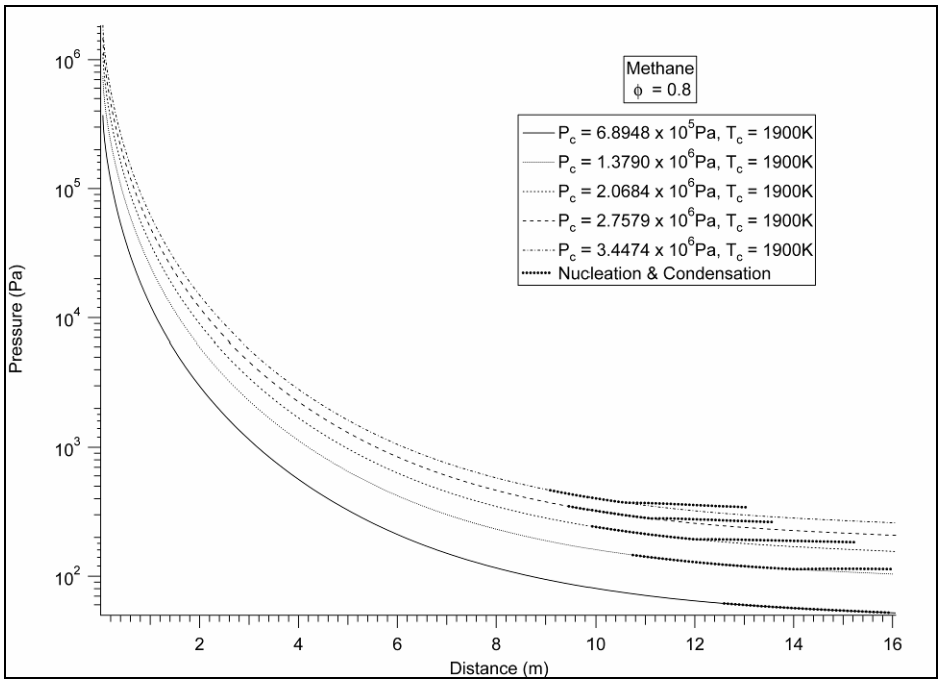

***Figure* H-3: Mixture Static Pressure Distribution Along the Nozzle for Cases 1.1.3, 1.2.3, 1.3.3, 1.4.3, and 1.5.3.**

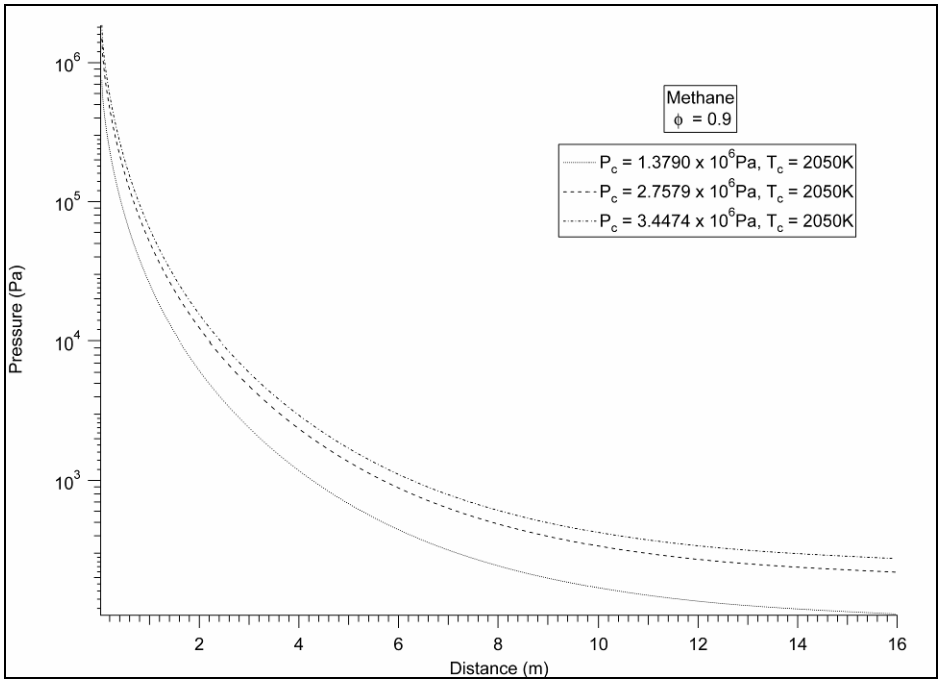

***Figure* H-4: Mixture Static Pressure Distribution Along the Nozzle for Cases METH 1.2.4, 1.4.4, and 1.5.4.**

Appendix I
Illustrations of the Mixture Stagnation Pressure Distribution Along the Nozzle

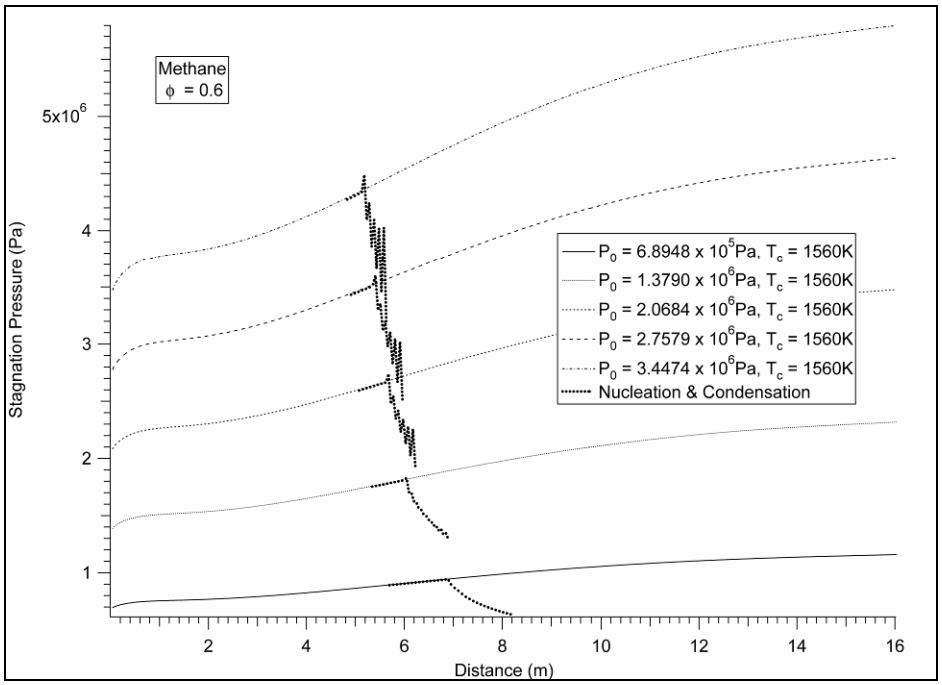

***Figure* I-1: Mixture Stagnation Pressure Distribution Along the Nozzle for Cases METH 1.1.1, 1.2.1, 1.3.1, 1.41, and 1.5.1.**

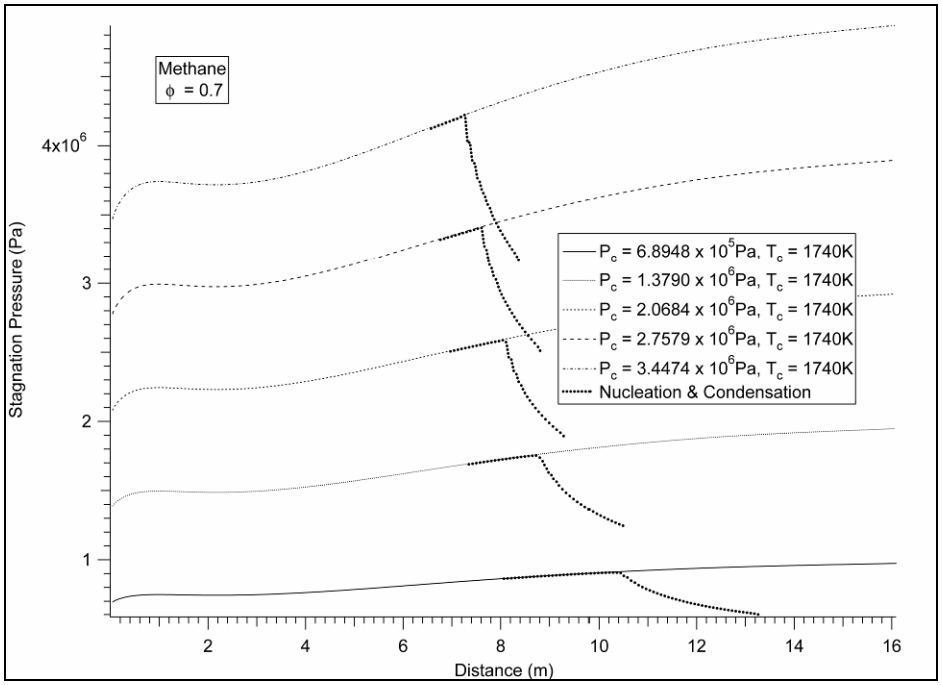

***Figure* I-2: Mixture Stagnation Pressure Distribution Along the Nozzle for Cases METH 1.1.2, 1.2.2, 1.3.2, 1.4.2, and 1.5.2.**

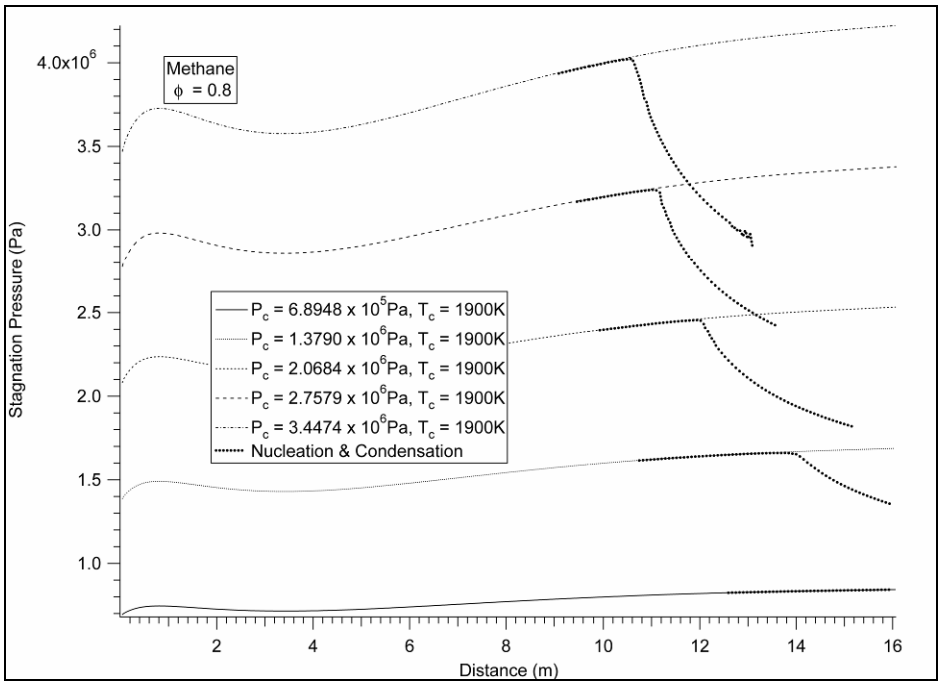

***Figure* I-3: Mixture Stagnation Pressure Distribution Along the Nozzle for Cases METH 1.1.3, 1.2.3, 1.3.3, 1.4.3, and 1.5.3.**

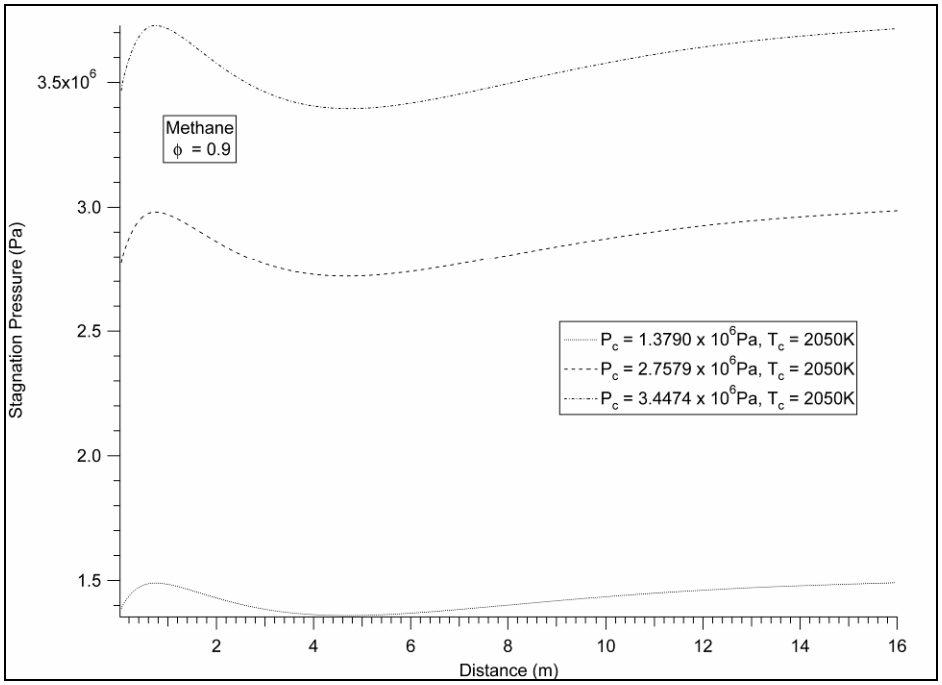

***Figure* I-4: Mixture Stagnation Pressure Distribution Along the Nozzle for Cases METH 1.2.4, 1.4.4, and 1.5.4.**

Appendix J
Illustrations of the Mixture Saturation Pressure Ratio Distribution Along the Nozzle

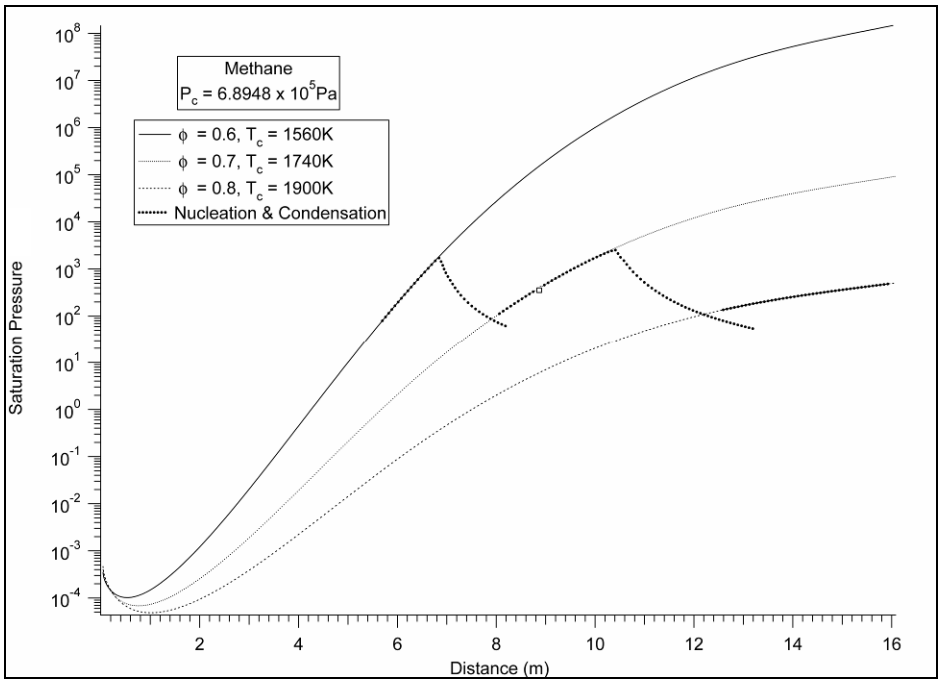

***Figure* J-1: Mixture Saturation Pressure Ratio Distribution Along the Nozzle for Cases METH 1.1.1, 1.1.2, and 1.1.3.**

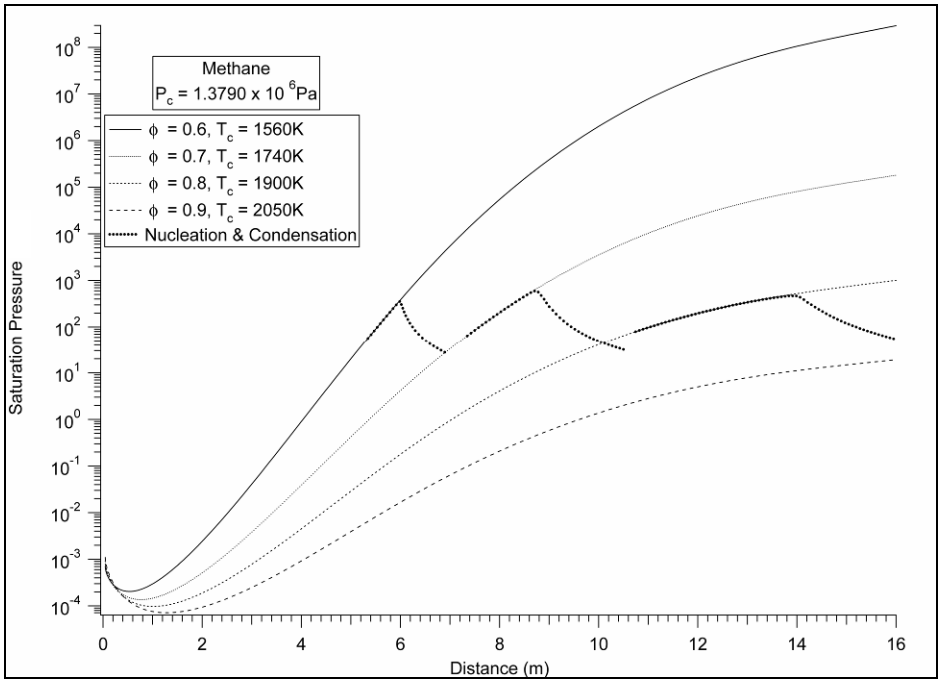

***Figure* J-2: Mixture Saturation Pressure Ratio Distribution Along the Nozzle for Cases METH 1.2.1, 1.2.2, 1.2.3, and 1.2.4.**

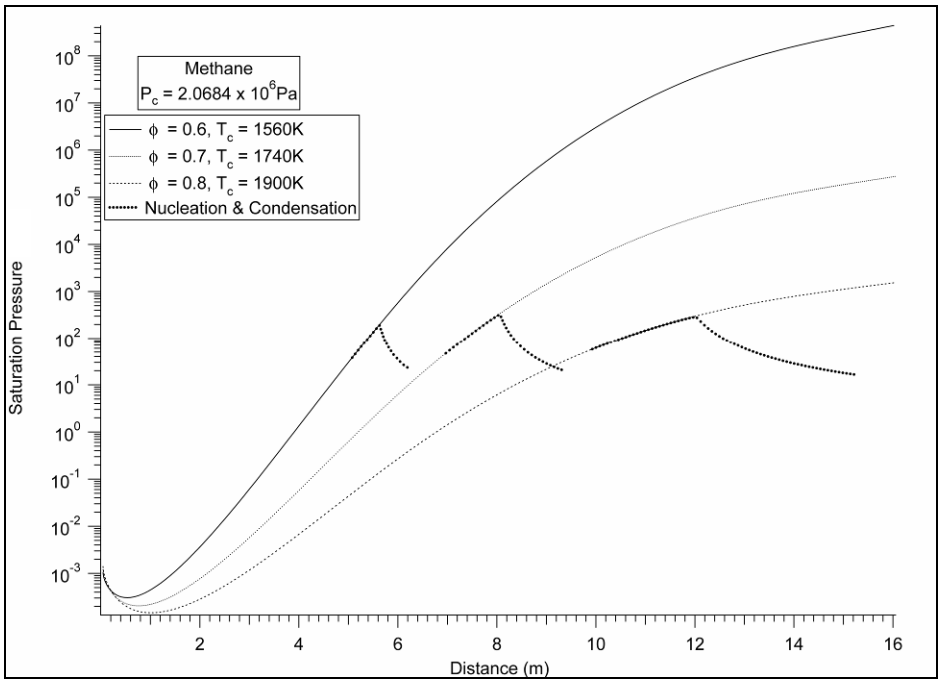

***Figure* J-3: Mixture Saturation Pressure Ratio Distribution Along the Nozzle for Cases METH 1.3.1, 1.3.2, and 1.3.3.**

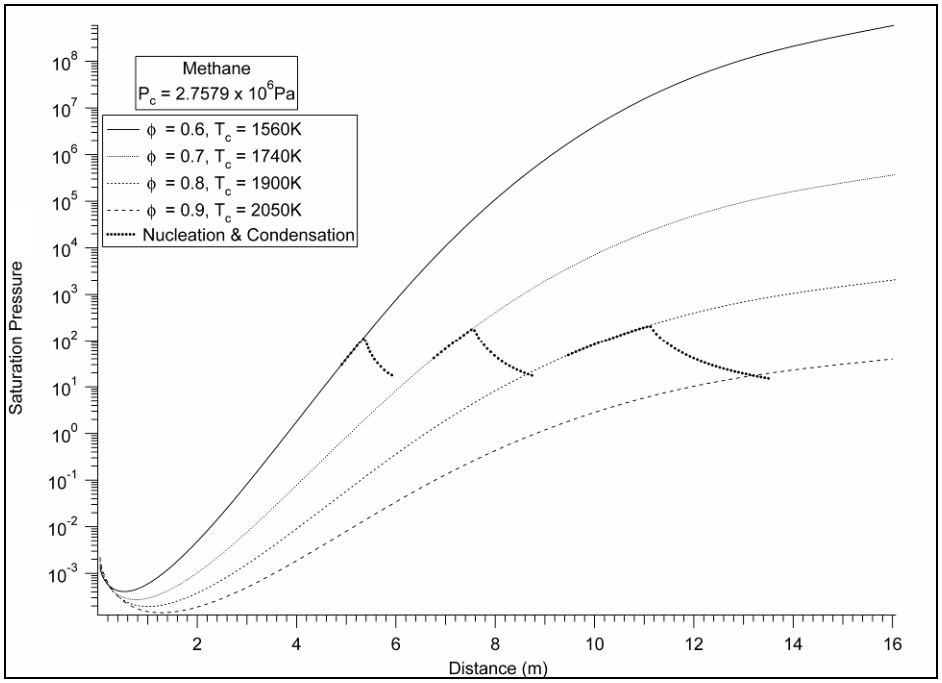

***Figure* J-4: Mixture Saturation Pressure Ratio Distribution Along the Nozzle for Cases METH 1.4.1, 1.4.2, 1.4.3, and 1.4.4.**

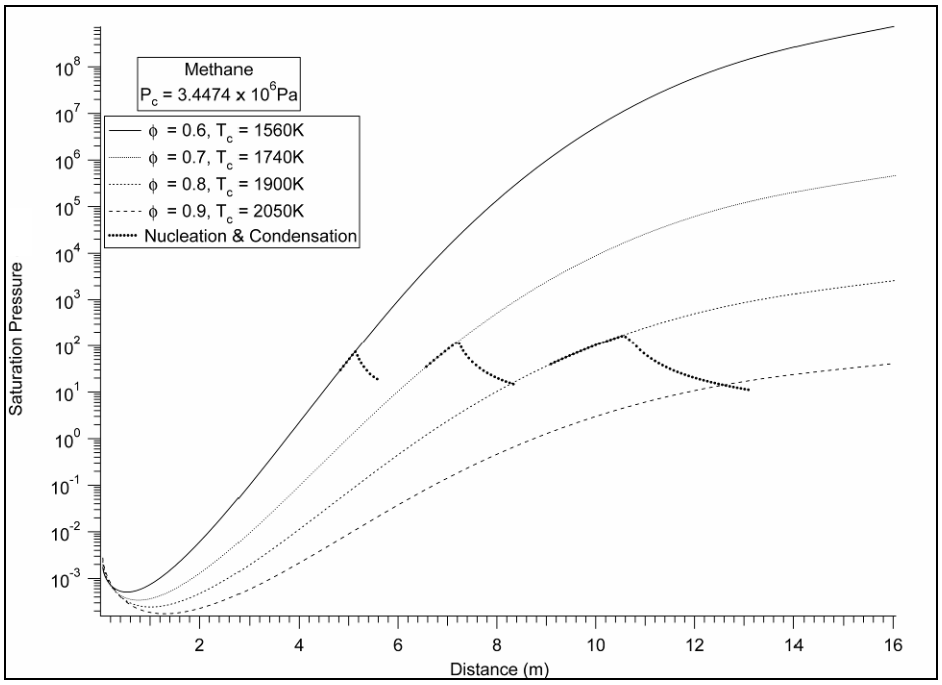

***Figure* J-5: Mixture Saturation Pressure Ratio Distribution Along the Nozzle for Cases METH 1.5.1, 1.5.2, 1.5.3, and 1.5.4.**

Vita

Todd VanPelt was born on Veterans Day of this country's bicentennial year. He was raised in Signal Mountain, TN for the majority of his early adolescent years followed by moving to Collierville, TN. In the May of 1995, he graduated from Collierville high school and later he was awarded a bachelor of science in mechanical engineering from the University of Memphis. His success in overcoming his learning disabilities resulting in the award of a bachelor's degree in engineering, inspired him to continue his studies towards more advance degrees. In the fall of 2000, he began attending the University of Tennessee Space Institute and received a master of science in mechanical engineering. He began his professional career in August 2004 as a research and development engineer for Aerospace Test Alliance which is the operating contractor for Arnold Engineering Development Center at Arnold Air Force Base. He is continuing his studies part time towards his final education goal of receiving a doctoral degree in engineering.